Minimizing the Cost of Wind Energy for Vashon Island – a Low Wind Speed Site

Eron Jacobson

A thesis submitted in partial fulfillment of
the requirements for the degree of

Master of Science in Mechanical Engineering

University of Washington

2005

Program Authorized to Offer Degree:
Mechanical Engineering

University of Washington

Abstract

Minimizing the Cost of Wind Energy for Vashon Island – a Low Wind Speed Site

Eron Jacobson

Chair of Supervisory Committee:
Professor Philip C. Malte
Mechanical Engineering

This study investigates the design of a wind farm on Vashon Island to meet the electricity needs of the local community at the lowest cost of energy. Vashon Island is located in Washington State's Puget Sound where wind speeds are usually low. The wind resource for the Puget Sound is generally considered to be Class 1 to Class 2 on a scale where Class 7 represents the greatest energy potential. An investigation into the cost of energy and appropriate turbine design for such low wind speeds has not been undertaken since higher wind resource sites exist elsewhere in the US. However, the desire for a sustainable community on Vashon Island may be great enough to facilitate the cost of a wind farm to provide the electricity supply. A wind resource assessment for proposed turbine sites on the island is developed, followed by an investigation of the optimum turbine parameters for the wind regime. Finally, the cost of integrating the wind farm into the local utility grid and the economic benefits of an energy storage system are determined.

Table of Contents

Page

List of Figures iii

List of Tables v

Introduction 1

1.0 Wind Resource Assessment 5

1.1 Wind Regime Characterizing Techniques 8
1.2 Data Sets 13
1.3 Directional Sector Analysis of the Data Sets 18
1.4 Computational Description of the Guidelines for Estimating Wind Speed Variations 23
1.5 Application of the Guidelines from the Data Collection Sites to the Turbine Site Locations 34
1.6 Annual Energy Yield 43
1.7 Sensitivities of the Model and Envelope Definition 47
1.8 Results 50
1.9 Summary and Conclusions 58

2.0 Optimum Wind Turbine Design for a Low Wind Speed Regime 61

2.1 Specific Power Description and Background 62
2.2 Turbine and Balance-of-Station Design and Cost Model 68
2.3 Results of the Wind Farm Cost and Energy Model Investigation 78
2.4 Future Component Cost Reduction 90
2.5 Summary and Conclusions 96

3.0 Grid Integration and Energy Storage 97

3.1 Grid Operation Background and Wind Energy Impacts 98
3.2 Wind Power Forecasting 100
3.3 Integration Timescales 101
3.4 Ancillary Services and Imbalances 102
3.5 Maury Wind Farm Integration into PSE System Analysis 107
3.6 Energy Storage 116
3.7 Summary and Conclusions 128

Conclusion 130

References 132

Appendix A. Wind Resource Figures 136

Appendix B. Turbine Site Description..... 140

Appendix C. Wind Resource Model Sensitivities 142

Appendix D. Turbine Component and System Design Description and Formulas 145

Appendix E. Balance-of-station Design Description and Cost Analysis..... 154

Appendix F. WindPACT Technology Impacts on Cost 168

List of Figures

Figure Number Page

Figure 1. Washington Wind Resources. [1] 2
Figure 2. Flow Chart of Analyses Used to Transform Collected Raw Wind Data to Projected Wind Velocities and Energy Yields at Maury Island Proposed Turbine Sites 7
Figure 3. Anemometer Locations for SeaTac and Beall Sites. [6] 14
Figure 4. SeaTac Airport Anemometer Location, 2002. [6] 15
Figure 5. Beall Anemometer Location [8] 17
Figure 6. Average Wind Velocity by Sector from SeaTac Data 1996-2004 at 10m. 18
Figure 7. Frequency Distribution by Sector from SeaTac Data 1996-2004 at 10m. 19
Figure 8. Weibull Distribution Fit Example 21
Figure 9. A Linear Correlation Fit Example for Beall and SeaTac 23
Figure 10. Guideline Flow Schematic [17] 25
Figure 11. Upstream Velocity Area of Puget Sound 33
Figure 12. An Example of Upstream Velocity Compared to Raw Velocity at SeaTac at 10m 36
Figure 13. A Comparison of Surface Roughness Lengths 38
Figure 14. Wind Turbine Site Locations on Maury Island [8] 41
Figure 15. Example of Projected Wind Speed Distribution at Turbine Site 8 at 50m 43
Figure 16. Generator, Power Electronics, and Drivetrain Efficiencies [30] 45
Figure 17. Average Velocity Shear Profile at Maury Island Turbine Sites – SeaTac Data 51
Figure 18. Average Velocity Shear Profile at Maury Island Turbine Sites –Beall Data 51
Figure 19. Average Distribution of Projected Wind Speeds, Beall Data Low Envelope at 50m 52
Figure 20. Average Distribution of Projected Wind Speeds, Beall Data High Envelope at 50m 52
Figure 21. Average Distribution of Projected Wind Speeds, SeaTac Data Low Envelope at 50m 53
Figure 22. Average Distribution of Projected Wind Speeds, SeaTac Data High Envelope at 50m 53
Figure 23. Average Wind Speeds Using the Beall Data, Low Envelope 54
Figure 24. Average Wind Speeds Using the Beall Data, High Envelope 54
Figure 25. Average Wind Speeds Using the SeaTac Data, Low Envelope 55
Figure 26. Average Wind Speeds Using the SeaTac Data, High Envelope 55
Figure 27. Annual Energy Production Using the Beall Data Low Envelope. 56
Figure 28. Annual Energy Production Using the Beall Data High Envelope. 57
Figure 29. Annual Energy Production Using the SeaTac Data Low Envelope. 57
Figure 30. Annual Energy Production Using the SeaTac Data High Envelope. 58
Figure 31. Previous Specific Power Studies for COE Minimization [24, 26] 65

Figure 32. Optimum Specific Power vs. Weibull Shape Parameter [24] 66
Figure 33. Specific Power of Commercial Utility Scale Turbines 68
Figure 34. Maury Island Wind Farm Top Level Diagram [8] 75
Figure 35. COE Investigation for Beall Data, High Envelope 80
Figure 36. COE Investigation for Beall Data, High Envelope 80
Figure 37. COE Investigation for SeaTac Data, Low Envelope 83
Figure 38. COE Investigation for SeaTac Data, High Envelope 83
Figure 39. Comparison of Specific Power Study 85
Figure 40. Comparison of COE vs. Wind Speed 86
Figure 41. Annual Energy Capture for Beall Data, Low Envelope 87
Figure 42. Annual Energy Capture for Beall Data, High Envelope 88
Figure 43. Annual Energy Capture for SeaTac Data, Low Envelope 88
Figure 44. Annual Energy Capture for SeaTac Data, High Envelope 89
Figure 45. Self-Erecting Tower Concept [39] 92
Figure 46. Schematic of Vanadium Redox Battery System 119
Figure 47. Hourly Wind Speed at SeaTac and Energy Output from the Maury Island Wind Farm 122
Figure 48. Yearly Load Shifted and Energy Loss 123
Figure 49. Normalized Load Following Error Reductions with Energy Storage 124
Figure 50. Losses of Energy Storage System for Load Following 125
Figure 51. Present Value of the Energy Storage System 127
Figure 52. Energy Storage System Present Value and ICC 128

List of Tables

Table Number Page

Table 1. Weibull Parameters for SeaTac Data....21
Table 2. Linear Correlations between SeaTac (at 10m) and Beall Data (at 49m)....22
Table 3. Summary of Roughness Lengths [4,5,14]....27
Table 4. Topography Coefficients [17]....28
Table 5. SeaTac Anemometer Site Characterization....35
Table 6. Roughness Length and Shear Exponents for Beall Site....37
Table 7. Envelope Assumptions....49
Table 8. Wind Speeds at Maury Island for Minimum and Maximum EnvelopesBased on SeaTac and Beall Reference Data.....50
Table 9. Summary of Wind Resource at Maury Island Wind Turbine Sites....59
Table 10. Turbine Site Ranking - Best to Worst....60
Table 11. Basic Parameters for WTGS Classes [3]....71
Table 12. Summary of Turbine Component and System Weight and Cost Calculations....74
Table 13. Summary of Balance-of-station Cost Calculations....77
Table 14. Optimum Turbine Parameters for Beall Data....81
Table 15. Optimum Specific Power for SeaTac Data....84
Table 16. Optimum Turbine Parameters for Beall Data....95
Table 17. Optimum Turbine Parameters for Beall Data....95
Table 18. Summary of Wind Integration Cost Estimate Studies [44]....105
Table 19. Wind Energy Impacts to PSE Power System [46]....106
Table 20. Wind Energy Impacts to the PSE System Extrapolated to 15MW....107
Table 21. Maury Island Wind Farm Estimated Hourly Forecast Errors....111
Table 22. Estimated PSE Forecast Errors....112
Table 23. Combined Standard Deviation of Hourly Forecast Errors....114
Table 24. California and New York Average Ancillary Service Prices for 2002 [45]....114
Table 25. Estimated Financial Impacts of Maury Island Wind Farm on PSE System....115
Table 26. Comparison of Financial Impacts of Maury Island Wind Farm on PSE System....116
Table 27. VRB Energy Storage System Costs [45, 52]....125
Table 28. Comparison of Financial Impacts of Maury Island Wind Farm on PSE System....129

Acknowledgements

The author wishes to express sincere appreciation to Committee members Professors Phil Malte, Jim Riley and Chris Stipe, and also to Dr. Rita Schenck, Director of the Institute for Environmental Research and Education, for sharing their expertise and providing encouragement and guidance. The author is grateful for the financial support provided by the Vulcan Fellowship on Renewable and Sustainable Energy, and expresses his thanks to Dr. Jim Boyden of Vulcan, Inc.

Introduction

This study investigates the theoretical cost of energy from a wind farm on Vashon Island located in the Puget Sound region. While a number of wind farms have been installed in south-central Washington, no wind farms have been developed west of the Cascades where high population densities exist. The reason for this is the lack of a good wind resource.

The Puget Sound region has largely been classified as a Class 1 to Class 2 wind resource by the Northwest Wind Mapping Project in 2002 [1]. The Olympic Mountains to the west of the Puget Sound create a sheltering effect from the weather patterns from this direction that results in low wind speeds. A western Washington State wind resource map is shown in Figure 1.

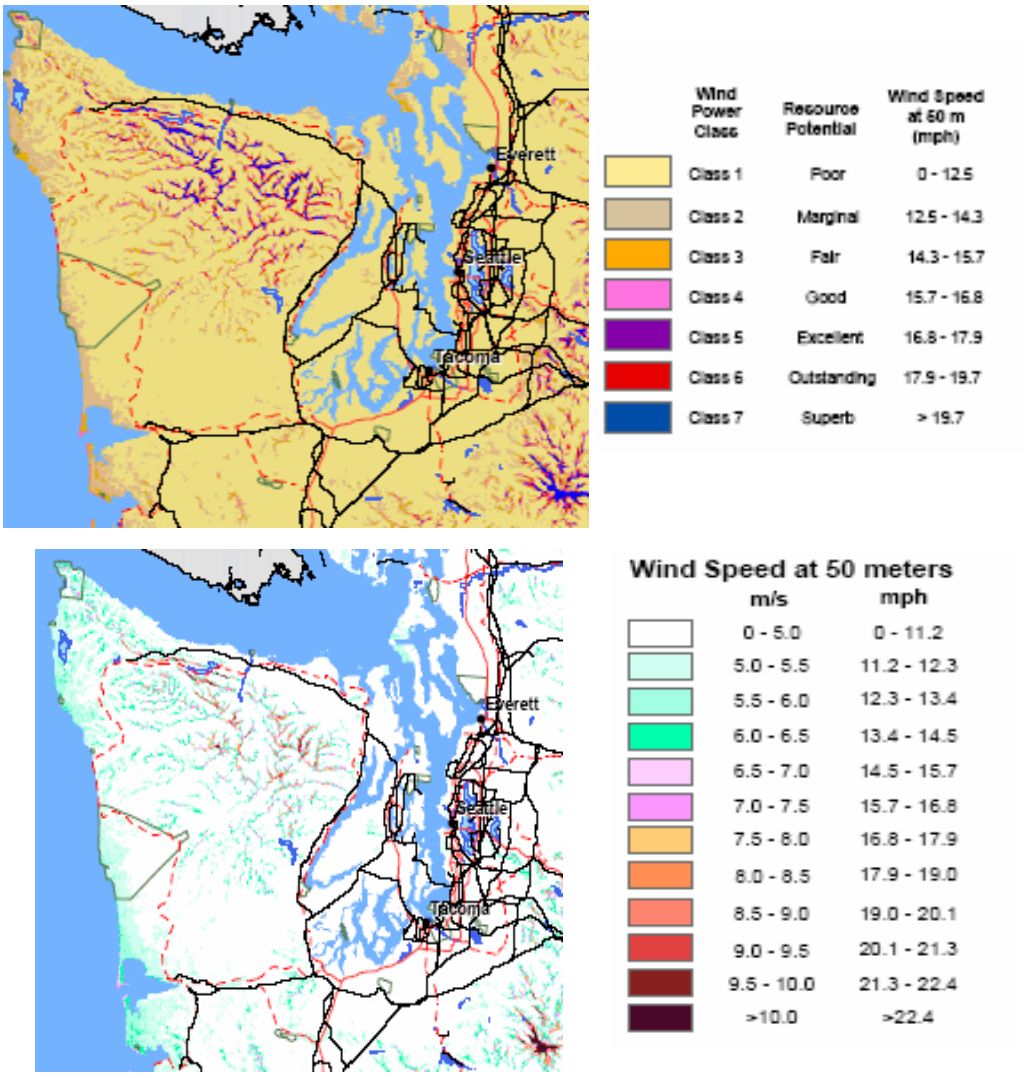

Figure 1. Washington Wind Resources. [1]

Class 2 wind resources do not typically elicit much attention from wind farm developers, but rather, most wind farms in the US are developed in resources of Class 4 or better. In fact, the goals of the Low Wind Speed Technology (LWST) program sponsored by the US Department of Energy (DOE) are largely aimed at minimizing costs for Class 4 wind resources [2]. The program recognizes that available prime Class 6 sites are running out in areas close to high density populations, and Class 4 sites are both abundant and generally much closer to cities (100 miles vs. 400 miles). The proximity to high population densities and the dwindling supply of high wind resource sites makes the

development of low wind resource sites necessary to continue wind energy development [2].

The cost of wind energy from a wind farm in a Class 2 resource such as Vashon Island is not likely to be competitive with the cost of energy from the ample hydroelectric and fossil fuel sources that make up Washington State's energy mix. Wind energy costs in Class 6 sites have become competitive with those of fossil fuels thanks to improved technology, acceptance, and economies of scale. The cost of wind energy in Class 4 sites is also competitive with the production tax credit of 1.8¢/kWh [2]. However, for a wind farm to be successful in the Puget Sound region there must be customers willing to pay more for the energy.

The Institute for Environmental Research and Education (IERE) has set a goal to make the Vashon Island community self-sustainable in its energy needs. IERE has surveyed the population on Vashon Island and has found that the community is willing to pay more for its electricity if it is from a "green" source. While the wind resource on the island is not expected to be superb, a preliminary study of the renewable energy sources for the island identified wind energy as a leading potential source [3]. IERE would like to provide the majority of the electrical energy needs through wind energy, or about 26 Gigawatt-hours (GWh) annually.

The goal of this study is to find the least cost to produce 26GWh annually from a wind farm on Vashon Island. This task necessitates identifying the best sites on the island to locate wind turbines, and the appropriate wind turbine design for the sites. Current wind turbines are designed for higher wind speed resources and may not be optimized for the low wind speeds of the Puget Sound.

This study takes the following steps to identify the minimum cost of wind energy from a wind farm on Vashon Island:

1. Perform a wind resource assessment for the optimal turbine locations on the island.
2. Identify the turbine and balance-of-station design that will minimize the end cost of energy, and identify technologies that may offer further cost reductions.
3. Assess the costs of grid integration and investigate possible energy storage systems to mitigate these costs.

1.0 Wind Resource Assessment

The wind regime is a quantitative description of how the wind blows at a site, and is the most important parameter in determining wind energy production. The power output from a turbine varies by the cube of the wind speed; a small error in the predicted velocity, 5% for example, will give about a 15% error in the turbine energy production. Lower wind speed sites are more sensitive to errors in predicted velocities [4]. Therefore, quantifying the wind regime characteristics becomes the critical task for a wind farm developer.

The wind resource assessment chapter characterizes the wind regime for proposed wind turbine sites along the south and southeastern ridges of Maury Island using long term wind data. Maury Island is connected to Vashon Island by a narrow isthmus and they are considered the same land mass. Two useful results are produced in this chapter: the first is identification of the wind regime for the ten turbine sites proposed for the wind farm. The second useful result is identification of which turbine sites have the best potential for energy capture. This information will be useful to the wind farm developer to place turbines in the most appropriate sites. The wind resource is then used to determine the optimum turbine design for the wind farm in Chapter 2.

The Chapter 1 outline is as follows:

1.1 Wind Regime Characterization Techniques: Background and descriptions of the data collection devices and the available methodologies for characterizing the wind regime are given in this section.

1.2 Data Sets: This section describes the two data sets that are used for the wind resource assessment, including the measurement site description and sampling information.

1.3 Directional Sector Analysis of the Data Sets: In this section, a description is given of how the raw data sets are analyzed and broken down into the components best suited to describe the wind regime at the data collection sites.

1.4 Description of the Guidelines for Estimating Wind Speed Variations: A computational description of guidelines for estimating wind speed variations are described in this section. These guidelines are designed to take a wind speed at a measured reference location and estimate the wind speed at another location. These guidelines are applied in Section 1.5.

1.5 Application of the Guidelines from the Data Collection Sites to the Turbine Sites: The topographic and surface coverage descriptions of the data collection sites and the turbine sites are developed in this section. These descriptions tailor the guidelines from Section 1.4 to the Maury Island application. The calculation methodology of the final projected velocities (projected from the data collection site) for the turbine sites is presented.

1.6 Annual Energy Yield: This section describes the calculation of the annual energy yield for the ten turbines given the final projected velocities.

1.7 Sensitivities of the Model: In this section, the sensitivity of the final projected velocities and annual energy yields to the assumptions made in the wind resource assessment model are investigated. Envelopes representing the lowest likely wind resource and the highest likely wind resource are defined.

1.8 Results: Final projected velocities and annual energy yields for the ten turbine sites are presented in this section.

1.9 Summary and Conclusions

A flow chart for the development of the wind resource for the turbine sites on Maury Island is shown in Figure 2. This starts with wind data collected at two sites within 10km of the Maury Island turbine sites: the SeaTac airport and the Beall location on Vashon Island.

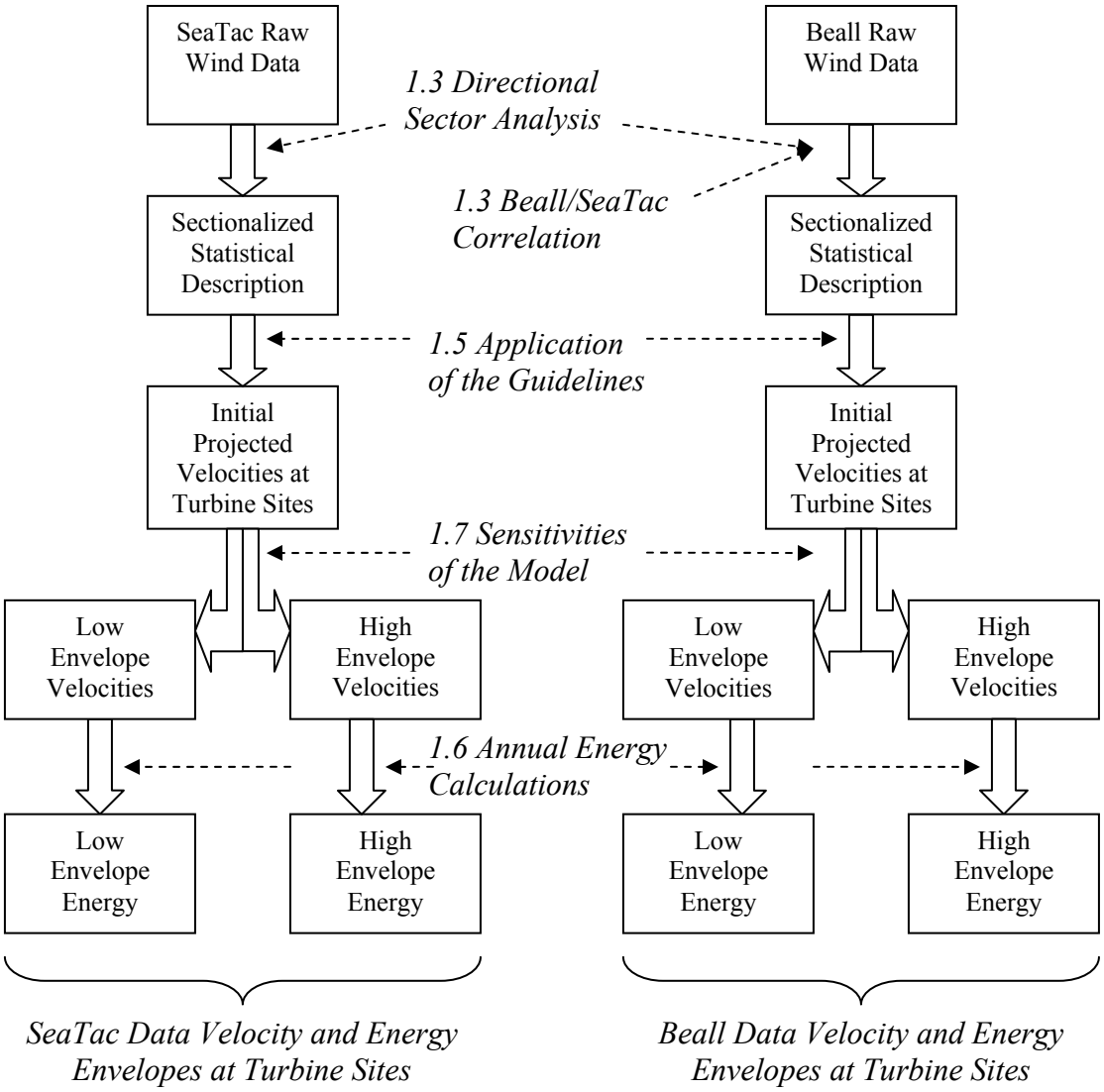

Figure 2. Flow Chart of Analyses Used to Transform Collected Raw Wind Data to Projected Wind Velocities and Energy Yields at Maury Island Proposed Turbine Sites

1.1 Wind Regime Characterizing Techniques

The wind regime for a location must be characterized in many ways to make an accurate prediction of annual energy production from a wind turbine at the site. This includes wind speed frequency distribution, directional frequency and velocity shear profile (change of velocity with respect to height). The most reliable way to make this characterization is to install a data collection system at each site of interest. The types of wind data collection devices include anemometer towers, SODAR and laser measurement systems. When data at a site is not available, analytical and numerical techniques are applied to extrapolate data from a nearby site to the site of interest.

1.1.1 Data Collection Devices

Data collection systems need to meet minimum requirements to provide useful data. The most useful measurement system is one that is installed at the proposed site of the wind turbine and at the exact hub height of the proposed turbine. In practice, one measurement system is installed at a location to measure data for multiple turbine sites around it. The area that one measurement system can cover is site dependent and based on topographical complexity and the surface coverage. For example, in complex terrain or heavily forested areas, one measurement system is typical for a 1km radius. This distance can be increased for smooth terrain and smaller vegetation coverage [4].

The predominant device used for collecting wind data is the anemometer tower. Anemometer towers range from 10m to 200m in height and normally have anemometers at multiple heights. The anemometers typically feed data to a data logger at 10 minute or one hour intervals. The data from the logger can be streamed to computers or downloaded at intervals for collection and analysis.

The anemometers will typically collect the following wind information:

- average wind speed (10 minute or one hour average)
- average wind direction (10 minute or one hour average)
- standard deviation
- maximum three second gust speed

Technical requirements for the anemometer systems are provided by the International Electrotechnical Committee (IEC), the International Energy Agency (IEA) and MEASNET. Good practices for installing collection equipment (i.e. in unsheltered areas), and the use of calibrated equipment can greatly improve the reliability of the data gathered [4].

Since wind turbine towers are becoming taller with applications well over 100m, it is often not economically viable to install an anemometer tower that will collect data at the hub height. Most anemometer towers installed for wind energy applications are 40m to 50m tall. This means that extrapolation of the data must be done to define the wind speeds at hub heights above this height.

1.1.2 Surface Boundary Layer Flow Software

Many software packages exist today explicitly for the purpose of estimating wind regimes for wind energy applications. These software packages, often called Wind Farm Design Tools (WFDT), are measure-correlate-predict type software programs which use available long-term meteorological data from one site to predict the wind regime at another site given the characteristics of the surrounding terrain. Many WFDTs come with features that can translate scanned topographic maps into their software, predict the energy output of a turbine given its power curve, and optimize turbine placement within given boundaries.

WFDTs use separate models to account for the local effects of terrain around the reference site. They correct the measured data for sheltering effects from obstacles near

the measurement location, the surface roughness of the terrain, and the topography of the site. The wind characteristics are then predicted for the nearby site of interest, accounting for the local terrain effects at the site of interest.

The software packages are limited in their predicting capabilities. The limiting factors to extrapolate the wind speeds from one site to another are as follows:

- The two sites must be in the same wind regime,
- The prevailing weather conditions must be close to neutrally stable (i.e. no strong thermal stratification of air currents), and
- The terrain must have limited complexity, and slopes must be within a critical limit to assure attached flow.

Numerous studies have been done that show the accuracy of these models to be fairly good [5]. It was found in studies that reasonable approximations are given on hilltops and upstream for grades less than 0.4. Wind velocity prediction errors in this type of software have begun to be thoroughly documented, and include effects from terrain with characteristics that fall outside the operating envelope of the program at either the reference or predicted site. The terrain characteristics that may fall outside operating envelopes include [9]:

1. Individual site ruggedness
2. Extensive flow separation
3. Topographic features outside the boundaries of the information given to the software
4. Site elevation
5. Hill height relative to the boundary layer height
6. Effective surface roughness length
7. The influence of large scale terrain effects.

1.1.3 WFDT Software Background

The basis for the WFDTs is the work of Jackson and Hunt [10], which is an analytical solution to adiabatic turbulent boundary layer flow over a two-dimensional hill with constant roughness. Linear equations of motion and a logarithmic velocity profile upstream of a hill are assumed in the analysis. The work assumes that two sections of flow result from the topographical change, an inner layer and an outer layer. A velocity perturbation in the outer layer caused by the vertical displacement of the flow in the inner region (from the hill) creates a pressure perturbation at the interface between the layers, which in turn drives a velocity perturbation in the inner layer. The result is given as a speed-up factor at the crest of the hill with a vertical distribution profile and a maximum velocity at a calculable height.

The two-dimensional theory of Jackson and Hunt is extended to three dimensions by Mason and Sykes [11] and later written into a model by Walmsley et al. [12] using Fourier series on a finite domain. The first version of the three-dimensional model was called MS3DJH/1 and after two subsequent revisions is known as MS3DJH/3R. This linearized flow model calculates changes in flow due to roughness changes and three-dimensional topography, and does not require that the wind data be taken upstream of the site of interest.

1.1.4 Meso-scale and Global Model Integration

The inherent limitations in boundary layer flow models have recently created interest in integrating global and meso-scale models with boundary layer flow models. Global weather analysis models such as NCEP/NCAR use meteorological data from around the world for applications such as weather forecasting. Such analysis and forecasting models have very course resolutions on the order of 30-40km. Meso-scale models can use these global analysis models as boundary conditions to predict wind conditions for areas on the order of several ten thousand square kilometers [13]. The meso-scale models also have

grids which are too coarse for wind turbine site analysis applications (~1-2km), but they can be used as forcing parameters for surface boundary layer flow programs. The integration of these three types of models has not yet been perfected. Future software along these lines may provide more accurate results than surface boundary layer flow programs alone.

1.1.5 Background of Guidelines for Estimating Wind Speed Variations

Unfortunately, WFDT software packages were not available for use in the Maury Island study. The next best option for performing a wind resource assessment is the use of guidelines developed by many of the same experts in boundary layer flow who have been involved in the development of the software algorithms. The guidelines use many of the same methods as in the software packages, though simplifications are made in the more computation intensive areas. Background on the development of these guidelines is briefly discussed here.

Taylor and Lee [14] developed simple guidelines for estimating speed variations due to small scale topographical features, including two-dimensional ridges and escarpments, three-dimensional hills, and rolling terrain. The guidelines address changes in wind velocity due to both topographical features and changes in surface roughness. One drawback is that the guidelines require the reference site (where data is collected) to be directly upstream of the site of interest. The boundary layer flow over hills that Taylor and Lee use is that developed by Hunt [15], which characterizes the change in flow by a speed up factor formula. The roughness change effects used by Taylor and Lee are based on the formulas developed by Elliot [16].

Walmsley, Taylor and Salmon [19] modified the guidelines developed by Taylor and Lee to allow the use of wind data from reference sites which are not directly upstream of the site of interest. They also suggest using a different formula than Elliot for the effect on boundary layer flow due to surface roughness changes. Resistance laws or geostrophic

drag laws allow the use of wind data from a reference site not upstream of the site of interest. This assumes that the geostrophic wind is the same above the reference site and the site of interest.

1.2 Data Sets

Wind speed and direction vary by day and night, by season, by year and by decade. The wind regime for a location can change up to 30% decade to decade, and even more so on shorter time scales [5]. Therefore, to accurately determine the energy potential for wind turbines installed on Maury Island, reliable data for long lengths of time are needed.

Two sources of wind data are available for use in this study: long term data from a National Climatic Data Center (NCDC) anemometer tower at SeaTac airport, and data for five months from an anemometer tower installed by the IERE on the central west side of Vashon Island at the Beall greenhouse site. The locations of the two anemometers are circled in red (SeaTac) and yellow (Beall) in Figure 3.

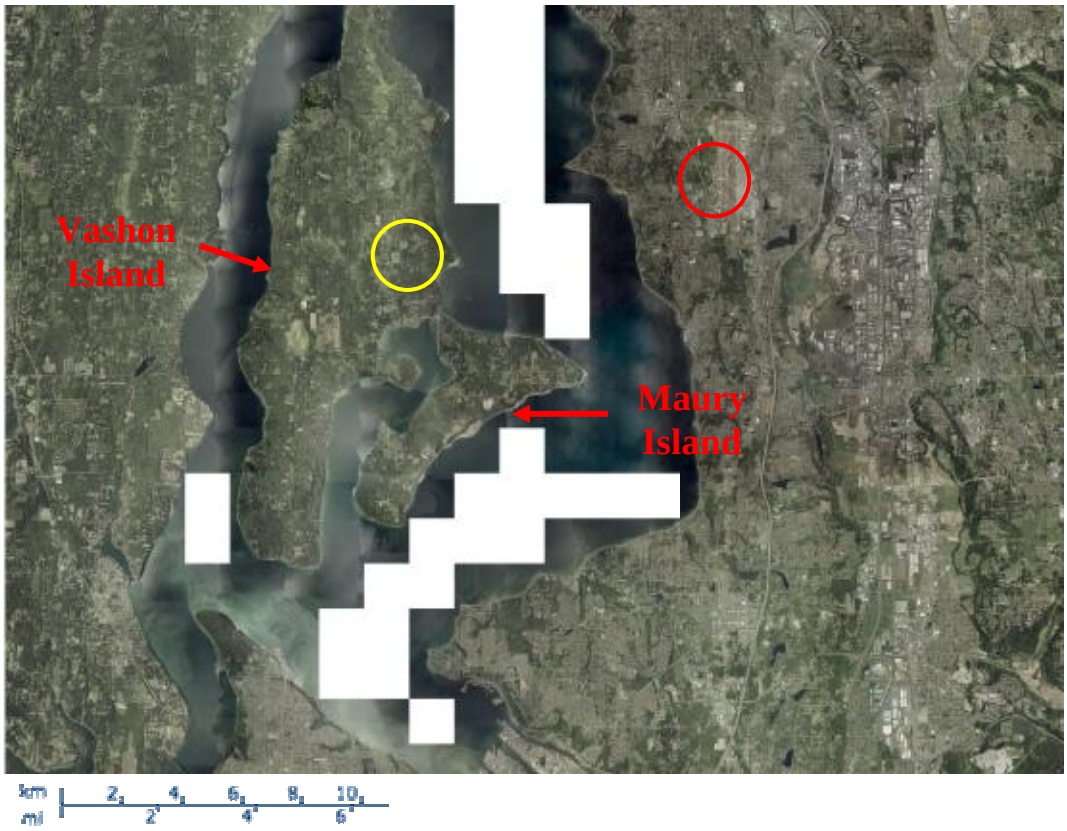

Figure 3. Anemometer Locations for SeaTac and Beall Sites. [6]

1.2.1 SeaTac Data Set

SeaTac airport is on the mainland of the Puget Sound region slightly east of Vashon/Maury Island by about 10 kilometers. The airport's close proximity to the island likely places it in the same wind climate as the island. Climatic data from SeaTac airport is available through the NCDC [7] in hourly increments with exceptions of seemingly random off-hour data points. The data set includes hourly average wind speeds and wind direction. The long term data used for this study is from 1996 through 2004, with an anemometer installation height of 10 meters.

The anemometer installation at SeaTac airport is on the west side of the north-south runways, slightly south of the central latitudinal location respective to the runways. Since the anemometer is located next to a runway, the topography surrounding the tower

is relatively flat. To the north and south of the anemometer location, the runways extend for about 2 km and 1¼ km respectively. The runway area extends for about ¾ - 1km in the directions 30º - 135º from north. On the west side of the anemometer location, from north to south, the terrain is covered by trees and suburbs.

The average wind velocity data from the SeaTac anemometer is recorded to the nearest knot and converted to meters per second. For example, recorded values include 2.6m/s (5 knots), 3.1m/s (6 knots), and 3.6m/s (7 knots). This inaccuracy in recorded values will undoubtedly add an inherent degree of error when utilizing the data.

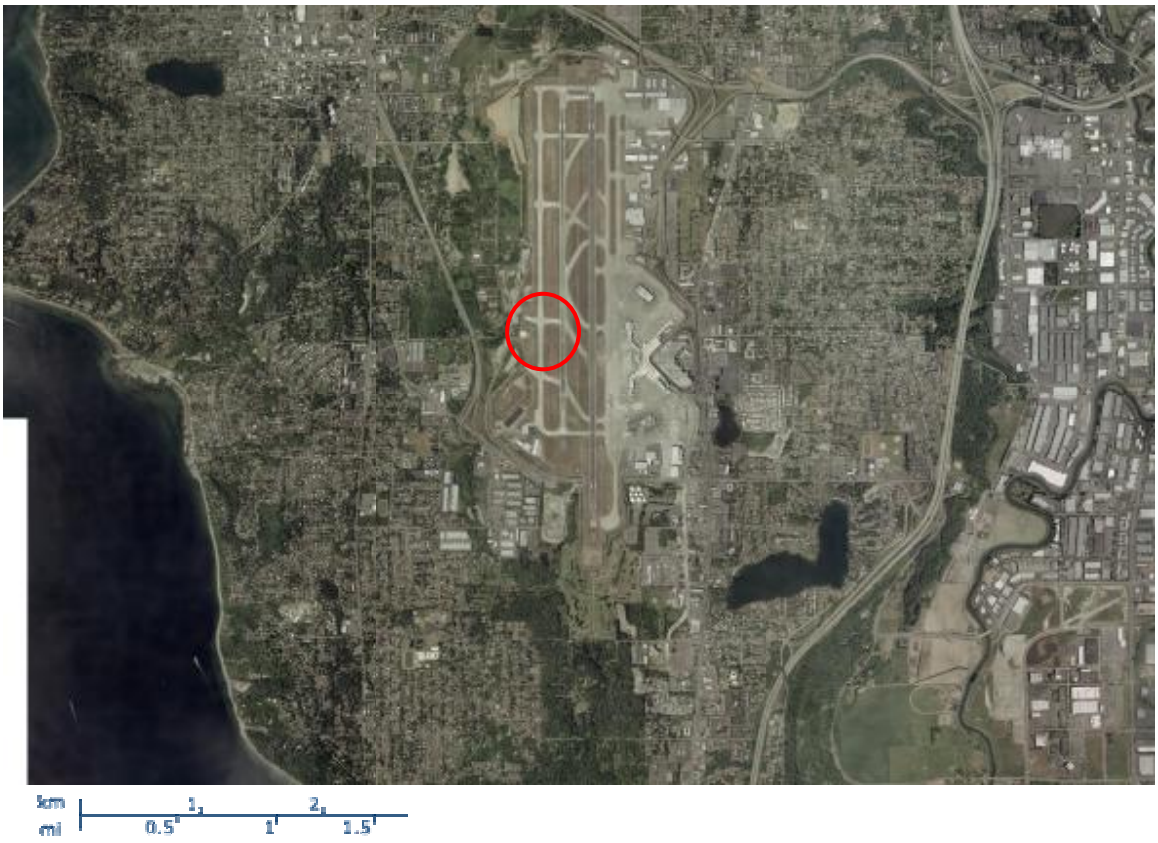

Figure 4. SeaTac Airport Anemometer Location, 2002. [6]

1.2.2 Beall Data Set

The Beall anemometer installation is on Vashon Island about 1 km south-southwest of the town of Vashon. This anemometer tower was installed by IERE on December 7, 2004 for the purpose of gathering data closer to the proposed turbine sites on Maury Island. The data set available for use in this study was provided by IERE for about five months, from 12/07/04 – 5/02/05. The anemometer tower has anemometers at four heights: 49m, 47.5m, 35m and 26.5m. It takes average wind speed and direction measurements every ten minutes.

The terrain surrounding the anemometer location is mostly woodlands and farmlands, with the exception of a large number of greenhouses to the east and southeast. The site is slightly depressed from surrounding terrain, but with a very shallow slope. Directly surrounding the tower, there are tree lines at about 50-200m from the tower base which are about 10-20m in height. The land leading up to the tree lines is flat and grassy, with the exception of lands lying to the east and southeast.

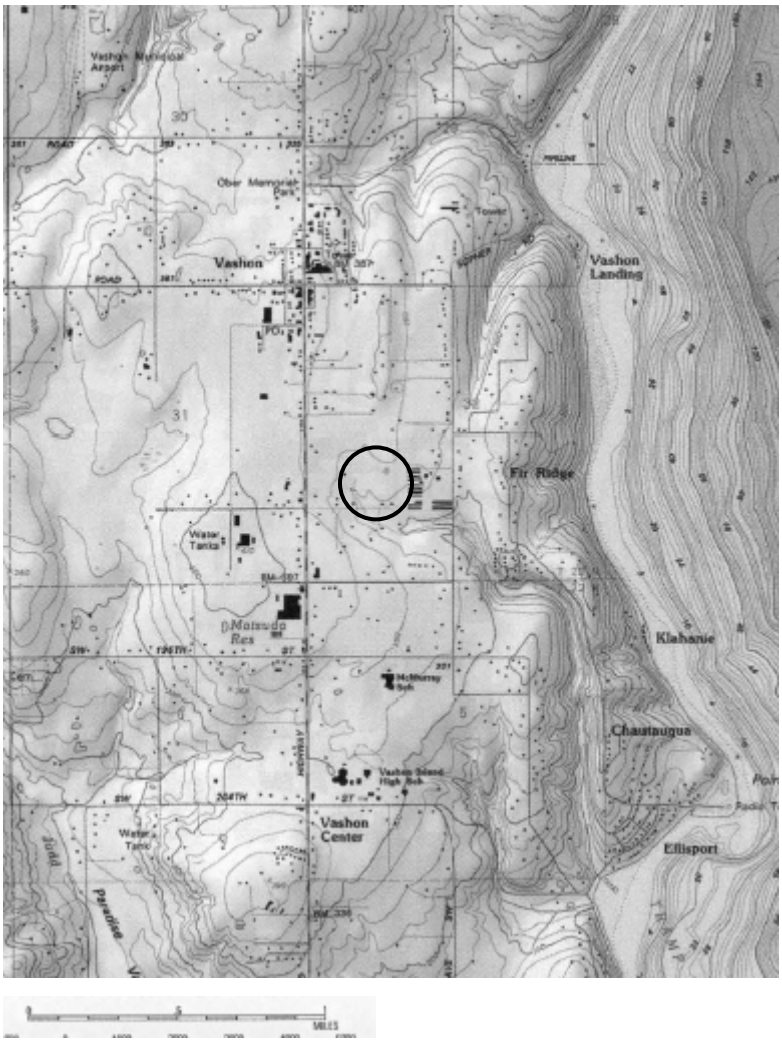

Figure 5. Beall Anemometer Location [8]

The data from the SeaTac and Beall anemometers provide two different sources to estimate the wind regime at Maury Island. The raw data are used to derive statistical distributions of wind speeds at the anemometer locations. Guidelines are then used to project wind speeds at Maury Island. The two different data sets help to reduce the uncertainty of the final results.

1.3 Directional Sector Analysis of the Data Sets

The data from SeaTac airport from 1996 to 2004 is broken into twelve directional sections of 30 degrees each and characterized in terms of the average wind speed at 10m, the Weibull distribution, and the roughness length. This technique is widely used in the wind industry [4, 5].

1.3.1 Average Wind Speed for SeaTac Anemometer

The average wind speed for each sector was simply calculated by using an equal weighting of each hourly data point. Additionally, the frequency of wind from each sector was calculated. The frequency of wind from a directional sector is the fraction of time that the wind blows from this sector. The highest frequencies and velocities are from the two southwestern directional sectors from 175º-205º and 205º-235º. The results are shown in Figure 6 and Figure 7.

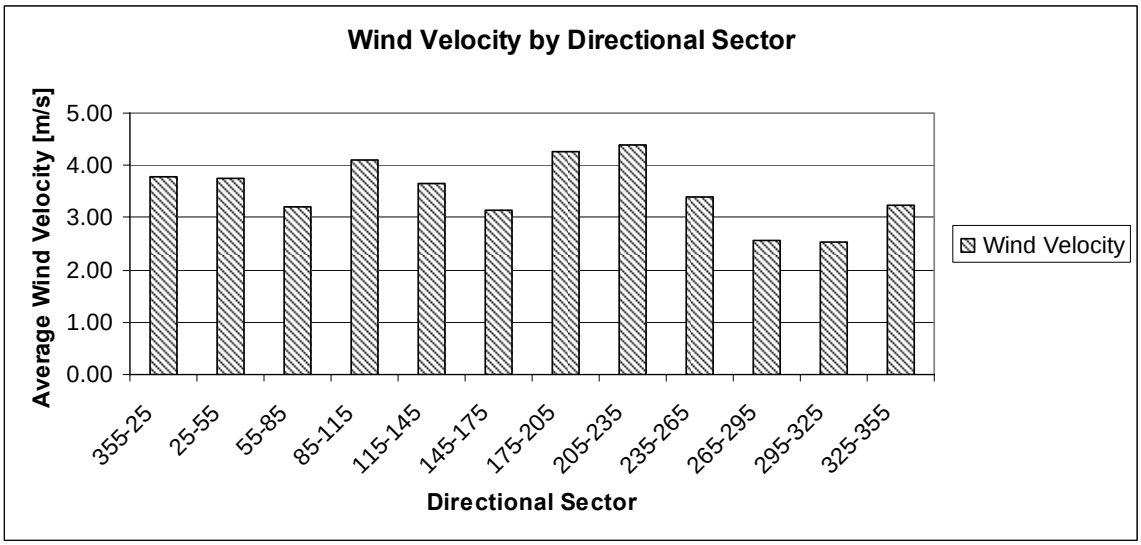

Figure 6. Average Wind Velocity by Sector from SeaTac Data 1996-2004 at 10m.

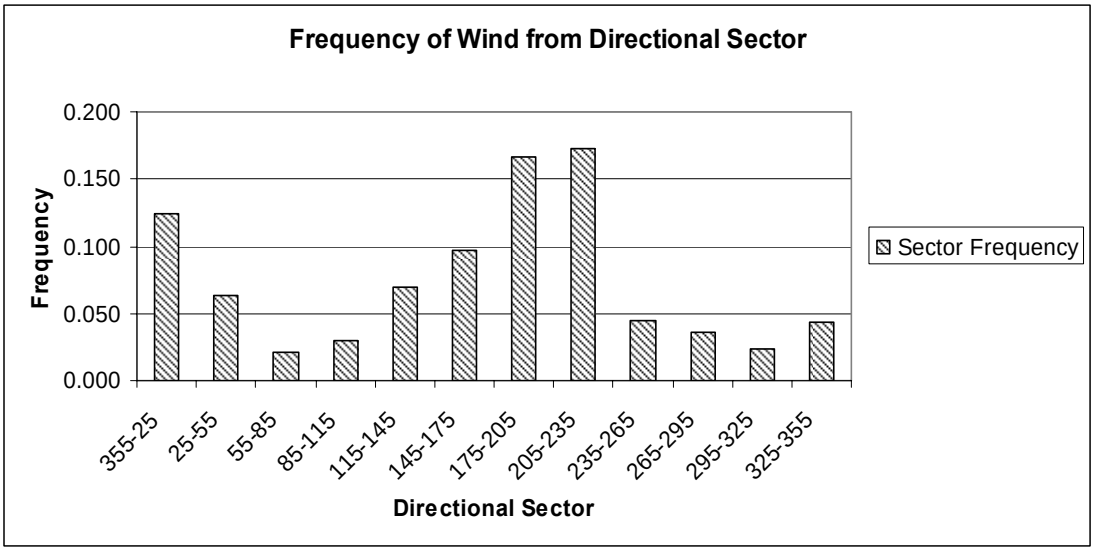

Figure 7. Frequency Distribution by Sector from SeaTac Data 1996-2004 at 10m.

1.3.2 Weibull Distribution Fit

It is thoroughly documented that the distribution of wind speeds is described well by Weibull distribution functions [5, 20, 21]. The two parameter Weibull distribution function is described by:

$$f(u) = \frac{k}{A}\left(\frac{u}{A}\right)^{k-1} \exp\left(-\left(\frac{u}{A}\right)^{k}\right)$$

Where: $f(u)$ = the frequency that the wind speed u occurs

A = the scale parameter

k = the shape parameter

The most common shape parameter characterizing wind data is $k = 2$ and is known as the Rayleigh distribution [5]. However, this distribution is not the case for all locations; thus, a fitting procedure must be used to determine the scale and shape parameters for the collected data. The goal of the fitting procedure is twofold: to maintain the total energy of the observed and fitted wind velocity distributions, and to maintain the frequencies of

velocities higher than the observed average speed equal in the fitted wind velocity distributions to that of the observed distribution [5].

The directional sector data from SeaTac airport was broken down into ranges, or buckets, of wind speed and then fit to a Weibull distribution. Twenty-five buckets were created to represent the 1m/s increments for the range of 0 to 25m/s. A few examples of buckets would be Bucket One: 0 to 1m/s, Bucket Two: 1 to 2m/s, and Bucket Three: 2 to 3m/s. The average velocity for each bucket was assumed to be the midpoint of the bucket range (e.g. 0.5m/s for Bucket One, 1.5m/s for Bucket Two, etc.).

Lun and Lam [21] found that using the maximum likelihood method for estimating the Weibull parameters produced the best fit. However, the modified maximum likelihood method also worked quite well, especially when smaller range buckets were used. The modified maximum likelihood method was chosen for use in this study because the data is already broken into velocity buckets. The estimation equations are:

$$k = \left(\frac{\sum_{i=1}^{25} u_i^k \ln(u_i) P(u_i)}{\sum_{i=1}^{25} u_i^k P(u_i)} - \sum_{i=1}^{25} \ln(u_i) P(u_i) \right)^{-1}$$

$$A = \left(\sum_{i=1}^{25} u_i^k P(u_i) \right)^{1/k}$$

Where: u_i = the wind speed central to the range

$P(u_i)$ = the frequency with which the wind speed falls into the bin, i

The equation for the shape parameter, k, is solved iteratively with an initial guess of 2. The scale parameter is then easily calculated by the second equation. This fitting

procedure minimizes the error of the cumulative frequency distribution. The conclusions of this analysis are listed in Table 1.

Table 1. Weibull Parameters for SeaTac Data

Direction [degrees]	Shape parameter, k	Scale parameter, A
355 to 25	3.04	4.37
25 to 55	3.06	4.36
55 to 85	2.57	3.75
85 to 115	2.57	4.77
115 to 145	2.48	4.26
145 to 175	2.66	3.61
175 to 205	2.40	4.96
205 to 235	2.57	5.08
235 to 265	2.50	3.99
265 to 295	3.25	3.02
295 to 325	2.99	3.00
325 to 355	2.63	3.80

An example of a Weibull distribution fit to collected directional sector data is shown in Figure 8. A complete set of figures for each direction sector is included in Appendix A.

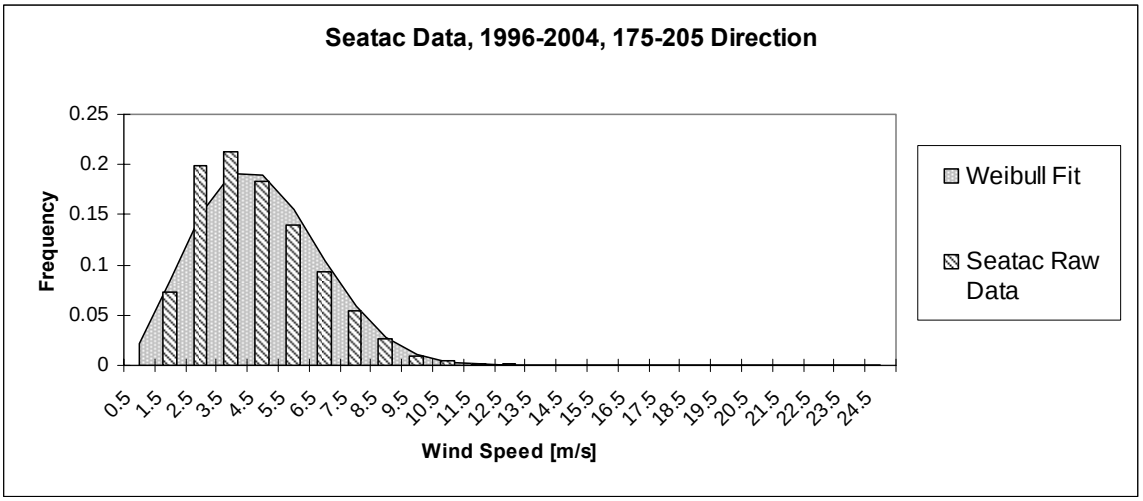

Figure 8. Weibull Distribution Fit Example

1.3.3 SeaTac – Beall Correlation

The short term data from the Beall site is not long enough in duration to be useful by itself for estimating the wind at the Maury Island proposed turbine sites. The five months of data from the Beall site can be useful if a correlation between the Beall site wind data and the SeaTac wind data is defined. The long term SeaTac data can be then adjusted by the correlation to represent long term data at the Beall site. The results should still be viewed with caution due to the relatively small amount of data available to develop a correlation.

Directional sector wind data was gathered from the Beall site on Vashon Island and SeaTac airport from December 7th, 2004 to May 3rd, 2005 and correlated using a linear relationship, as is standard in wind resource assessment [22]. The correlation was made between the 49m anemometer height on the Beall tower and the 10m anemometer location (the only height) at SeaTac airport for wind velocities greater than 3m/s [22]. The linear correlations and the correlation coefficient are described in Table 2.

Table 2. Linear Correlations between SeaTac (at 10m) and Beall Data (at 49m)

Direction [degrees]	**Beall/ SeaTac**	**R^2**	**No. of Hours**
355 to 25	1.0654	0.93	177
25 to 55	1.0006	0.95	153
55 to 85	0.7926	0.96	11
85 to 115	0.6071	0.72	9
115 to 145	0.713	0.94	14
145 to 175	0.6317	0.93	4
175 to 205	0.8639	0.94	37
205 to 235	1.1088	0.96	172
235 to 265	1.1377	0.96	75
265 to 295	1.1673	0.98	3
295 to 325	1.3202	1	1
325 to 355	0.7701	1	1

An example of the linear correlation fit is shown in Figure 9. As can be seen, the linear fit holds for the full range of velocities recorded at the two anemometer locations. However, at least 7 of the 12 sectors lack enough data for confidence in the correlation.

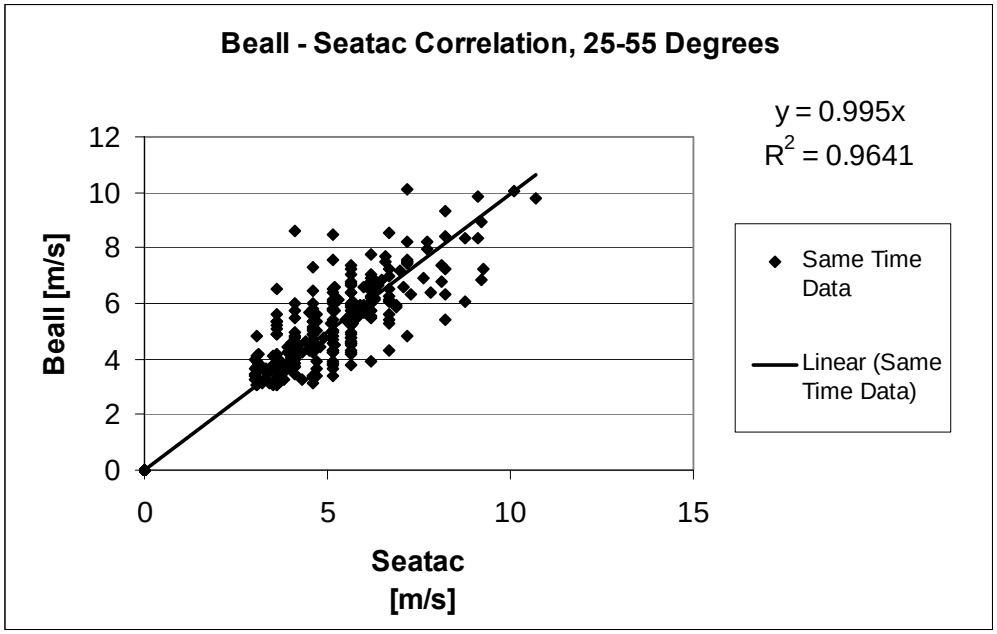

Figure 9. A Linear Correlation Fit Example for Beall and SeaTac

1.4 Computational Description of the Guidelines for Estimating Wind Speed Variations

The guidelines for estimating wind speed variations are used to take a wind speed at a measured reference source and estimate the wind speed at another location given the topographical and surface coverage description of the earth around the two locations. The background of the development of these guidelines is discussed in Section 1.1.5. They will be referred to as "the Guidelines" throughout this paper. The calculation methodology of the Guidelines is described here.

The wind climate at a location has two factors which affect it: the overall weather system above the location and the topography and ground cover around the location [5]. The overall weather system defines the geostrophic wind speed or the free stream velocity, the

velocity for which the effect of surface friction of the earth has no significant impact [19]. The surface roughness of the earth creates an atmospheric layer next to it called the atmospheric boundary layer. This layer extends from 100m on a clear night to 2km on a clear summer day [5]. The Guidelines are methods for calculating how the wind profile at a reference location, *R*, can be used to describe the wind profile at a location of interest, *P*. This concept is shown well by Figure 10.

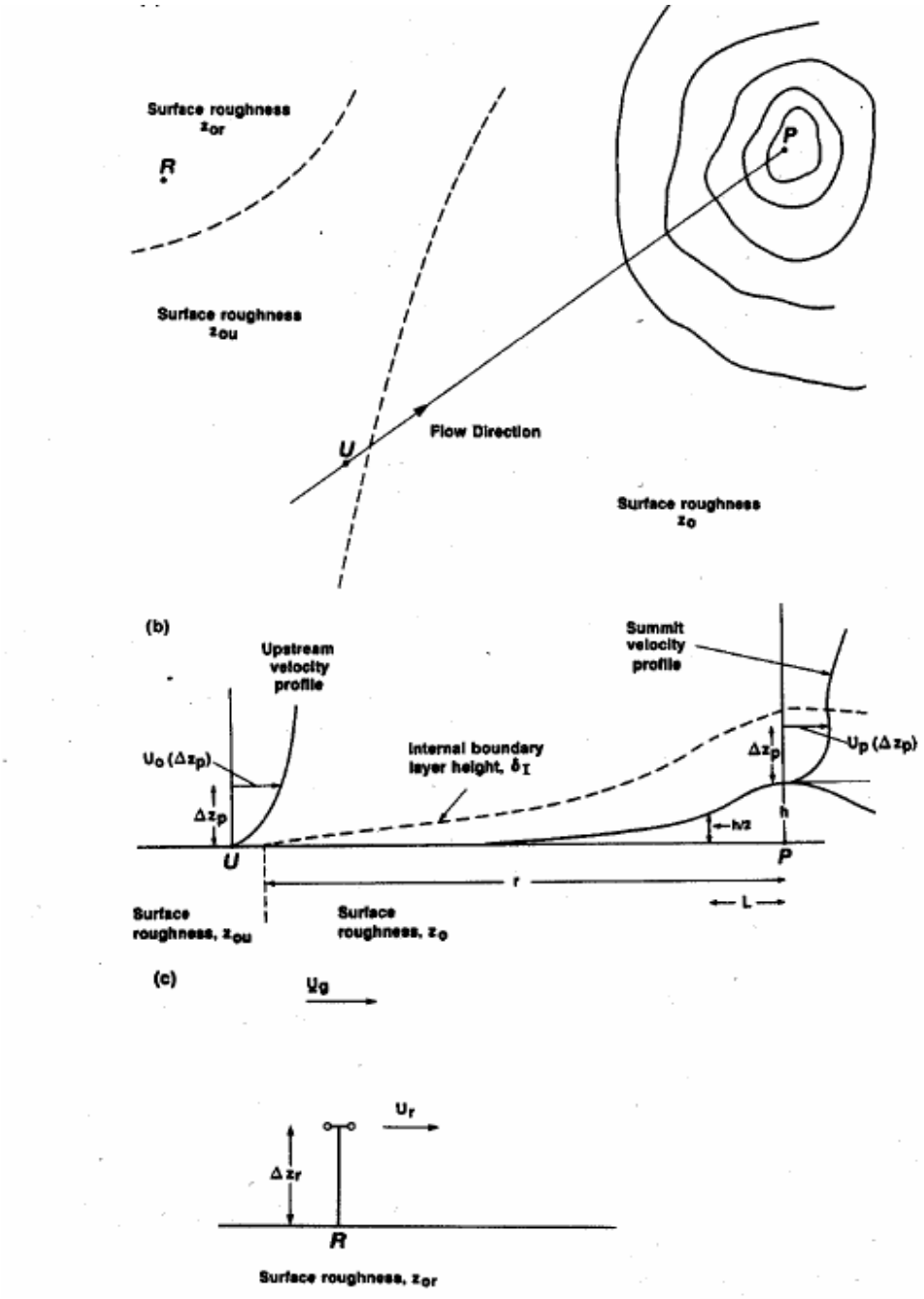

a) Plan view or map.
- - - - - - Roughness boundaries.
-------- Contour lines.
b) Topographic cross-section.
c) Reference site.

Figure 10. Guideline Flow Schematic [17]

1.4.1 Logarithmic Shear Profile Law and Surface Roughness

The lowest part of the atmospheric boundary layer is called the surface layer. It is estimated at roughly 10 percent of the atmospheric boundary layer, and is assumed to be 100m or higher for wind energy applications [5]. Within this layer, up to 100-150m, the logarithmic law approximates the wind speed well for neutrally stratified flows and moderate wind speeds [5, 14]: Neutrally stratified flows are flows where strong thermal stratification does not exist.

$$\mathrm{U}(\Delta z) = \frac{u_*}{\kappa} \ln\left(\frac{\Delta z}{z_o}\right)$$

Where: $U(\Delta z)$ = the wind speed at height Δz above the ground

u_* = friction velocity

κ = 0.4, the von Karman constant

z_o = the surface roughness length

The logarithmic law is also often written in terms of a known reference wind speed at a reference height:

$$U(\Delta z) = U(\Delta z_r) \frac{\ln\left(\Delta z / z_0\right)}{\ln\left(\Delta z_r / z_0\right)}$$

Where: $U(\Delta z_r)$ = the wind speed at the reference height Δz_r

As can be seen from the two formulas:

$$u_* = \frac{\kappa * U(\Delta z)}{\ln\left(\frac{\Delta z}{z_o}\right)}$$

The surface roughness length is a characteristic determined by the type and density of the ground coverage. A rule of thumb for the roughness length is that $z_o \approx 1/30$ to $1/10$ the size of the roughness elements [14]. Roughness lengths from numerous sources are shown in Table 3.

Table 3. Summary of Roughness Lengths [4,5,14]

Surface	Comments	z_o [m] [14]	z_o [m] [5]	z_o [m] [4]
Ice	Smooth	.00001	-	0.00001
Water	Windspeed dependent	10^{-5}-10^{-3}	0.0001	0.0001
Snow	Assumed smooth	.001	0.001	0.001
Sand, desert		.0003	0.003	0.0003
Bair Soil		10^{-3}-10^{-2}	0.005	0.005
Grass	0.2-0.1m high	0.003-0.1	0.08	.01
	0.25-1.0m high	0.04-0.10	-	-
Agricultural Crops	Can be windspeed dependent	0.04-0.20	-	-
Airports	Runways	-	0.01	-
	Runways with buildings	-	0.03	-
Rural Area / Farmland	Open farmland	0.01	0.03	0.05
	Farmland with isolated trees & buildings	0.10	0.10	-
Shelter Belts	-	-	0.3	0.3
Orchards	May be seasonally dependent	0.5-1.0	-	-
Forests		1.0-6.0	0.8	0.5
Suburban Areas / Small Towns	Low housing, trees, etc	0.10-2.0	0.5	0.8
City Centers	Buildings 10-50m high	1-10	1.0	1

The logarithmic law is used to extrapolate data from one height to another at a location where the roughness length is known. For instance, a wind speed recorded at a height of 10m over an open runway (such as at SeaTac airport) can be extrapolated to the wind

speed at 50m above the runway by assuming the roughness length is $z_o = 0.01$ and applying the logarithmic law.

1.4.2 Topographical Speed-up

Wind speed changes when flowing over hills or valleys. The change in wind speed at the crest or trough due to flow over slopes of height h is represented by ΔU_T. If the slope is positive, such as for a hill, ΔU_T is positive, and conversely for a negative slope, such as for a valley, ΔU_T is negative.

$$\Delta U_T = \Delta S * U_0(\Delta z_p), \text{ for } \Delta z_p < \delta_1$$

$$\text{Where: } \Delta S = \Delta S_{\max} \exp\left(\frac{-A\Delta z}{L}\right),$$

$$\Delta S_{\max} = \frac{Bh}{L},$$

$U_0(\Delta z_p)$ = the upstream wind speed at height Δz_p above the surface,

h = the height of the slope

L = the length from the peak of the slope P to the point where the slope is ½*h

δ_1 = the internal boundary layer depth

A,B are defined in Table 4. For simplicity, 2D ridges were assumed for all locations in this study.

Table 4. Topography Coefficients [17]

Terrain Type	**A**	**B**
2D hills (ridges)	3.0	2.0
3D hills	4.0	1.6
2D escarpments	2.5	0.8
2D rolling terrain	3.5	1.55
3D rolling terrain	4.4	1.1
Flat terrain	0.0	0.0

The internal boundary layer is the layer of air that is affected by the change in surface roughness. The layer depth is zero at the point of surface roughness change and increases downstream. It is defined as δ_1, and is described in the following equations [17]:

$$r' = a\left[\delta'\left(\ln\delta' - 1\right) + 1\right]$$

Where: $r' = \frac{r}{z_o}$, $\delta' = \frac{\delta_1}{z_o}$, and $a = 2$.

z_o = the roughness length at the point P

r = the distance from the point P to the beginning of roughness length z_0

This equation is solved iteratively using Newton's method with an initial guess of δ_1 to be:

$$\frac{\delta_1}{z_0} = 0.75\left(\frac{r}{z_0}\right)^{0.8}$$

Newton's method for finding the internal boundary layer thickness is described by the following equation:

$$\delta_{1,i+1} = \delta_{1,i} - \frac{f(\delta_{1,i})}{f'(\delta_{1,i})}$$

Where: $f(\delta_{1,i}) = a\left(\delta'\left(\ln\delta' - 1\right) + 1\right) - r'$,

$f'(\delta_{1,i}) = a * \ln\delta'$

The method is iterated until the incremental change in boundary layer thickness is less than 5m.

The topographical speed-up is used to determine the increase in wind speed as air flows up a ridge. The Maury Island turbine sites are located at the crest of the ridgeline near

the south and south-eastern coast of the island. As wind flows over the ridge to the turbine sites, it will accelerate, resulting in a higher wind speed. The topographical speed-up equations allow this increase in wind speed to be calculated.

1.4.3 Surface Roughness Changes

The wind speed change due to the roughness length change from the upstream reference location to the site of interest at point *P*, is defined by the equation:

$$\Delta U_R = \left[\left(\frac{\ln\left(\Delta z_p / z_o\right)}{\ln\left(\delta_1 / z_o\right)} \right) \left(\frac{\ln\left(\delta_1 / z_{ou}\right)}{\ln\left(\Delta z_p / z_{ou}\right)} \right) - 1 \right] U_o\left(\Delta z_p\right)$$

Where: z_{ou} = the roughness length of the upstream reference location

Changes from a smooth surface such as water or ice to a rough surface such as tall grass or woodlands will cause ΔU_R to be negative. A change from a rough surface coverage to a smooth surface coverage will cause ΔU_R to be positive. For example, the surface roughness change equations allows calculation of the wind speed increase for wind traveling from the suburbs of Tacoma, across the waters of the Puget Sound to the coastline of Maury Island.

1.4.4 Surface Layer Similarity Laws

The Guidelines have the limitation that the wind resource reference site is in the ideal location: upstream of the site of interest at point *P* (refer to Figure 10). Since this is not the case for the anemometer locations and the proposed Maury Island turbine sites, an additional wind change calculation must be used. A procedure was developed using the "Resistance Laws" for a neutrally-stratified planetary boundary-layer. This procedure assumes the geostrophic wind, U_g, is constant for both the anemometer site, *R*, and the

upwind site, U. The proximity of the anemometer locations and Maury Island proposed turbine sites make this assumption valid. This also assumes an equilibrium relationship between the surface friction velocities for the two sites, u_*, and is defined by [5]:

$$U_g = \frac{u_*}{\kappa}\left[\left(\ln\left(\frac{u_*}{fz_o}\right) - A\right)^2 + B^2\right]^{1/2}$$

Where: A = 1.8,

$B = 4.5$,

$f = 2\Omega\sin(\phi)$, where f is the Coriolis parameter and

Ω = 7.27e-5 rad/s, the Earth's angular velocity

ϕ = 47.45º, the Latitude of Vashon Island

The Resistance Law equation is used to compute U_g assuming a logarithmic surface layer profile at the reference site with friction velocity u_{*r} and surface roughness z_{or}. Next, U_g is used to determine u_{*u} corresponding to the surface roughness upstream of the site of interest, z_{ou}. This is again done through the use of Newton's method:

$$u_{*u,i+1} = u_{*u,i} - \frac{f(u_{*u,i})}{f'(u_{*u,i})}$$

Where: $f(u_{*u,i}) = \frac{u_{*u,i}}{\kappa}\left(\left(\ln\left(\frac{u_{*u,i}}{fz_o}\right) - A\right)^2 + B^2\right)^{1/2} - U_g$

$$f'(u_{*u,i}) = \frac{1}{\kappa}\left(\left(\ln\left(\frac{u_{*u,i}}{fz_o}\right) - A\right)^2 + B^2\right)^{1/2} + \frac{\ln\left(\frac{u_{*u,i}}{fz_o}\right) - A}{\kappa fz_o\left(\left(\ln\left(\frac{u_{*u,i}}{fz_o}\right) - A\right)^2 + B^2\right)^{1/2}}$$

From this, the upstream velocity U_o can be computed assuming a logarithmic profile for any height, Δz_p. For example, the surface layer similarity laws allow a wind speed measured by the Beall anemometer to determine the geostrophic wind speed over the Puget Sound. With the geostrophic wind speed known, the surface layer similarity laws can be applied again to determine the wind speed at a location upstream of the turbine sites for any height. However, the surface layer similarity laws can only be utilized when a logarithmic profile can be assumed to exist. This concept is discussed in the following sub-section.

1.4.5 Definition of the Upstream Velocity Profile

To determine a geostrophic wind speed, a fully developed surface boundary layer must be assumed at an upstream position. This means that at the upstream position there is a consistent surface roughness for an adequate distance to assume that the change from the previous roughness length, ΔU_R, has gone to zero. For moderate wind speeds, changes in roughness length can affect the flow 1-2 km downstream of the line of change, and for lower wind speeds, this length can be up to 10km [14]. In initial attempts at characterizing the wind regime, it was assumed that the distance of the water between the land surrounding Puget Sound and Maury Island was large enough to assume a fully developed surface boundary layer over the water. However, subsequent investigations revealed this to not be the case; this assumption produced wind speeds that were far beyond those expected and recorded at the island.

The upwind position with a fully developed surface boundary layer is assumed to be over the land surrounding the Puget Sound. The land of the Puget Sound is assumed to have a universal surface roughness length characteristic of a suburban area. A fully developed surface boundary layer is assumed over the land based on this surface roughness length. This means that as the wind is coming from each directional sector it has an unchanging velocity right before it reaches the water of the Puget Sound. It then experiences an increase in velocity ΔU_R due to the change in surface roughness from land to water. The increase in velocity ΔU_R changes as it travels across the water to the coastline of Maury Island. The red cross-hatched area in Figure 11 shows where the constant surface roughness length and upwind velocity are assumed. When the wind reaches the blue line of the water around Vashon/Maury Island, the wind begins its acceleration.

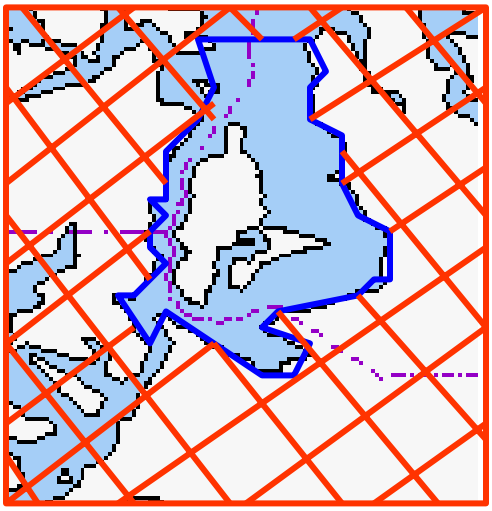

Figure 11. Upstream Velocity Area of Puget Sound

The determination of the constant upstream velocity profile is a key step in the analysis. It acts as the "clean slate" for the analysis; all topographic and surface coverage features downstream act on this clean state.

1.5 Application of the Guidelines from the Data Collection Sites to the Turbine Site Locations

Application of the Guidelines from the anemometer location (either SeaTac Airport or the Beall Site) to the turbine sites on Maury Island requires a topographic and surface coverage description of areas surrounding the two locations. The following sections provide these descriptions. Also included in this section is a summary of the methodology for calculating the final wind velocity at the turbine sites.

1.5.1 SeaTac Site Characterization and Upstream Profile Definition

The SeaTac airport anemometer location is surrounded by different surface covers which must be considered before applying the logarithmic law to the data. As can be seen from Figure 4, the runways surround the anemometer tower in all directions, but at different lengths in each direction. Beyond the runways are suburbs and trees where the upstream velocity profile is assumed to hold true. The wind will tend to speed up as it crosses the smooth surface of the runway and registers on the anemometer. The wind speeds that the anemometer records are therefore higher than the upstream wind speeds. This "speed-up" needs to be subtracted from the recorded speeds to identify the true wind speed upstream.

The calculation applied to the SeaTac data is essentially the reverse of that described in Section 1.4.3 (the wind speed change due to roughness change section). The known wind velocity from a sector recorded by the anemometer is assumed to incorporate the wind speed change due to the roughness change caused by the runways.

$$U_{SeaTac} = U_o\left(\Delta z_p\right) + \Delta U_R = U_o\left(\Delta z_p\right) + U_o\left(\Delta z_p\right)\left[\left(\frac{\ln\left(\Delta z_p / z_o\right)}{\ln\left(\delta_1 / z_o\right)}\right)\left(\frac{\ln\left(\delta_1 / z_{ou}\right)}{\ln\left(\Delta z_p / z_{ou}\right)}\right) - 1\right]$$

Where: U_{SeaTac} = the SeaTac recorded velocity data

Δz_p = 10, the height of the anemometer

δ_1 = the internal boundary layer depth

z_o = the roughness length of the airport, Table 5

z_{ou} = the upstream roughness length of the surrounding land

The roughness lengths assumed for each sector at the airport site and the distance to the change in surface roughness (the edges of the runway) are listed in Table 5.

Table 5. SeaTac Anemometer Site Characterization

Direction [degrees]	**Distance of Runway, r [m]**	**Roughness Length, z_o [m]**
355 to 25	2200	.01
25 to 55	1500	.01
55 to 85	800	.01
85 to 115	700	.01
115 to 145	1100	.01
145 to 175	1500	.01
175 to 205	1100	.03
205 to 235	300	.03
235 to 265	200	.03
265 to 295	200	.01
295 to 325	200	.01
325 to 355	300	.01

Solving for the upwind velocity (the raw velocity minus the speed-up effect) yields:

$$U_o(\Delta z_p) = \frac{U_{SeaTac}}{1 + \left[\left(\frac{\ln\left(\Delta z_p / z_o \right)}{\ln\left(\delta_1 / z_o \right)} \right) \left(\frac{\ln\left(\delta_1 / z_{ou} \right)}{\ln\left(\Delta z_p / z_{ou} \right)} \right) - 1 \right]}$$

The upwind velocity is calculated for each bucket in the Weibull distribution for each sector. An example of the upstream velocity compared with the raw velocity for each velocity bucket is shown for the 205-235º directional sector in Figure 12.

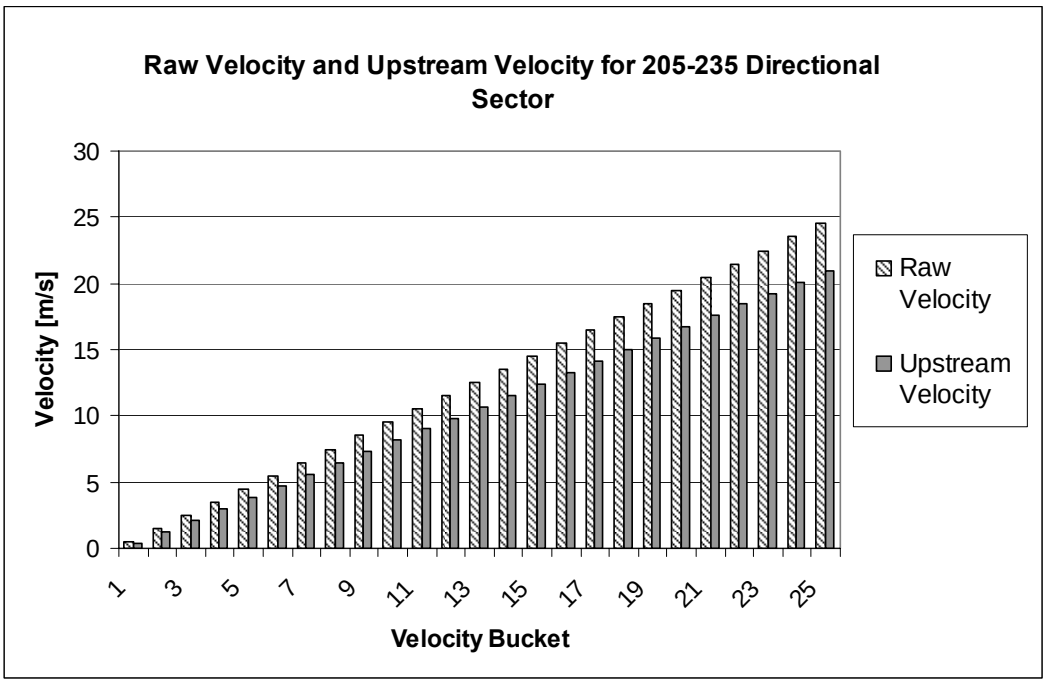

Figure 12. An Example of Upstream Velocity Compared to Raw Velocity at SeaTac at 10m.

In summary, the upstream velocities at 10m are determined from the SeaTac anemometer data by using the surface roughness change equations. With the upstream velocities known at 10m and an assumed roughness length for the upstream position, the upstream velocities are calculated for any height using the logarithmic law.

1.5.2 Calculating the Roughness Length of the Beall Anemometer Site

The Beall anemometer has three heights at which it samples data: 26.5, 35.2, and 49 meters. The empirical wind shear exponent for the Beall anemometer location in each directional sector can be calculated by using the simple power law below [19] and the wind speed data from anemometers mounted at 26.5m and 49m. The shear exponent is

averaged for each data point in each directional sector. This analysis is performed using data that is 3m/s or greater since below this speed buoyancy effects take over.

$$U(\Delta z) = U(\Delta z_r)\left(\frac{\Delta z}{\Delta z_r}\right)^{\alpha}$$

Where: α = empirical wind shear exponent

The results of the curve fitting for the wind shear exponent are in Table 6. Also included in the table are the roughness lengths that have the best correlation with the average data at each height of the anemometer (26.5, 35.2 and 49 meters). The roughness lengths are calculated according to a sum of least squares between the natural log of the height and the wind velocity. The roughness length is the y-intercept of this linear regression.

Table 6. Roughness Length and Shear Exponents for Beall Site

Direction	α	z_0
355-25	0.40	1.7
25-55	0.37	2.3
55-85	0.30	1.1
85-115	0.28	0.6
115-145	†	†
145-175	0.65	7.4
175-205	0.50	4.6
205-235	0.34	1.7
235-265	0.32	1.4
265-295	0.33	1.7
295-325	***	***
325-355	0.47	4

† Notes that the data does not fit the power law profile

*** Notes that there is insufficient data.

These results show an unusually large logarithmic rise in velocity with height at the Beall anemometer. With the large amount of fields, buildings and trees surrounding the Beall

anemometer location, it is likely that the roughness length would be between z_o = 0.3 and z_o = 0.8 [4]. A comparison of roughness lengths and associated velocity shear profiles for a 5m/s wind speed at 50m is shown in Figure 13, including:

- the roughness length of the predominant sector at Beall, z_o = 1.7,
- an extreme roughness length at Beall, z_o = 4,
- a roughness length that would be expected at the Beall site, z_o = 0.5 (for small towns, suburbs, orchards),
- and the roughness length for farmland z_o = 0.1 (typical to most wind farms).

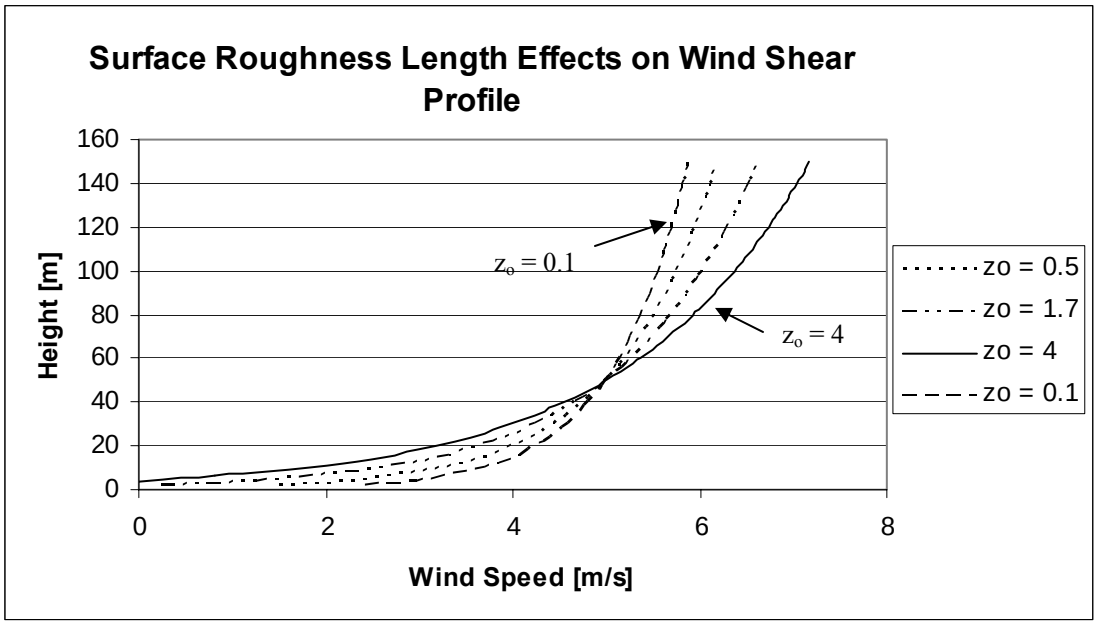

Figure 13. A Comparison of Surface Roughness Lengths

The calculated roughness lengths at the Beall site are much higher than would be expected for the site. According to Table 3, the surface roughness at Beall is more characteristic of city centers or tall forests. It is hard to explain such high roughness lengths since the land around the anemometer is relatively flat and the surface coverage is similar to a suburban area (fields, trees, and small buildings). Sheltering effects from trees and the local buildings likely influence the anemometer measurements at the lowest

height (26.5m), but these effects would be limited since they are not that tall (<25m) and not that close to the anemometer (>50m). This phenomenon decreases confidence that the wind speeds measured by the Beall anemometer represent the true wind speeds. Assumed roughness lengths of z_o = 0.5-2.0 are used in the subsequent analyses instead of the suspect results shown in Table 6.

The geostrophic wind speed can be calculated from data collected at the Beall anemometer site with an additional assumption: the surface boundary layer at the Beall anemometer is fully developed. This assumption is valid since the surface coverage of the island within a few kilometer radius is roughly the same, and the effects of topography and surface coverage changes from the edge of the island would likely dissipate before reaching the anemometer tower. Using the surface layer similarity laws, the geostrophic wind speed is determined. Finally, the upstream velocities for the land surrounding the Puget Sound are calculated at any height using the logarithmic law and the geostrophic wind speed.

1.5.3 Maury Site Descriptions

The ten proposed turbine sites on the Southern and Eastern shores of Maury Island, as shown in Figure 14, are chosen for a number of reasons. Since the turbine sites mostly face the water of the Puget Sound in the predominant south and southwestern direction, there will likely be good speed up factors and little turbulence from this direction at the sites. There will also be good speed-up factors due to the high ridgeline along the coasts. The sites were reviewed for bird migratory routes, homes and businesses, and soil conditions, and were found to be satisfactory in these regards [57]. The close proximity to the substation on the eastern tip of Maury Island is also a positive attribute of these sites.

To apply the Guidelines for wind speed variation, the roughness lengths and topographical features must be described for the proposed turbine sites on Maury Island.

Each of the proposed turbine sites along the Maury Island ridge line have distinct characteristics in terms of:

(1) direction to the ridgeline,
(2) the height of the ridgeline (h),
(3) the length from the peak of the ridge (or hill) to half the height of the ridge (L),
(4) and the distance from the site to the change in roughness length (r).

Each site was measured by 30º sectors using a USGS topographical map with a scale of 1:30,750. The characteristics for each sector for each turbine site are described in Appendix B. Maury Island is largely covered by forests with trees approximately 15 - 20m in height. A roughness length of $z_o = 0.8$ is originally assumed for each turbine site due to the forest coverage of the island [4].

The characteristics of each turbine site are plugged into the topographical speed up and surface roughness change equations discussed in Section 1.4 and written in a Matlab file. The changes to the upstream velocity due to roughness change and topography for each sector at each turbine site are then calculated in Matlab.

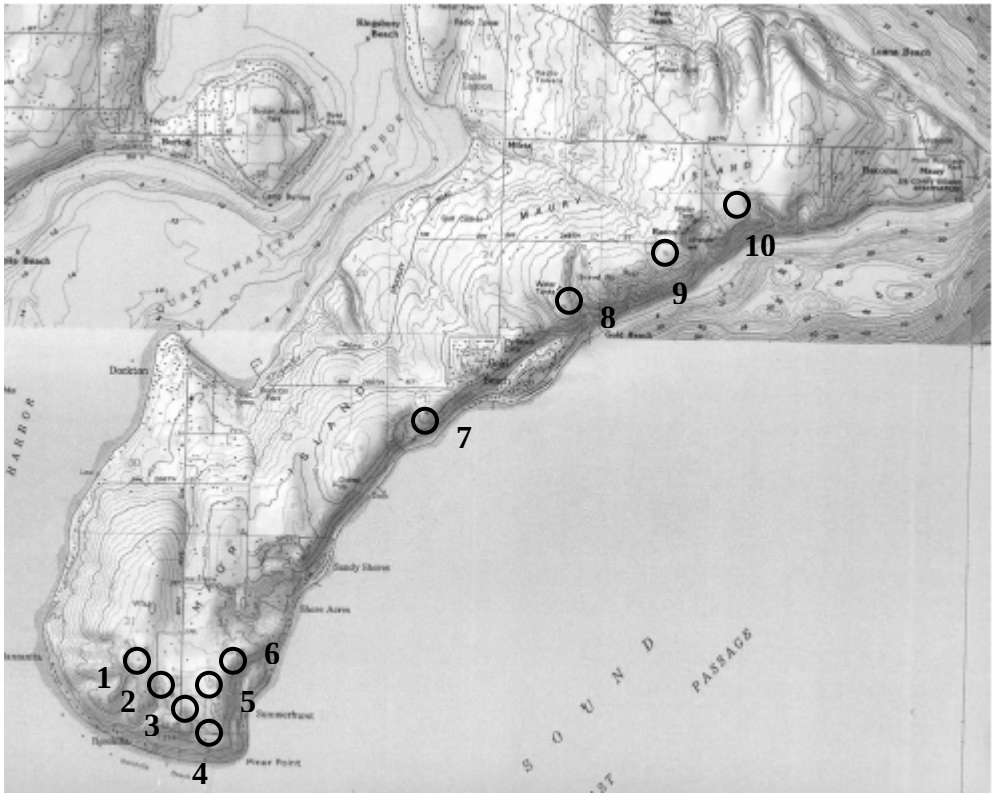

Figure 14. Wind Turbine Site Locations on Maury Island [8]

1.5.4 Application of Velocity Changes

With the upstream velocity profile and the turbine site speed-up effects defined, the final velocity at the turbine sites can be calculated. This calculation is performed for each wind speed bucket in every directional sector for all the wind turbine sites. The change in velocity is applied to each initial velocity bucket with an average velocity greater than 3m/s with the following formula:

$$U'_{i,j,k} = U_{i,j,k} + \Delta U_{T,i,j,k} + \Delta U_{R,i,j,k}$$

Where: i = the turbine site

j = the directional sector

k = the wind speed bucket

$U_{i,j,k}$ = the upstream wind velocity of the bucket

$U'_{i,j,k}$ = the projected wind speed at the turbine site for the bucket

$\Delta U_{T,i,j,k}$ = the topographical speed-up

$\Delta U_{R,i,j,k}$ = the wind speed change due to surface roughness change

The total formula above is applied only to velocities above 3m/s because of the limitations of the Guidelines. The contribution of velocities under 3m/s (buckets 1, 2, and 3) to the turbine power is nil.

The final outcome of this analysis, $U'_{i,j,k}$, is a matrix of the projected wind speeds at the Maury Island turbine sites according to each original velocity bucket. For example, the velocity bucket 7 representing an average wind speed of 6.5m/s at the SeaTac anemometer from the directional sector 115-145º may correlate to a 7.8m/s velocity at Turbine Site 8. If the frequency the wind blows at 6.5m/s from directional sector 115-145 º is 1% of the time, then the Turbine Site 8 will see a 7.8m/s velocity from directional sector 115-145 º for 1% of the time. An example of the distribution of projected wind speeds (for Turbine Site 8) versus the wind speed distribution measured at SeaTac is shown in Figure 15. A significant drop between Bucket 3 and Bucket 4 exists because the Guidelines for this example are only applied to wind speeds greater than 3m/s. Below this wind speed, the speed-up effects can't reliably be predicted by the Guidelines, and the buckets remain unaffected. With the projected wind speeds at each turbine site, the annual energy yield from the wind turbines can be calculated.

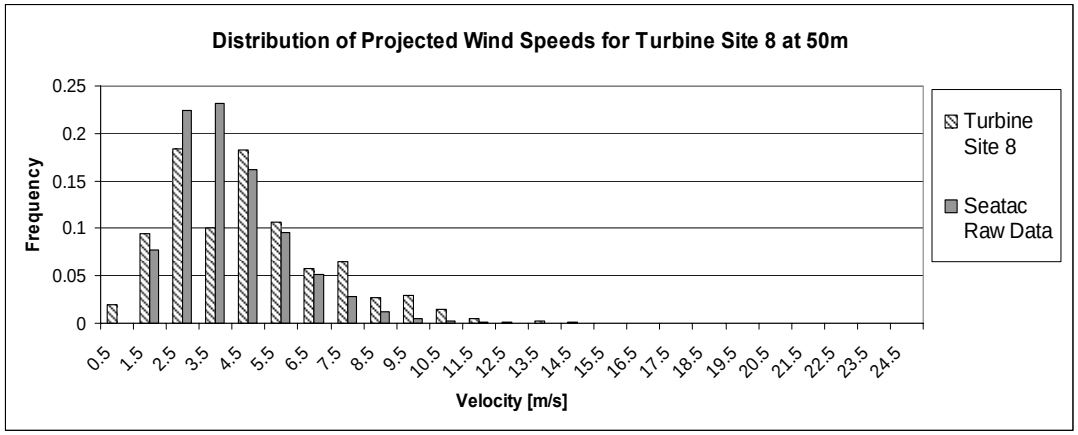

Figure 15. Example of Projected Wind Speed Distribution at Turbine Site 8 at 50m

1.6 Annual Energy Yield

The annual energy yield is the final product of the wind resource assessment and prediction model. The calculation of the annual energy yield begins with the calculation of the average turbine power. The power produced by a wind turbine at each site is a function of the wind speed, which means the power must be calculated for each wind speed bucket and sector at each site:

$$P_{i,j,k} = \eta_t \eta_g \eta_{pe} \frac{1}{2} \pi \rho_a C_p U'^{3}_{i,j,k} \frac{D^2}{4}$$

Where: i = the turbine site

j = the directional sector

k = wind speed bucket

$P_{i,j,k}$ = power for the wind speed bucket

η_t = the gearbox efficiency

η_g = the generator efficiency

η_{pe} = the power electronic efficiency

ρ_a = 1.225 kg/m^3, the density of air

C_p = 0.50, the aerodynamic rotor power coefficient

$U'_{i,j,k}$ = the changed wind speed for the bucket

D = the diameter of the turbine rotor

The aerodynamic rotor power coefficient is held constant for all wind speeds because the turbine is assumed to be variable speed. Variable speed wind turbines are able to operate at the maximum aerodynamic rotor power coefficient for all wind speeds since their rotational speed isn't determined by the electrical grid frequency. According to the European Wind Energy Association, state-of-the-art turbines have aerodynamic rotor power coefficients of C_p = 0.50 [4]

The annual energy yield is in terms of total kilowatt-hours (kWh) of energy production per turbine per annum. A summation over wind speed buckets and sectors of each power, $P_{i,j,k}$, multiplied by the frequency of the wind speed bucket, $fb_{i,j,k}$, and the frequency for the sector, fs_j, gives an average power output for the turbine. Multiplying the average power output of the turbine by 8760 hours in a year gives the annual energy yield in units of kWh. The annual energy yield equation for the i^{th} turbine is:

$$E_i = 8760 * \sum_{j=1}^{12} \sum_{k=1}^{25} P_{i,j,k} * fs_j * fb_{i,j,k}$$

Where: E_i = the annual energy for turbine i

$P_{i,j,k}$ = the power for the wind speed bucket

fs_j = the frequency of the sector

$fb_{i,j,k}$ = the frequency of the wind speed bucket

The generator and power electronic efficiencies tend to be functions of the percentage of rated power, but the gearbox efficiency stays roughly constant. The efficiencies used in the annual energy production models are shown in Figure 16.

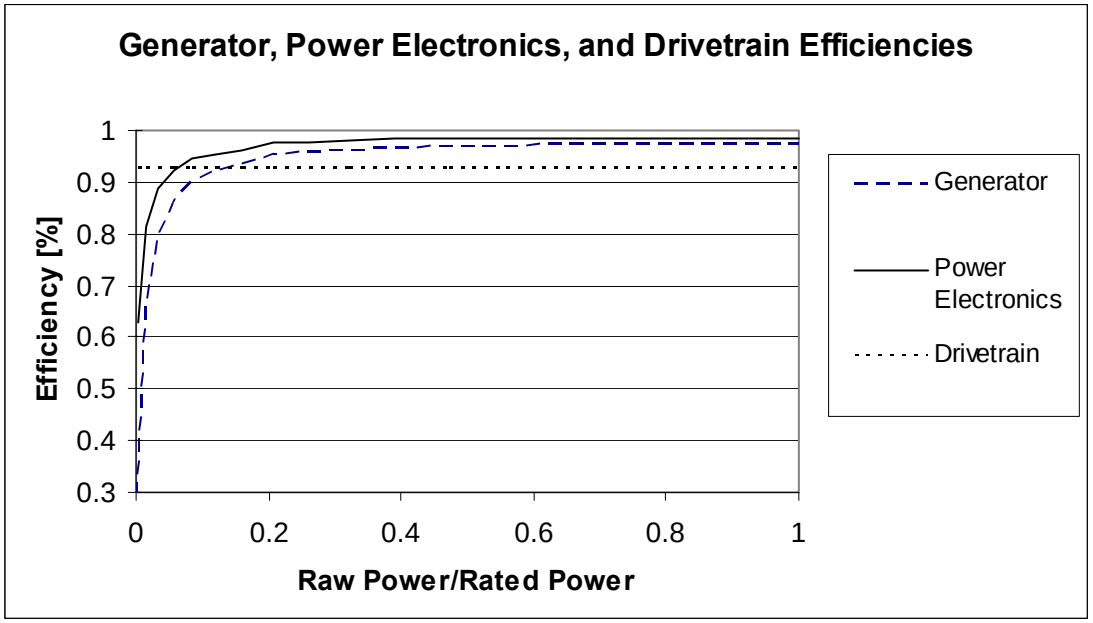

Figure 16. Generator, Power Electronics, and Drivetrain Efficiencies [30]

In addition to the power calculations mentioned to this point, there exist restrictions on the cut-in wind speed of the turbine and the maximum power output of the generator. The cut-in wind speed of a turbine is the wind speed at which the turbine will begin to produce energy. The range for typical turbines is between 3 and 5m/s. The lower cut-in wind speeds are for turbines designed to operate in lower wind speed regimes. The model assumes a cut-in speed of 3m/s.

The generator and power electronics limit the power output of the wind turbine. Wind turbines usually produce rated load far before their cut-out speed. The cut-out speed is the speed at which the turbine will cease producing electricity and adjust to a feathered or safe position. This is required so that large overturn moments caused by drag on the rotor do not drive up the design costs of the turbine. The cut-out speed for commercial wind turbines is typically between 20 and 25m/s. For this study, a cut-out speed of 25m/s is assumed. Once the rated wind speed (the lowest wind speed at which the turbine produces rated power) is reached, at say 10-15m/s, the generator does not produce more power even if the wind speed increases. Therefore, in the annual energy production

model, if the power for a particular wind speed bucket theoretically predicts a power higher than the rated power, the rated power is assumed.

1.6.1 Additional Losses

In addition to the above described efficiency losses, energy losses can occur due to availability of the turbines, blade soiling losses, array losses and electrical losses. These losses reduce the annual energy yield calculated in the model.

The availability of a wind turbine is the percentage of time that the turbine is available to produce electricity. A turbine is unavailable when a failure occurs or when maintenance is taking place. The availability of current production wind turbines is targeted at 97.5% [4]. The WindPACT study [32] took a more conservative approach to availability and assigned a value of 95%, which is adopted here.

- Availability 95%

Dirt build-up on the turbine blades cause a decrease in efficiency called blade soiling losses. The WindPACT studies [30,32] assume this decrease in efficiency is equal to about 2% over the lifetime of the turbine.

- Blade soiling losses 2%

Aerodynamic interference from one wind turbine to another can occur when the turbines are within 20 rotor diameters from one another and the wind is coming from such a direction that the wake from one turbine influences the other [19]. This interference is termed array loss. Array losses can have significant impacts on the energy yield of turbines depending on the turbine spacing, the frequency distribution of wind directions, the number of turbines, the turbine characteristics and the turbulent intensity of the wind. The array losses are greater for a larger number of turbines in the wind farm, for

increases in the turbine rotor diameters, and for decreases in distances between turbines. The greater the turbulent intensity of the wind, the quicker the wake generated by the turbine will be diffused into the ambient resulting in a smaller array loss. The turbine sites at the southern tip of Maury Island are few and they are at a minimum 200m apart. Coupled with the relatively high turbulent intensities from the vegetation coverage of the island, array losses can be expected to be minimal. The value for array losses assumed here is 5% [19,30,32].

- Array losses 5%

The conductor line losses are calculated using a collector system described in Chapter 2 of this study. The line losses at the maximum operating output power for all turbines is less than 1.5%. Since the line losses are related to the square of the current output, the losses are much smaller when the turbines are not operating at capacity. The wind farm is not likely to operate close to maximum power often, so the electrical line losses are negligible and ignored in energy yield calculations.

1.7 Sensitivities of the Model and Envelope Definition

Many assumptions for the wind speed prediction model have been discussed previously such as the roughness lengths for the anemometer and turbine sites. Assumptions are necessary in wind resource assessments when long term wind data for the exact site of a turbine is not available. This section discusses the sensitivity of the wind speed model to these assumptions, but first, limitations of the Guidelines requiring additional assumptions are presented.

The Guidelines assume that conditions of neutral thermal stability exist, and should work fairly well for near-neutral and unstable conditions [14]. The stability of the atmosphere is its tendency to allow or restrict vertical motion. In unstable conditions vertical motion is enhanced, and turbulent mixing in the surface boundary layer allows vertical

momentum transfer. In stable conditions, vertical flow is inhibited and thermal stratification occurs, giving rise to high wind shear values. For conditions of moderate or strong stable stratification, the Guidelines may give erroneous results. For strong stable stratification, speed-up factors are reduced. Predicted departures from neutral thermal stability are offered by Taylor and Lee [14], but are not considered in this study because of the necessary characterization of surface heat fluxes for numerous sites. Taylor and Lee [14] note that the Guidelines are most appropriate for speeds greater than 6m/s where aerodynamic effects will dominate the flow and should not be used for velocities less than 3m/s where thermal effects are likely to dominate.

In addition to the above assumptions, the Guidelines have restrictions on the slope of terrain that can be analyzed without separation occurring and the speed-up factor departing from the suggested values. Walmsley, Taylor and Salmon [19] put this slope limit at 0.6, and suggest adjusting slopes greater than 0.6 down to 0.6. This slope adjustment is adopted here. Woods [18] found analytically that the lower bound for separation to occur is at a slope greater than 0.31 depending on factors such as the surface roughness, the length of the slope and the height of the slope.

An investigation into the sensitivity of the annual energy production model to certain assumed parameters is documented in Appendix C. The parameters investigated are:

- Water Roughness Length: the surface roughness of the water surrounding the island
- Maury Island Roughness Length: the roughness length of the surface coverage at the Maury Island turbine sites
- Beall Roughness Length: the roughness length of the surface coverage at the Beall site
- Critical Slope: the slope at which separation of airflow over the surface occurs
- Applicable Velocities: the lower limit of velocities to which the Guidelines are applicable (i.e. the velocity at which speed-up effects are applied)

- Puget Sound Roughness Length: the roughness length of the land surrounding the Puget Sound or the "upstream location"

Values are assumed for these variables which provide the lowest and highest velocities likely at the turbine sites. The result is an envelope definition that encompasses the combined effects of the assumptions leading to the lowest and highest realistic annual energy production values. This sensitivity investigation shows the large inherent capacity for error in predicting wind velocities using the Guidelines applied in this study. The assumptions listed in Table 7 are considered to provide the minimum and maximum total annual energy productions.

Table 7. Envelope Assumptions

Assumed Parameter	Minimum Envelope Assumptions	Maximum Envelope Assumptions
Upstream Water Roughness Length, z_{ou}	0.001	0.0001
Maury Island Roughness Length, z_{op}	0.8	0.6
Beall Roughness Length, z_{or}	0.5	1.0
Critical Slope, θ_c	0.31	0.6
Applicable Velocities, $U(\Delta z_r)$	> 5m/s	> 3m/s
Puget Sound Roughness Length, z_{ps}	0.4	0.7

Some parameters are larger for the minimum envelope and some are larger for the maximum envelope. At first glance this may appear contradictory; however, the effects of the parameters are site dependent. Larger roughness lengths at the data measurement sites (Beall and Puget Sound roughness lengths) correlate to higher geostrophic wind speeds and higher wind speeds at the turbine sites. On the other hand, larger roughness lengths at the turbine sites (Maury Island and Upstream Water roughness lengths) correlate to lower wind speeds at the turbine sites (for the same height).

1.8 Results

The simplest result of the wind regime at Maury Island is the average wind speed. The average speeds for the ten turbine sites are shown in Table 8. These average speeds are fairly low, but are consistent with the average wind speeds found by Northwest Wind Mapping Project [1].

Table 8. Wind Speeds at Maury Island for Minimum and Maximum EnvelopesBased on SeaTac and Beall Reference Data.

Height [m]	SeaTac Data		Beall Data	
	Minimum [m/s]	Maximum [m/s]	Minimum [m/s]	Maximum [m/s]
50	4.85	5.66	3.50	4.17
60	5.01	5.77	3.62	4.26
70	5.14	5.84	3.71	4.33
80	5.24	5.90	3.79	4.38
90	5.33	5.95	3.85	4.43
100	5.41	5.99	3.91	4.46

The velocity shear profile gives a very good visual picture of the wind speeds at the Maury Island turbine sites. The average velocity shear profiles for the ten turbine sites are shown in Figure 17 and Figure 18 for the Beall data and SeaTac data respectively.

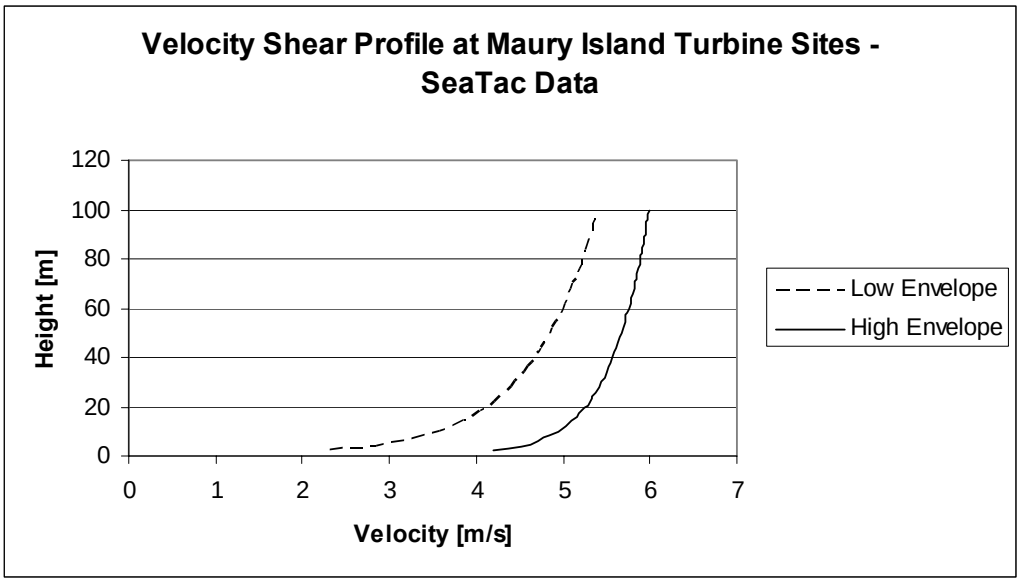

Figure 17. Average Velocity Shear Profile at Maury Island Turbine Sites – SeaTac Data

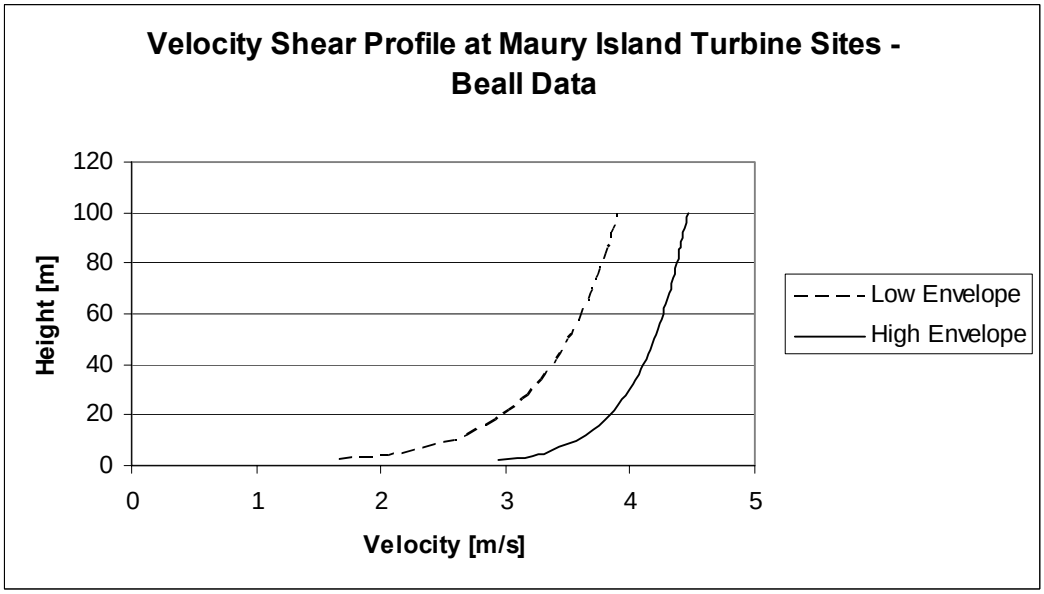

Figure 18. Average Velocity Shear Profile at Maury Island Turbine Sites – Beall Data

The projected distribution of wind velocities averaged for the 10 turbine sites are shown in Figures 19 – 22. The application of speed-up factors skews the original Weibull shape of the wind speed distribution. All the distributions have a larger frequency of higher

velocities due to the speed-up factors, which results in the distribution having a long "tail." Fitting a Weibull distribution to the projected distribution shows that the Weibull shape parameter, k, for the distributions is much lower than the measured distributions at SeaTac. This is caused by the long tail in the actual wind speed distributions. The Weibull shape parameters for the individual turbine sites range from k=1.56 to 1.9 and k=1.49 to 1.68 for the Beall low and high envelopes respectively, and k=1.46 to 1.74 and k=1.53 to 1.89 for the SeaTac low and high envelopes.

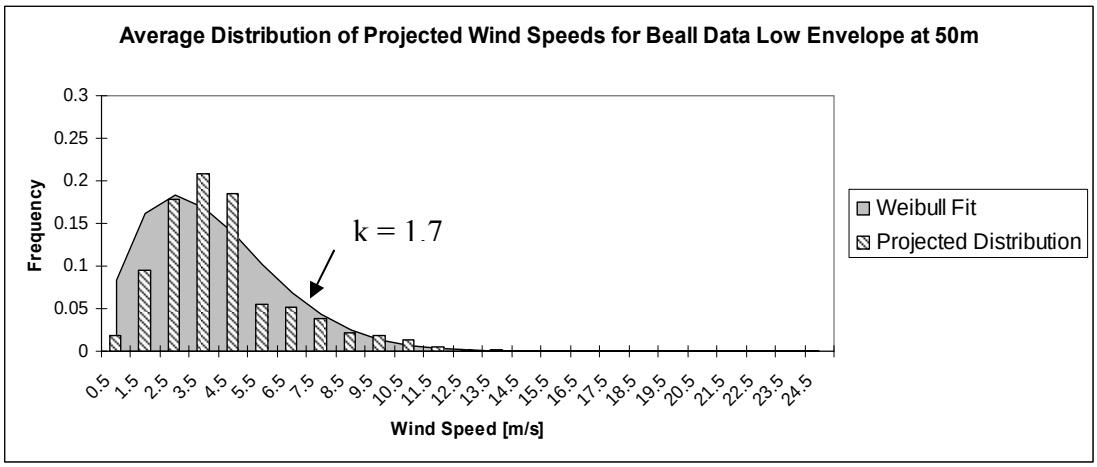

Figure 19. Average Distribution of Projected Wind Speeds, Beall Data Low Envelope at 50m

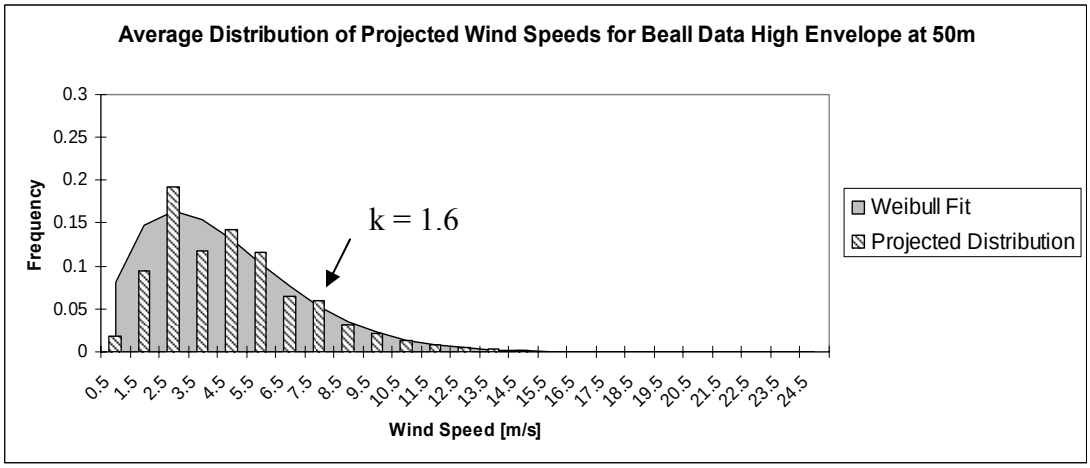

Figure 20. Average Distribution of Projected Wind Speeds, Beall Data High Envelope at 50m

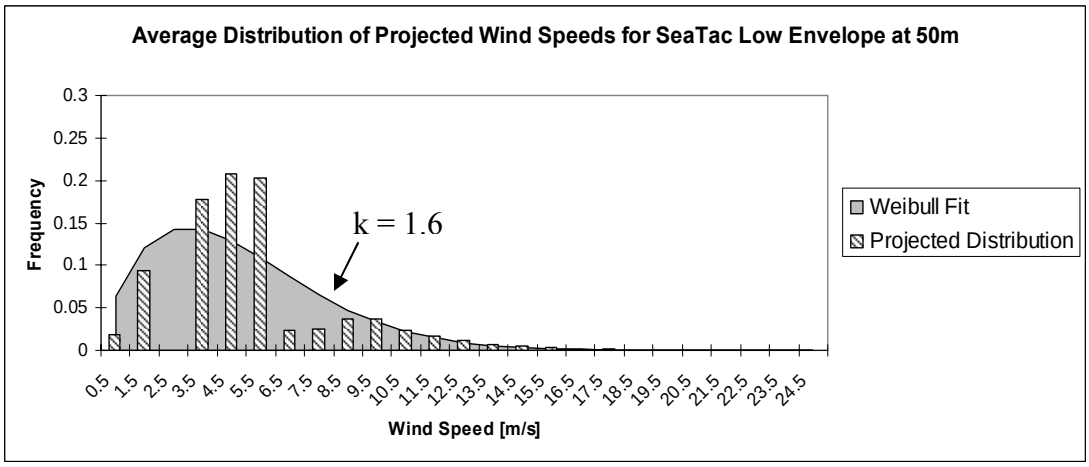

Figure 21. Average Distribution of Projected Wind Speeds, SeaTac Data Low Envelope at 50m

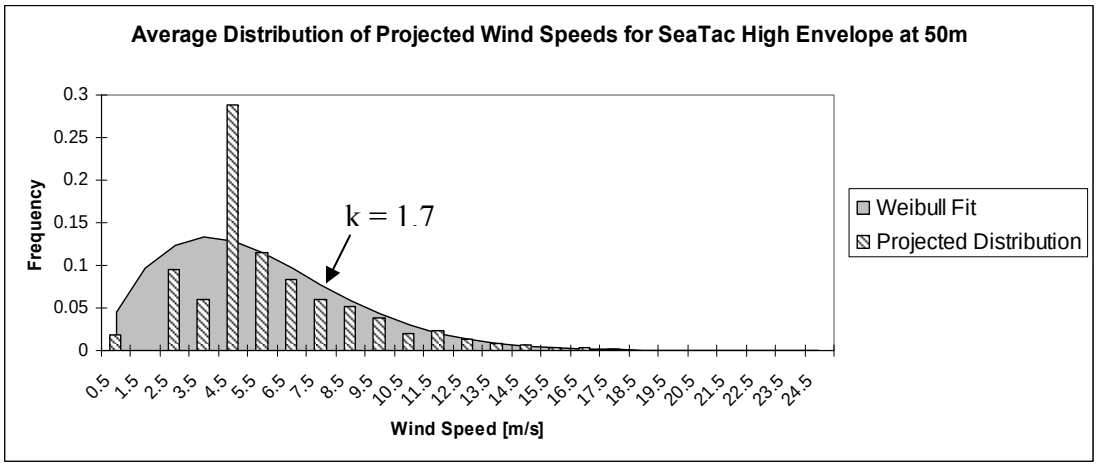

Figure 22. Average Distribution of Projected Wind Speeds, SeaTac Data High Envelope at 50m

Some gaps exist in the distribution at very low velocities where the velocity buckets were shifted up from the original distribution into the next higher bucket. The shift is caused by the increase in velocity with height between the measured height, 10m, and the height in the figures, 50m. The sharp decreases between Bucket 3 to Bucket 4 for the high envelopes and Bucket 6 to Bucket 7 in the low envelopes exist because the speed-up effects of the Guidelines are applied only to wind speeds greater than 3m/s and 6m/s for the high and low envelopes respectively.

1.8.1 Average Velocity by Sector and Turbine Site

The aggregate data for the ten turbine sites are discussed in the previous section, but there are more interesting results available if the average velocities are analyzed site by site and sector by sector. The average velocities for each sector and turbine site are shown in Figure 23 through Figure 26. They vary substantially. The two southwestern sectors from 175 - 235º have the highest velocities. The reason for this is twofold: these sectors have the largest measured velocities (from the anemometer data), and the speed-up effects from the ridgeline and smooth water surface are greatest in this direction.

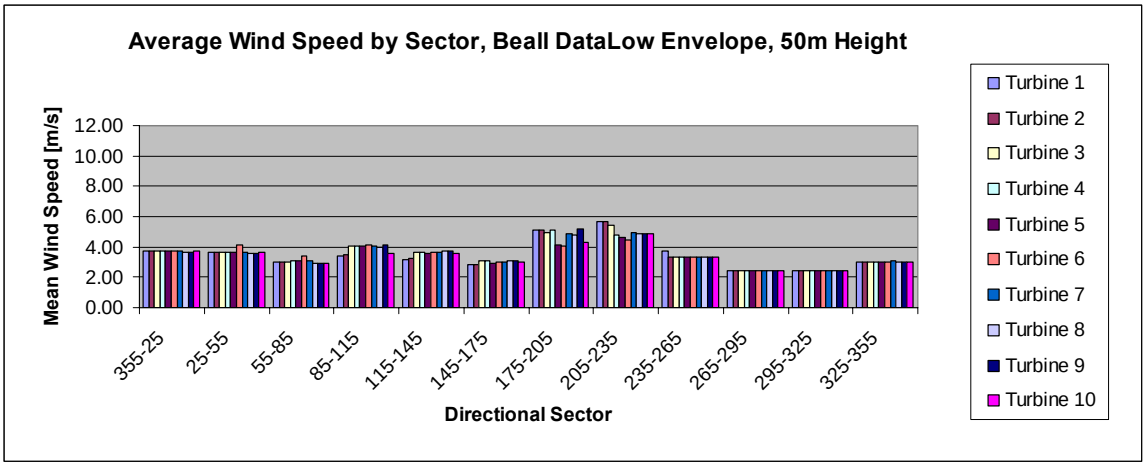

Figure 23. Average Wind Speeds Using the Beall Data, Low Envelope

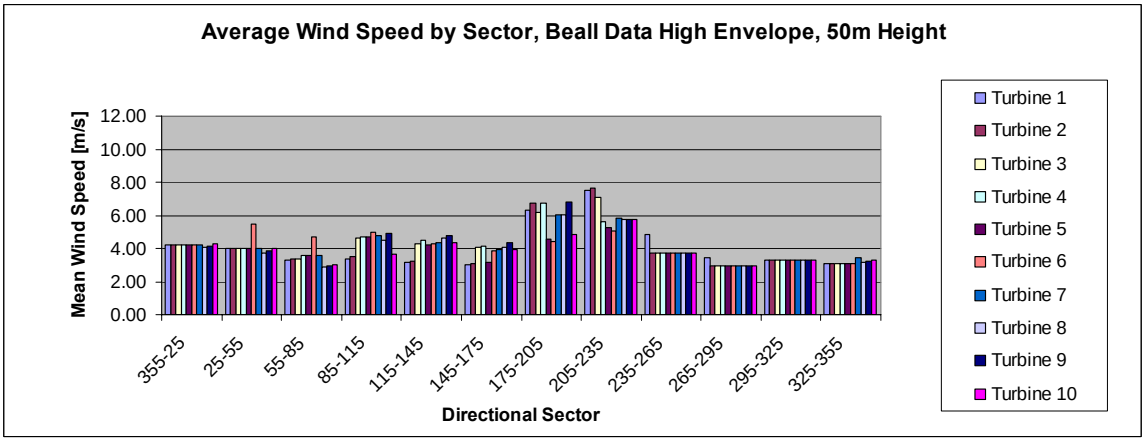

Figure 24. Average Wind Speeds Using the Beall Data, High Envelope

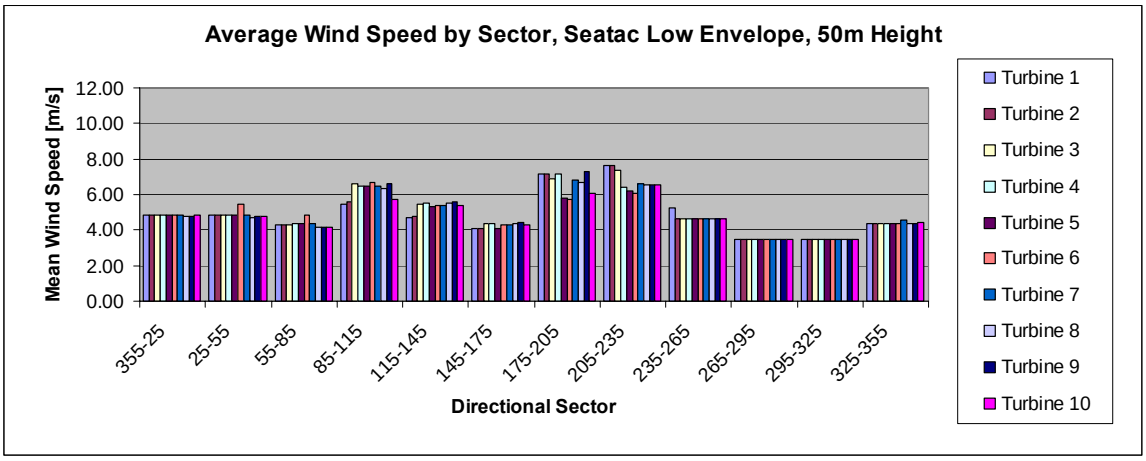

Figure 25. Average Wind Speeds Using the SeaTac Data, Low Envelope

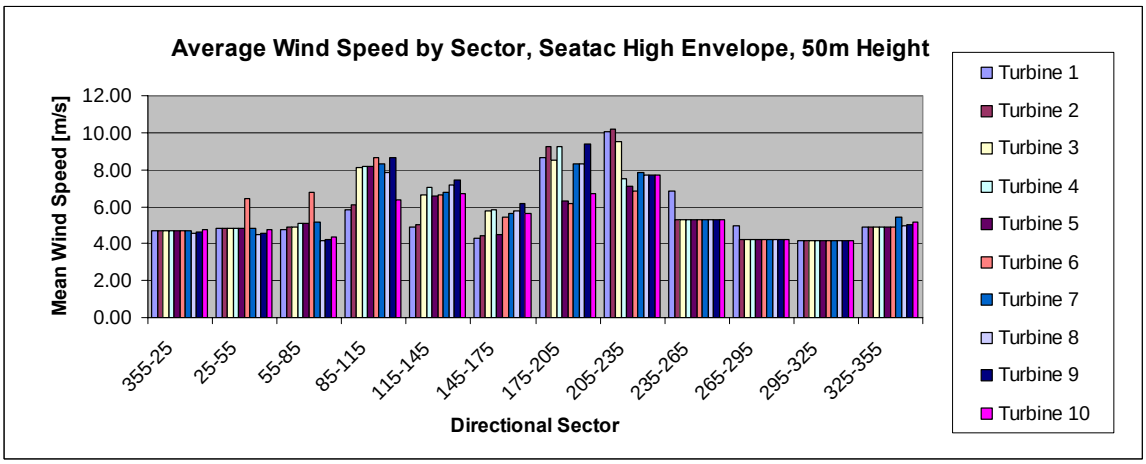

Figure 26. Average Wind Speeds Using the SeaTac Data, High Envelope

1.8.2 Annual Energy Production by Sector and Turbine Site

The annual energy produced from each sector is a better way to analyze the model results than by the velocities because it incorporates the effects of the distribution frequencies of the wind from each sector in addition to the velocities. Certain sectors are bound to be more valuable in terms of energy potential than others. More importantly, this is the best way to identify which turbine sites have the greatest energy production potential.

The annual energy production for each turbine site was calculated assuming a rotor diameter of 70 meters and a rated capacity of 1.5MW. The results are shown in Figure 27 through Figure 30. The most notable characteristic of these figures is that the annual energy is primarily produced from the two southwestern sectors from 175 - 235º. This can be expected since the largest velocities and the highest frequencies are seen from these directions. These sectors compromise 50-70% of the annual energy production.

The turbines at sites 1, 2, and 3 are the greatest energy producers. These sites have the benefit of the south facing ridge with open water to the south and south west. Sites 4, 7, 8, and 9 represent the next best energy producing sites, and sites 5, 6 and 10 are the worst. Sites 5 and 6 are poor because they are inland from the southern ridgeline and thus experience less wind speed-up effects from the predominant south and south west directions.

The sector and site energy productions are good tools for the final selection of turbine sites. It is possible that additional sites near turbine sites 1, 2, 3 and 4 or sites 7, 8, and 9 would be available and more productive than sites 5, 6, and 10.

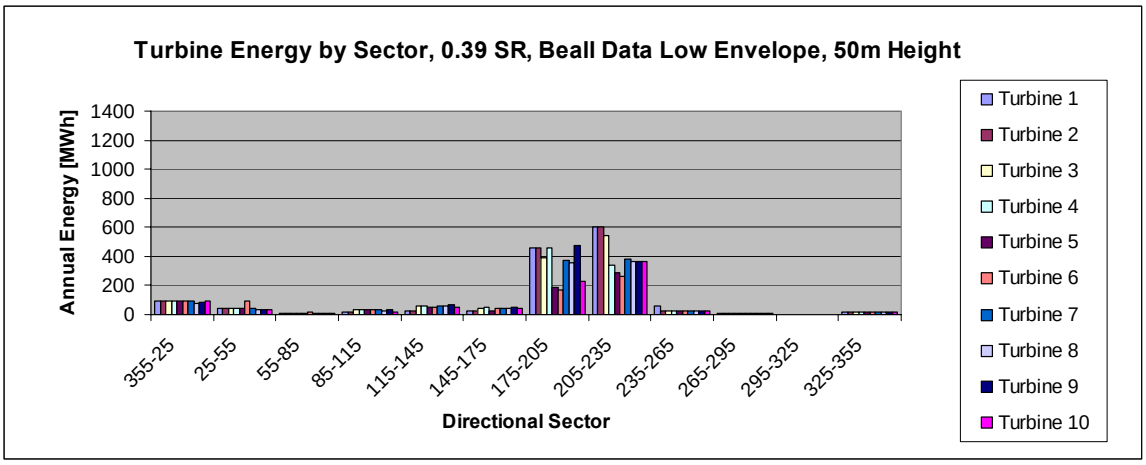

Figure 27. Annual Energy Production Using the Beall Data Low Envelope.

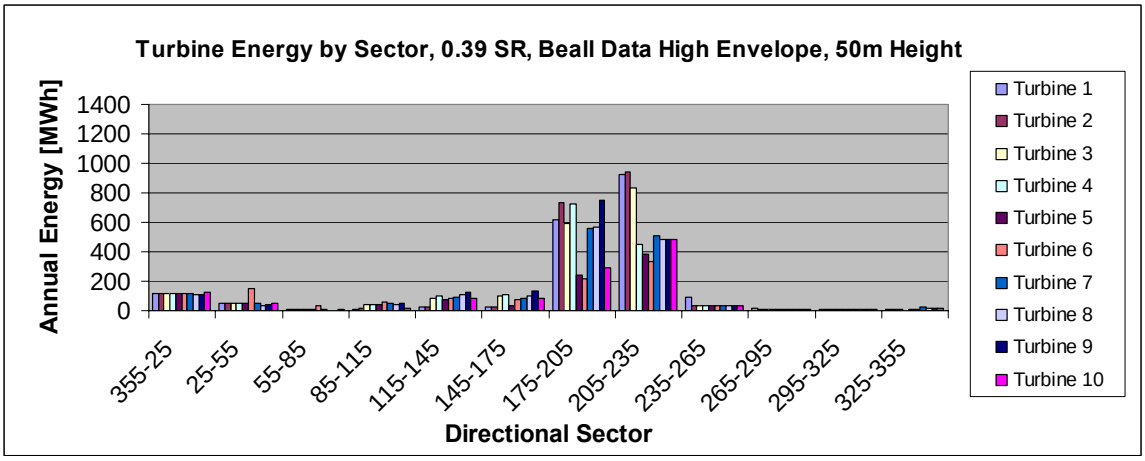

Figure 28. Annual Energy Production Using the Beall Data High Envelope.

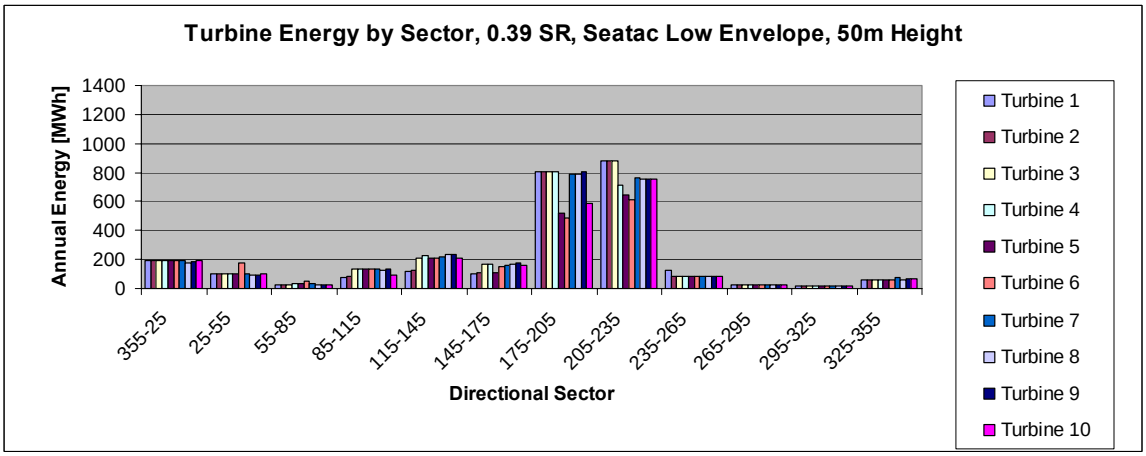

Figure 29. Annual Energy Production Using the SeaTac Data Low Envelope.

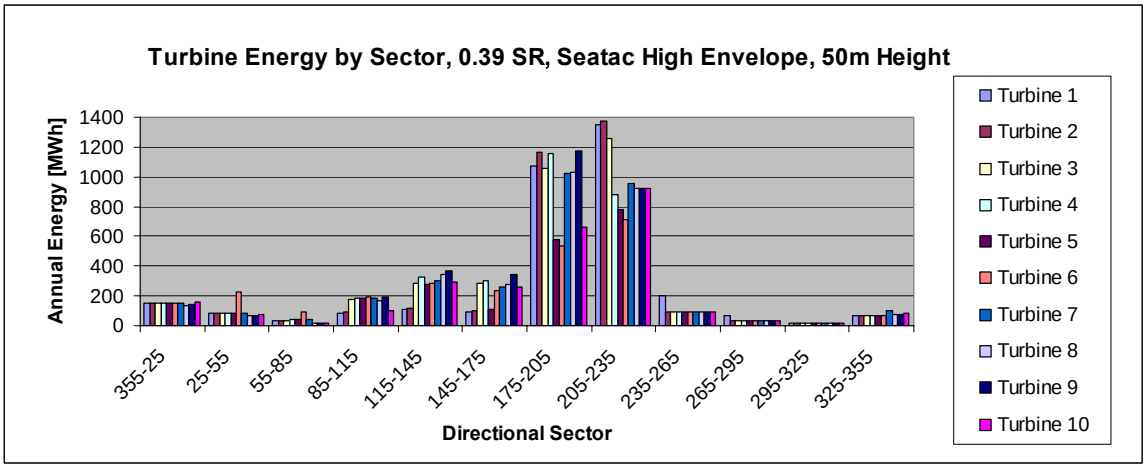

Figure 30. Annual Energy Production Using the SeaTac Data High Envelope.

1.9 Summary and Conclusions

An analysis has been presented in this section that determines the wind resource at the proposed turbine sites on Maury Island. Long term wind data from the SeaTac airport anemometer and short term wind data from the Beall site anemometer provided two different measurements of the winds near the Maury Island turbine sites. The data from these sites were grouped into 30º directional sectors and described using statistical analyses that are well established in the wind energy field. Finally, projected wind speeds at the turbine sites and annual energy yields were estimated using simple guidelines.

The Guidelines used for the wind velocity calculations cannot capture all the complexities of boundary layer flow, and offer only an approximation. Boundary layer flow analysis requires many assumptions regarding the topography and surface roughness of the land. High and low envelopes were established as the best way to bound the effects of the many assumptions. It is likely that the actual wind velocities and annual energy captures lie within these envelopes. A summary of the wind resources for each envelope are shown in Table 9.

Table 9. Summary of Wind Resource at Maury Island Wind Turbine Sites

	SeaTac		Beall	
	Low	High	Low	High
Average Velocity at 50m [m/s]	4.85	5.66	3.50	4.17
Wind Power Class	Class 1-2	Class 2	Class 1	Class 1

The SeaTac data and the Beall data produce very different wind resource results. The SeaTac data shows there is a much greater wind resource at the Maury Island turbine sites than the Beall data. The question arises: which wind resource is more accurate? This question can be answered by looking at the characteristics of the two data sets.

Both the SeaTac and Beall data sets are less than perfect. The SeaTac anemometer data was collected at the low height of 10 meters, but is nine years in duration. The Beall anemometer data, while collected at up to 49 meters, has only been collected for five months and exhibits high characteristic roughness lengths inconsistent with the surface coverage of the area. The SeaTac data is probably more accurate than the Beall data since it represents a much longer timescale of measurement and is unobstructed by local objects. The low envelope for the SeaTac data is probably the best choice since the results from the Beall data suggest a conservative assumption should be made.

A more accurate wind resource assessment can be made by installing an anemometer tower on the south end of Maury Island for at least a year. A WFDT software package can then confidently be utilized to extrapolate the data from this anemometer tower to other turbine locations on the Island.

Finally, a list of the turbine sites ordered from best to worst is presented in Table 10. The average energy produced at each turbine site is presented as a percent of the energy produced at the best turbine site. This information will help future studies choose the most appropriate site for further assessment.

Table 10. Turbine Site Ranking - Best to Worst

Turbine Site	Energy [% of Best Site]
Turbine 3	100
Turbine 2	97
Turbine 1	97
Turbine 9	96
Turbine 4	92
Turbine 7	90
Turbine 8	88
Turbine 10	76
Turbine 6	72
Turbine 5	67

2.0 Optimum Wind Turbine Design for a Low Wind Speed Regime

The wind regime for Vashon and Maury Island is a low wind speed regime. The average wind speed at 50m makes the site at Maury Island a Class 2 wind speed site at best. Wind turbines have not been designed for low wind speeds simply because of the abundance of sites with higher wind speeds [2]. In fact, the DOE Low Wind Speed Turbine (LWST) development program is aimed at reducing costs for wind energy in Class 4 environments [2]. Simply stated, there is no off-the shelf wind turbine that is advertised as suited for a Class 2 wind speed site.

The design parameters that can be used to tailor wind turbines to a specific wind regime are the turbine hub height, the rotor diameter, and the generator rating. Many wind turbine manufacturers are now offering turbines with more than one choice of rotor diameter including GE, Vestas, and others. Generally, in lower wind speed environments, turbines with larger rotors (compared to the installed generator capacity) and taller towers are installed [24, 23, 40].

The goal of this chapter is to identify the wind turbine design which would provide the minimum COE from the Maury Island wind farm. Background on tailoring wind turbines for specific wind regimes is discussed. An investigation into the optimum turbine hub height, the rotor diameter, and the generator rating is presented and the minimum COE identified. Additionally, a projection of COE reductions over the next ten years is made considering cost reductions in turbine design.

The Chapter 2 Outline is as follows:

2.1 Specific Power Description and Background: This section defines the specific power of a turbine and the importance of this parameter for optimizing a turbine

design for the Maury Island wind farm. Background into previous research on this topic is discussed.

2.2 Turbine Design and Cost Model: A modeling tool is described in this section that allows the total cost of the turbines, balance-of-station, and operation and maintenance to be scaled with the turbine design parameters investigated here (i.e. rotor diameter, generator rating, and tower height). The combination of this model with the annual energy yield model developed in Chapter 1 provides the critical parameter for the wind farm design: the COE in terms of ¢/kWh.

2.3 Results of the Wind Farm Cost and Energy Model Investigation: This section presents the results of the investigation into minimizing the COE from the Maury Island wind farm by identifying the optimum turbine design.

2.4 Future Component Cost Reduction: Turbine technology improvements and the projected reductions in the COE from these improvements are described in this section.

2.5 Summary and Conclusions

2.1 Specific Power Description and Background

The specific power of a wind turbine is defined as the generator nameplate capacity divided by the rotor swept area of the turbine. Specific power is also referred to as specific rating. This parameter has been found to be useful when tailoring a wind turbine to a particular wind regime. Theoretically, for each wind regime there exists a specific rating that will minimize the COE.

$$Specific\ Power = \frac{Generator\ Rating}{Rotor\ Swept\ Area}$$

The COE for a wind turbine is dependent on both its energy production and its costs. Generally, an increase in turbine size leads to higher costs. However, the effects of increasing turbine size on the energy production are slightly more complicated.

The annual energy production from a wind turbine is a function of the rotor diameter, the efficiencies of the system, and the rating of the generator. The turbine power is proportional to the square of the rotor; thus, increasing the rotor diameter (which decreases the specific power) will increase the energy production of the turbine for a given generator size. Increasing the rotor diameter while maintaining a constant generator size increases the time the turbine operates near generator capacity. The efficiencies of systems such as the generator are greater when operating at higher percentages of capacity. Thus it is most efficient to operate the turbine at the highest possible capacities.

Similarly, decreasing the generator rating decreases the specific power and increases the time that the system is operating at capacity. However, this does not necessarily correlate to a larger energy capture. Decreasing the generator size for a given rotor diameter may increase the efficiency that the system operates at, but the power that is available beyond the capacity of the generator is unable to be captured. For example, hypothetically, two turbines are able to capture 250kW of power with equivalent 50 meter rotor diameters at 8m/s wind speed. The generator of the first turbine is rated at 250kW and is operating slightly below maximum efficiency yielding 225kW. The second turbine has a generator that is rated at 500kW and is operating at much less than maximum efficiency so it produces 210kW. When the wind speed increases to 15m/s, the turbine with the 250kW generator can produce 250kW, but the turbine with the 500kW generator rating would produce 500kW. This may be a disadvantage for the turbine with the 250kW generator unless the wind speeds in the location of interest very rarely increases beyond 8m/s. Clearly, the wind regime affects the choice of generator size for a turbine.

The trade off for increasing energy capture with a larger rotor diameter is cost. Many of the components of a wind turbine are scaled as a function of the rotor diameter. For instance, if the rotor diameter is increased, the hub thickness will have to be increased to carry the extra weight. With the increased hub and rotor weights, there is a need to increase the size of other components such as the bearings, the bedplate, the tower, and the foundation. These increases in size and weight have associated increases in cost.

The same is true for increasing generator size. Increasing the generator size can increase the energy capture, but it will also increase the cost of the turbine. With increasing generator size, the costs of the generator, power electronics system and electrical hardware also increase.

Finding the optimum specific power of a turbine for a particular wind regime takes consideration of both energy production and turbine costs. This quickly becomes a complex analysis. A few studies that have investigated this topic are discussed.

2.1.1 WindPACT Study

The WindPACT study of specific power [24] is a detailed investigation that includes the effects of the wind regime on the optimum specific power of the turbine. The approach is to find the optimum specific power for a given wind regime by holding either the rotor diameter or the generator capacity constant while changing the other to affect a range of specific powers from 250W/m^2 to 600kW/m^2. In this way, investigations into effects of the wind regime on the optimum specific power are undertaken including average wind speed and the Weibull shape parameter.

The investigation involving average wind speed shows that the lower the average wind speed is, the lower the optimum specific power. The study investigates average wind speeds from 6m/s up to 10m/s with a Rayleigh wind speed distribution (Weibull shape

parameter k = 2). The tower height is kept constant throughout the investigation. For each wind speed a distinct minimum value of COE is determined correlating to a particular specific power. This optimum specific power value decreases as the mean wind speed value decreases. Figure 31 shows a summary of the findings from the WindPACT Study [24] and also those from Burton et al. [26] which is described in Section 2.1.2.

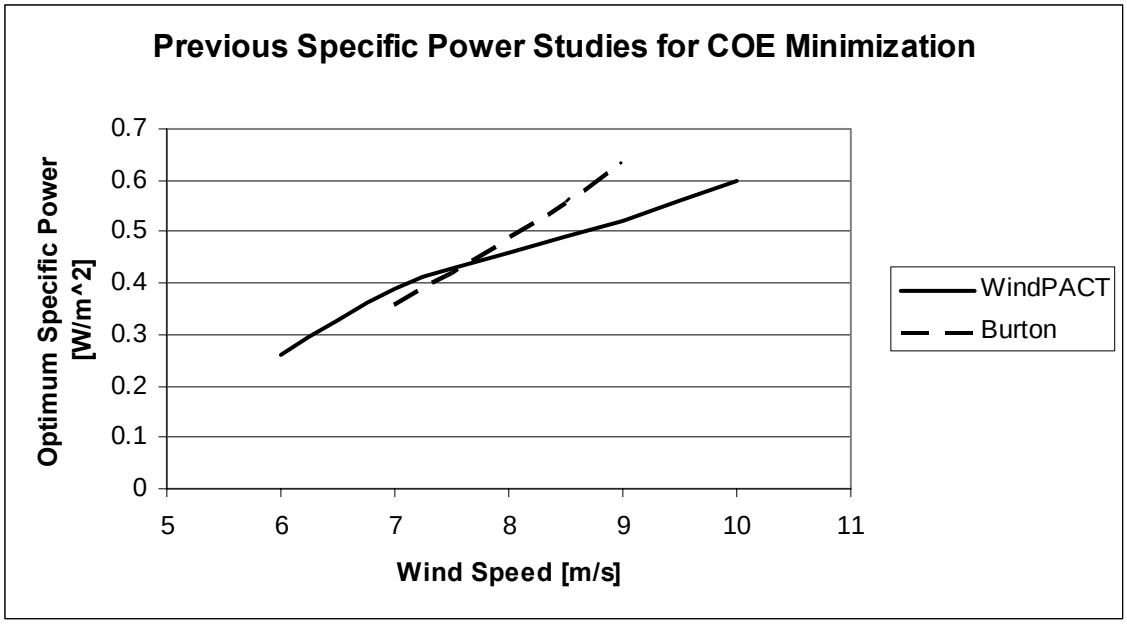

Figure 31. Previous Specific Power Studies for COE Minimization [24, 26]

Neither the WindPACT study [24] nor Burton et al. [26] determine the optimum specific power for average wind speeds less than 6m/s where the Maury Island average wind speed lies.

The Weibull shape parameter investigation determines that a lower Weibull shape parameter leads to a higher optimum specific power. In wind regimes of the same average speed of 7.86m/s, a high specific power (500W/m^2) is optimum for a low Weibull shape parameter value (k = 1.6), and a low specific power (390W/m^2) is optimum for a high Weibull shape parameter value (k = 2.5). This phenomenon is

explained by the overlap of the wind speed distribution and the turbine power curve. In each situation, the most time spent near rated capacity is the deciding factor. Figure 32 shows this trend graphically.

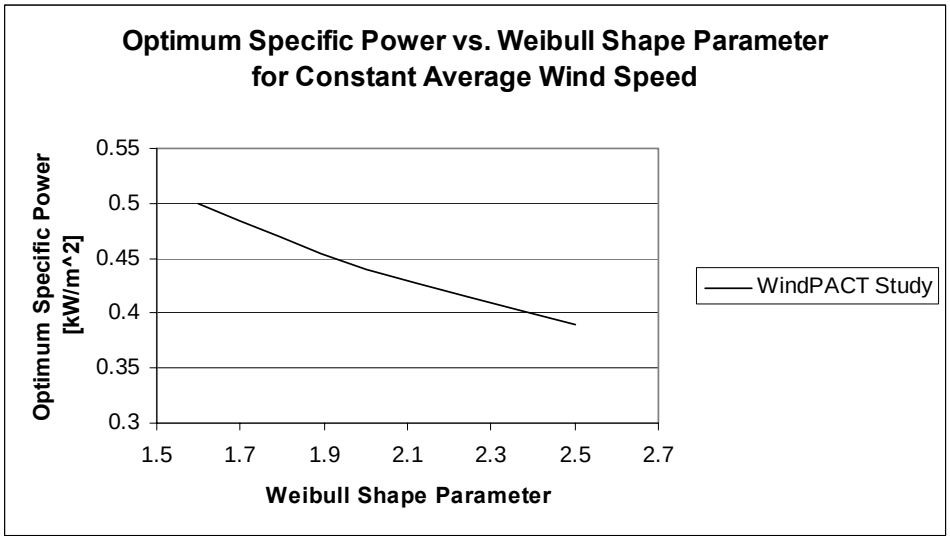

Figure 32. Optimum Specific Power vs. Weibull Shape Parameter [24]

2.1.2 Wind Energy Handbook

A brief section of the Wind Energy Handbook written by Burton et al. [26] discusses optimizing the specific power of a wind turbine using a simplified cost model. The authors suggest utilizing a baseline turbine design where component costs are known, to scale to larger sizes. Component weight relations are determined as a function of the rotor diameter or the rating of the turbine. The costs of the components are then scaled linearly by their weight. The weight and cost relations are then combined into one formula that relates the cost of the new wind turbine as a function of the baseline turbine and the ratio of the rated wind speeds.

The results of the study are reflected in Figure 31. They are quite similar to those found in the WindPACT study [24], but with a much smaller range of mean wind speeds. This

study also suggests that a linear relation between optimum specific power and the mean wind speed exists.

2.1.3 Additional Literature

A few other studies have looked at optimizing wind turbine design for particular wind regimes and have come to the same conclusion that lower wind regimes call for turbines with lower specific powers. Jackson et al. [23] characterize the optimum specific power for the wind regime in Tehachapi, California with respect to annual energy production and the daily electrical demand. The optimum specific power is related to the site-specific wind regime and the hourly value of the generated energy. The study concludes that wind turbines with a low specific power will have larger initial capital costs (due to larger components), but have benefits that may outweigh this cost in terms of increased capacity factors. However, this study does not investigate the COE from the turbines, only the annual energy production and the resulting time-valued sale price.

Janganshetti and Rau [25] investigate three parameters which describe the wind turbine power curve: the cut-in wind speed, the rated wind speed, and the cut-out wind speed. For a given wind regime with known Weibull scale and shape parameters, the three turbine power curve parameters can be chosen to maximize the energy production. The goal for defining the rated wind speed is to maximize the energy yield at a high capacity factor. This method is well suited for maximizing the energy yield for a given site, but it does not consider the COE.

2.1.4 Specific Power of Current Wind Turbines

From the above literature review of the relationship of turbine specific power with site-specific wind regime, it is concluded that wind turbines with low specific powers are best suited for the Maury Island application. It is therefore of interest to know what the

industry has to offer in terms of large turbines with low specific powers. Specific powers currently available for large wind turbines are shown in Figure 33.

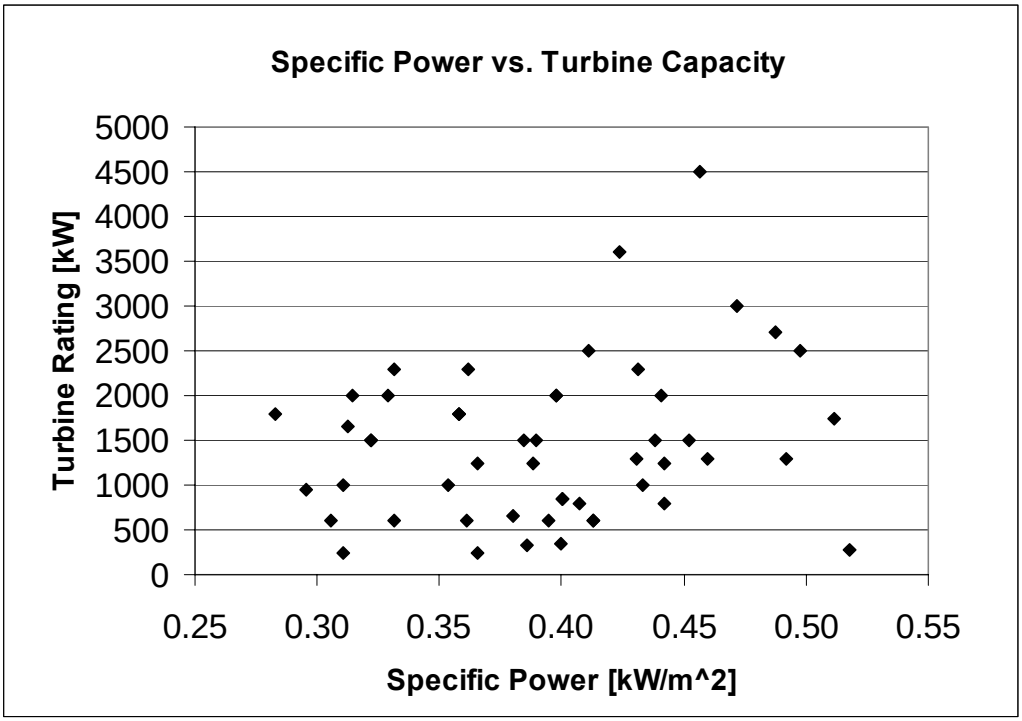

Figure 33. Specific Power of Commercial Utility Scale Turbines

The range in specific powers of current production wind turbines is quite large. In part, this reflects the site specific design tailoring that occurs in the industry. The lower limit of specific power for current production wind turbines is 0.270 kW/m^2. There are a number of turbines with ratings between 500kW and 2MW near the specific power of 0.30kW/m^2, which are suited for low wind speed sites. The turbines with the larger ratings tend to be for off-shore applications and typically have higher specific powers.

2.2 Turbine and Balance-of-Station Design and Cost Model

The studies discussed above do not determine the optimum specific power or turbine characteristics for wind speeds as low as those on Maury Island. The lowest average wind speed investigated is 6m/s (at hub height) which is well above the Maury Island

average wind speed. A study to determine the optimum turbine design for the Maury Island wind regime is necessary. To accomplish this study, a turbine design model is created.

A scalable turbine design model is developed that calculates the weight of the turbine components based on the rotor diameter, generator capacity, and tower height. These three turbine parameters and a few other site characteristics determine critical design loads of the turbine referred to here as major design drivers. The size and weight of the turbine components are determined largely by these major design drivers. The costs of the turbine components are calculated based largely on their weight. Additionally, the design of the wind farm balance-of-station is developed and cost estimates determined. The turbine component design and balance-of-station are all scalable with the rotor diameter, generator capacity and tower height.

The two main sources of information used in the development of the turbine model were *Large Wind Turbines: Design and Economics* [29] and the WindPACT studies [24, 27, 28, 30, 31, 32]. *Large Wind Turbines: Design and Economics* [29] is based on the turbine mass and cost model developed at the University of Sunderland. The WindPACT studies [24, 27, 28, 30, 31, 32] investigate the costs of the wind turbine subsystems based on their weight.

The turbine and balance-of-station model is essentially a tool to determine the optimum turbine design for Maury Island. The turbine design is investigated by varying the specific power (via the rotor diameter), the generator rating, and the tower height in the following ranges:

- Specific Power: 150 – 400 W/m^2
- Rated Capacity: 1.0MW, 1.5MW, 2MW
- Tower Height: 50 – 100 meters

The turbine and balance-of-station model is described in the following sub-sections. A Matlab program is created using the formulas detailed below.

2.2.1 Major Design Drivers

The loads on a wind turbine ultimately determine the weight and costs of the turbine components. Once the loads of the turbine are calculated, material allowable stress levels define section modulii and finally component dimensions and weight. The design of turbine components can either be fatigue driven or ultimate load driven. This study uses ultimate loads to determine component design. The two main design drivers are rated torque and extreme thrust on the rotor.

Rated torque is the single most important design driver needed to model the weight and cost of the rotating machinery [29]. It is defined by the following equation:

$$Q_R = \frac{1}{16}\rho_a C_p \pi \frac{V_R^3}{V_T} D^3$$

Where: V_R = the rated wind speed,

$V_T = \lambda * V_R$ the rotor tip speed

λ = the tip speed ratio

The tip speed ratio is the velocity of the tip of the rotor blade compared to the wind velocity. It is held constant in the model at 9.5 for two-bladed turbines and 7 for three-bladed turbines to achieve the maximum aerodynamic efficiency [32].

The extreme thrust on the rotor affects the weight of the bearings, the nacelle bedplate, the tower and the foundation [29]. It is dependent on the extreme wind speed, the rotor solidity, the drag of the blades and the diameter.

$$T_R = \frac{1}{8}\rho_a (0.85 * V_{EX})^2 C_D S \pi D^3$$

Where: V_{EX} = the fifty year extreme wind speed

C_D = 1.8, the drag coefficient of parked rotor blades [19]

S = the solidity of the rotor

The fifty year extreme wind speed is a design parameter determined by the International Electrotechnical Commission (IEC) class of the turbine [3] by:

$$V_{EX}(z) = 1.4 * V_{ref} * \left(\frac{z}{z_{hub}}\right)^{0.11}$$

Where: V_{ref} is defined in Table 11

z = the height of interest (in this case the hub height)

z_{hub} = the hub height of the turbine

Table 11 describes the reference velocities (V_{ref}) for determining the fifty year extreme wind speeds. The average velocity at the hub of the turbine (V_{ave}) determines the design class of the wind turbine.

Table 11. Basic Parameters for WTGS Classes [3]

Turbine Class	V_{ref} [m/s]	V_{ave} [m/s]
I	50	10
II	42.5	8.5
III	37.5	7.5
IV	30	6

Few utility scale turbines are designed to IEC classes less than Class II. The fifty year extreme wind speed defined for a Class II turbine is assumed in the model unless otherwise specified.

The solidity of the rotor blades is the area of the blade profile perpendicular to the wind compared to the rotor swept area. The solidity of the rotor is optimized according to the design tip speed ratio and has a value of 0.5 [19].

2.2.2 Turbine Components and Systems

Wind turbine technology is maturing, and with this maturation, a standard turbine design is coalescing. The design of wind turbines currently dominating the market is characterized by a horizontally mounted upwind three-bladed rotor, an active yaw control drive, and a free-standing tower [23]. Doubly fed induction generators (or wound rotor induction generators) are becoming the generators of choice because they allow a large range of variable-speed operation and require power electronic systems rated to only one third the generator rating. These generators operate by feeding one-third of the power from the generator through a power electronic system to control the generator slip and frequency to match the grid frequency. The power electronic system can control the power factor of the generator and thus the wind farms do not require reactive power support. A wind turbine with the following characteristics is assumed:

- Upwind three-bladed rotor
- Full pitch control of the rotor blades
- Active yaw control
- Free-standing tower
- Doubly-fed induction generator

Wind turbines are complex conglomerates of fully integrated systems from a wide range of technical fields. To create a turbine design that is scalable as a function of the rotor diameter, generator rating and tower height, the turbine design is described by 16 components and systems. The 16 component and system weights (where necessary) and costs are calculated based on formulas that are functions of:

- Q_R: the rated torque of the rotor
- T_R: the extreme thrust on the rotor
- V_{EX}: the extreme wind speed
- D: the rotor diameter
- Rating: the generator rating
- HH: the hub height of the turbine (tower height)
- YS: the yield strength of the component materials
- $V_{cut\text{-}in}$: the cut-in wind speed, 3m/s (the wind speed at which the turbine begins to produce energy)

The components and systems may also be functions of other component sizes and weights. Therefore, the model calculates in a top down manner beginning with the rotor, followed by the drive train, nacelle and tower. Descriptions of the component and system weight and cost formulas are given in Table 12. Where the formulas are too complicated to be simply stated in the table, the formula variables are defined instead. A full description of the component and system design and cost calculations is provided in Appendix D.

Table 12. Summary of Turbine Component and System Weight and Cost Calculations

Component/ System	Weight and Cost Model	Source
Rotor Blades	$M_{blade} = 0.21 * (D/2)^{2.89}$ [kg] Cost = \$10.95/kg	[32]
Hub	$M_{hub} = 0.24 * D^{2.5765}$ [kg] Cost = \$4.25/kg	[28,32]
Pitch Mechanism and Bearings	$M_{pitch} = 2.992E\text{-}4 * D^{2.9935}$ [kg] Cost = $M_{pitch} * 6.689 + 953$ [\$]	[32]
Low-speed Shaft	$M_{LSS} = f(D, M_{pitch}, M_{hub}, M_{blade}, YS)$ Cost = \$7.00/kg	[29,32]
Main Bearings	$M_{bearing} = 2.613E\text{-}5 * (D_{o,\,LSS})^{2.77}$ [kg] $M_{housing} = 6.744E\text{-}5 * (D_{o,\,LSS})^{2.64}$ [kg] Cost = \$17.60/kg. (Note: $D_{o,LSS}$ = Low-speed Shaft Outer Diameter)	[32]
Gearbox	$M_{gearbox} = f(D, V_{cut\text{-}in}, T_R)$ Cost = $(0.000647 * Rating + 13.26) * M_{gearbox}$ [\$]	[29,32]
Generator	$M_{generator} = 3.3 * Rating + 471$ [kg] Cost = \$52.00/kW	[29,30, 32]
Variable-speed Electronics	Cost = \$54.00/kW	[30,32]
Bedplate	$M_{bedplate,} = f(Q_R, T_R, D, M_{blade}, M_{hub}, M_{pitch})$ Cost = \$4.25/kg	[29,32]
Nacelle Cover	$M_{nacelle} = f(bedplate\ length)$ Cost = \$10.00/kg	[29,32]
Yaw Drive and Bearings	$M_{yaw} = f(T_R, M_{rotor}, M_{gearbox}, M_{generator}, M_{bedplate,} M_{nacelle,} M_{HSS})$ Cost = $2* (M_{yaw} * 6.689 + 953)$ [\$]	[29,32]
Mechanical Brake, High-speed Shaft and Coupler	$M_{HSS,brake,coupler} = f(D, V_{cut\text{-}in}, T_R)$ Cost = \$10.00/kg	[29,32]
Electrical Connections	Cost = \$40.00/kW	[30,32]
Hydraulic and Lubrication Systems	Cost = \$4.50/kW	[32]
Controls and Safety Systems	Cost = $9500 + 10 * D$ [\$]	[32]
Tower	$M_{tower} = f(T_R, V_{EX}, HH, YS)$ Cost = \$1.50/kg	[28,32]

2.2.3 Wind Farm Layout and Balance-of-station

The proposed wind farm on Maury Island has ten turbine sites along the southern and south-eastern bluffs grouped into three regional locations. The electricity generated by the turbines would be collected at each of the three regional locations and transmitted to the substation located on the eastern tip of Maury Island via overhead lines. Figure 34 shows the turbine locations, substation location, and overhead line routing.

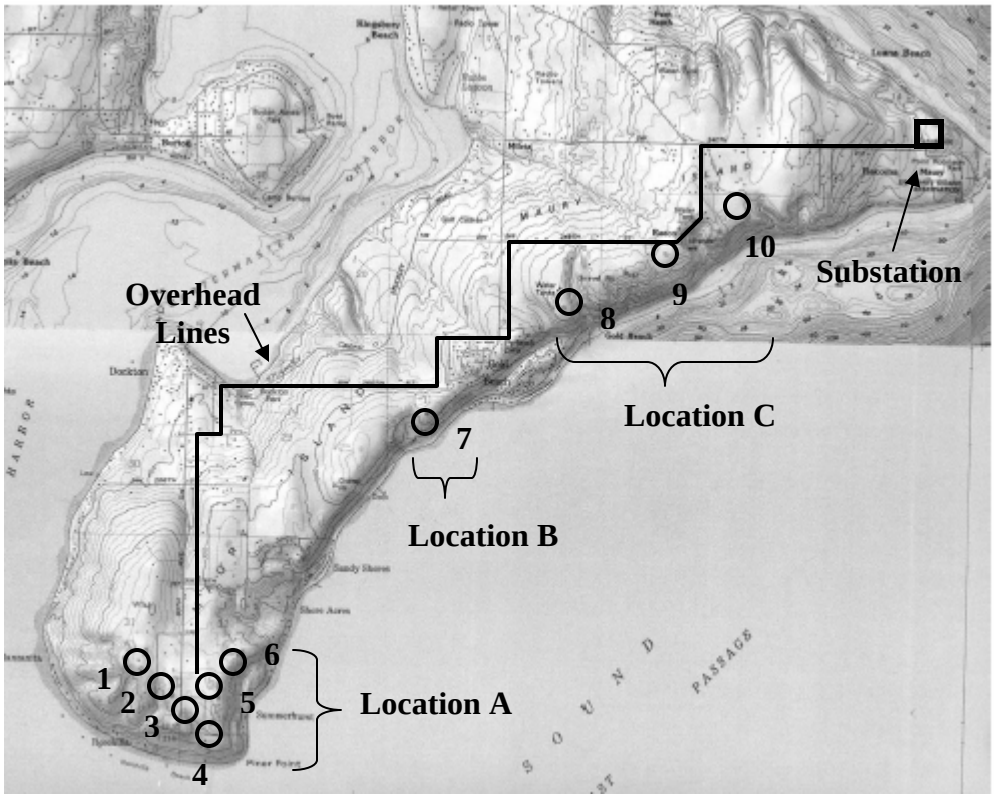

Figure 34. Maury Island Wind Farm Top Level Diagram [8]

The balance-of-station cost for each turbine typically makes up 20-25% of the total installed cost [36]. This percentage may be higher for Maury Island due to the fact that the turbines are quite spread out around the island. The balance-of-station for a wind farm is a broad category covering everything from electrical integration, such as transformers and circuit breakers, to crane pads for turbine installation. A full analysis of

the balance-of-station design and costs are provided in Appendix E. The analysis is based on the following variables:

- D: the rotor diameter
- Rating: the generator rating
- HH: the hub height of the turbine (tower height)
- Conductor Length: the length of conductors running from the turbines to the substation
- Road length: the length of service roads to provide access to turbine sites
- Site Area: the area of the turbine sites

A summary of the balance-of-station cost equations are provided in Table 13.

Table 13. Summary of Balance-of-station Cost Calculations

Component/ System	Cost Model	Source
Electrical Interface and Connections	Cost = *f(Rating, Conductor Length)*	[26,30, 31,37, 58]
Roads and Civil Works	Cost = *f(Road Length)*	[31]
Crane Pad	$Cost_{cranepad} = 1.3348 * (HH)^{2.3081}$ [$]	[31]
Foundation	Cost= $510*(Moment_{max,\ base})^{0.465}$ [$] (Note: $Moment_{max,\ base}$ = the maximum moment at the base of the tower)	[31]
Transportation	$Cost_{blade,transport} = 0.1722 * D^{2.4181}$ [$] $Cost_{hub,\ transport} = 0.782 * D^{2.0083}$ [$] $Cost_{nacelle,transport} = 0.3251 * D^{2.4212}$ [$] $Cost_{tower,\ transport} = \left(\frac{1160}{1111}\right) * 0.0121 * (HH)^{3.3649}$ [$] $Cost_{barge,head} = 1830.9 * D^{0.3716}$ [$]	[28,31]
Crane Cost	$Cost = 0.017 * (HH)^{3.3058}$ [$]	[31]
Assembly and Installation	$Cost = 0.1324 * (HH)^{2.815}$ [$]	[31]
Permitting Costs	Cost = 9.94E-4 * Rating + 20.31 [$/kW]	[31]
Engineering Costs	Cost = 0.07 * Balance Subtotal [$]	[31]
Surveying Costs	Cost = 6562 * Site Area [$]	[31]
Inspection Costs	Cost = 6 * 10,000 [$]	[31]
Manufacturer Mark-up	Cost = 25% * (Cost of Turbine – Cost of Tower) [$]	[29,32]

2.2.4 Operation and Maintenance

Operation and maintenance (O&M) costs can comprise a large portion of the cost for a wind turbine, upwards of 20-25% of the lifetime cost. Unfortunately, available O&M cost data vary widely, and in general, long-term reliable O&M data is not readily available. One reason for the data not being available is the relative newness of wind turbine technology and the vast number of changes in characteristics such as size and system designs over the past 20 years, which makes O&M data for older smaller turbines relatively inapplicable to newer larger turbines [36]. Additionally, since O&M costs can

be such a large portion of a wind turbine's life cycle cost, turbine manufacturers may view this data as proprietary and do not release their data for public investigation [32].

Operation costs are calculated as part of the fixed finance charge rate in the cost model discussed in the next section. Research revealed a number of maintenance costs ranging from 0.0048¢/kWh to 0.0127¢/kWh [30, 32, 36]. The maintenance costs are assumed to be 0.0127¢/kWh [32] unless otherwise specified.

2.2.5 Cost of Energy Model

The formula used to calculate the cost of energy specified by the NREL in the WindPACT studies [32] is assumed in this study:

$$COE = \frac{(FCR * ICC)}{AEP_{net}} + O\,\&\,M$$

Where COE = Levelized cost of energy ($/kWh)
FCR = Fixed charge rate (0.106/year)
ICC = Initial capital cost ($)
AEP_{net} = Net annual energy production (kW/yr)
= AEP_{gross} adjusted for availability, array losses, soiling, etc.
O&M = Operating and maintenance cost ($/kWh)

2.3 Results of the Wind Farm Cost and Energy Model Investigation

The results presented in this section constitute investigations into the optimum turbine design for minimizing the Maury Island installation COE, including the rotor diameter, the generator rating and the tower height. Rotor diameter and generator rating were investigated in one parameter, the specific power. The specific power was investigated

both by varying the rotor diameter with the rating held constant, and by investigating three generator ratings. Ranges of the parameters investigated are as follows:

- Specific Power: 150 – 400 W/m^2
- Rated Capacity: 1.0MW, 1.5MW, 2MW
- Hub Height (tower height): 50 – 100 meters

These investigations were carried out using a Matlab program of the turbine and balance-of-station model previously described.

2.3.1 Beall Data COE Results

The COE calculations using the Beall data reveal that there is in fact a distinct minimum in the COE pertaining to an optimum specific power. This is consistent with previous studies [24,26] and is true for both the high and low envelopes. The results are shown graphically in Figure 35 and Figure 36. The optimum hub heights are identified in the keys.

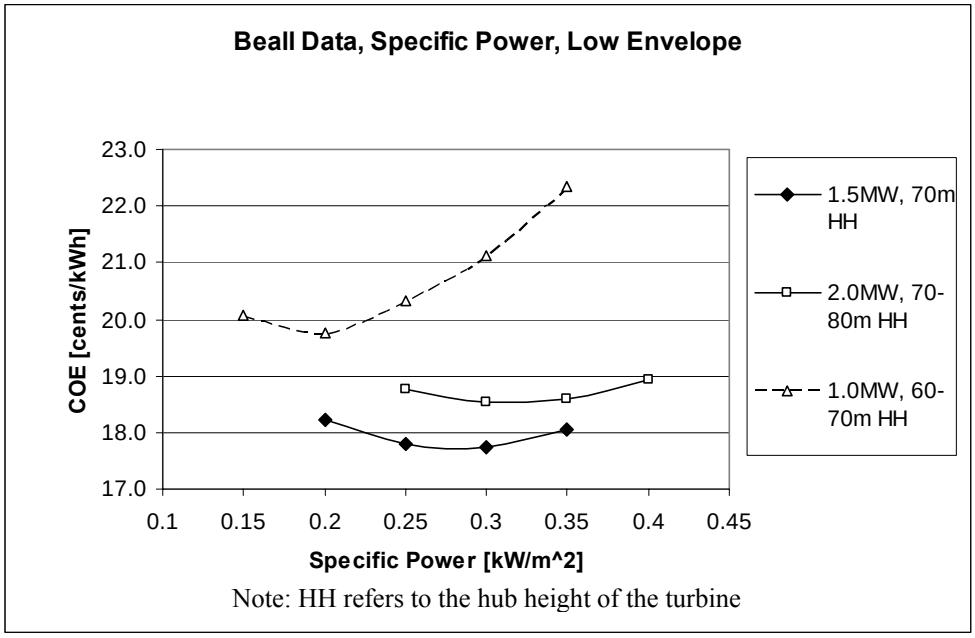

Figure 35. COE Investigation for Beall Data, High Envelope

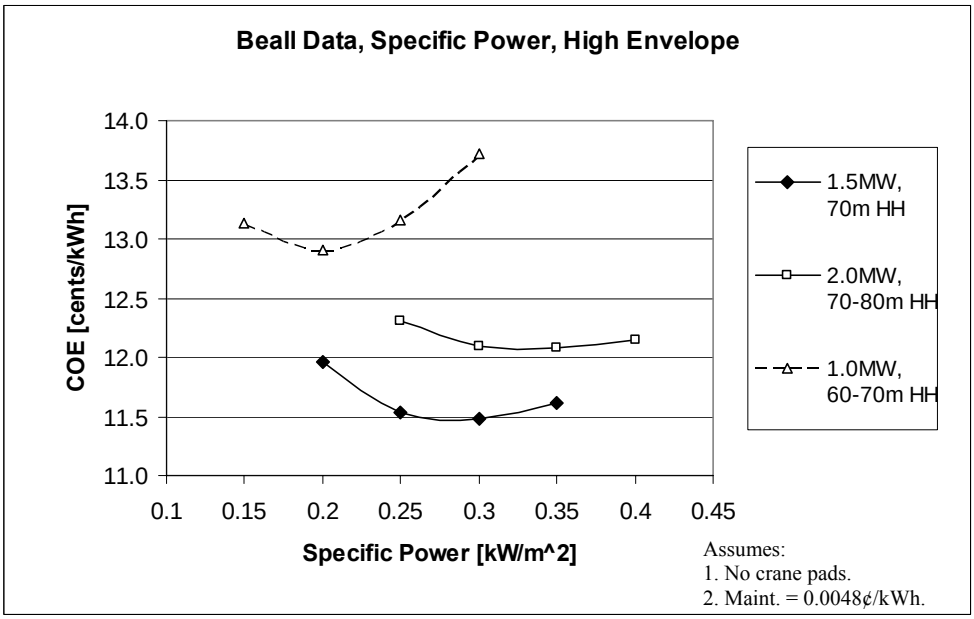

Figure 36. COE Investigation for Beall Data, High Envelope

The 1.5MW turbine is seen to be the optimum rating for the Maury Island wind regime. If the rating is increased to 2MW, the additional energy capture from the larger turbine is not great enough to compensate the greater cost of larger turbine components. If the

rating is decreased to 1MW, the decrease in energy capture outweighs the reduction in cost from smaller turbine components. The 1.5MW rating has a minimum COE about 1¢/kWh lower than the minimum COE for the 2.0MW rating. The minimum COE rating for the 1MW turbine is 2-3¢/kWh higher than that for the 1.5MW turbine. Optimum turbine parameters for the Low and High Beall Data Envelopes are defined in Table 14.

Table 14. Optimum Turbine Parameters for Beall Data

Turbine Parameter	Low Envelope	High Envelope
Rotor Diameter [m]	83.5	80
Generator Rating [MW]	1.5	1.5
Tower Height [m]	70	70
Specific Power [kW/m^2]	0.275	0.30
COE [¢/kWh]	17.8	11.5

As would be expected, the optimum specific powers of the low and high envelopes differ. The low envelope, which has a lower average wind speed, has a lower optimum specific power than the high envelope. This trend is consistent with past studies which show a positive linear relationship between average wind speed and optimum specific power [24,26].

The optimum specific power is lower in value for lower turbine ratings. This result is not unexpected. As previously stated, the specific power is the ratio of the generator rating to the rotor swept area. Holding the specific power constant, a larger rated capacity means a larger rotor diameter than that for a smaller rated capacity. Since many turbine component costs scale as a power of the rotor diameter, a larger rated capacity means the component costs are increased significantly. As specific power is decreased for a constant rated capacity, at some point, the component costs associated with the larger rotor diameter outpace the additional energy capture. This turning point occurs at a higher specific power for turbines with larger rated capacities because the rotor diameter and component costs are much greater than those for a turbine with a smaller rated

capacity and the same specific power. The minimum of the curves in the Figures 35 and 36 represent this turning point.

The result of the optimum specific power decreasing for smaller turbine ratings is important because it means that characterizing an optimum turbine for a given wind regime is not dependent on specific power alone, but also on the turbine rating. The approach developed in this study is a thorough strategy to identify the optimum turbine design for a particular wind regime.

The optimum hub height increases from 60-70m for the 1MW turbine to 70-80m for the 2MW turbine. The increasing optimum hub height for increasing turbine ratings is easily explained by the design of the tower. The tower design is dependent on both tower height and tower head mass (the mass of all of the components the tower supports). As the turbine rating increases, the tower head mass increases due to the larger components. The increased tower head mass drives up the necessary thickness of the tower. Increasing the height of the tower for the larger turbine ratings has less of an effect on the COE since the towers are already thicker. In other words, the increased tower cost for the taller towers are somewhat masked by the increased tower cost to support the larger components. The benefit from the taller tower is a larger annual energy capture since wind speeds increase with height.

2.3.2 SeaTac Data Results

The COE results using the SeaTac data are shown in Figure 37 and Figure 38. The COE results using the SeaTac data are far smaller than those using the Beall data. However, the shapes of the curves are quite similar.

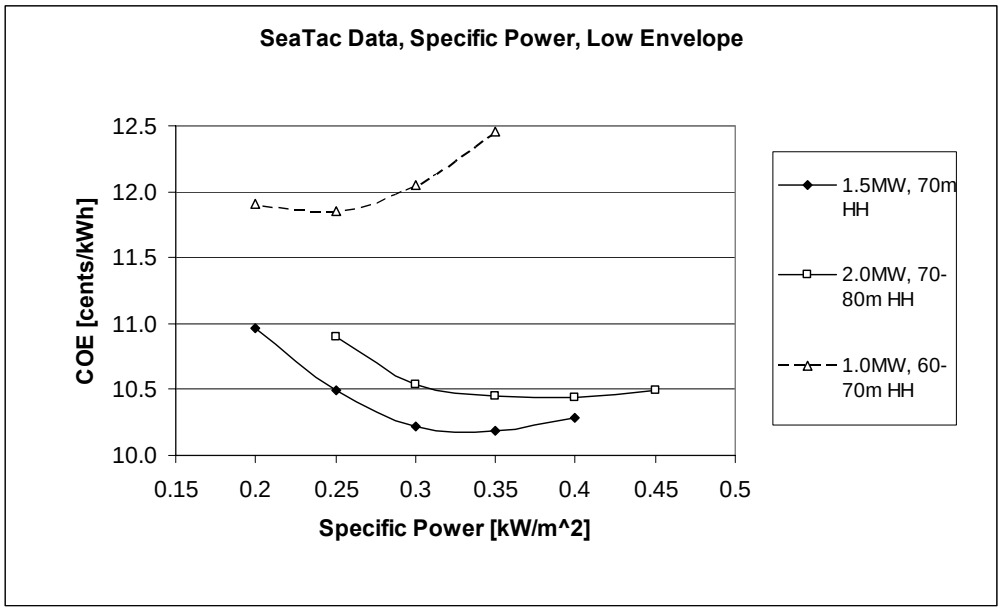

Figure 37. COE Investigation for SeaTac Data, Low Envelope

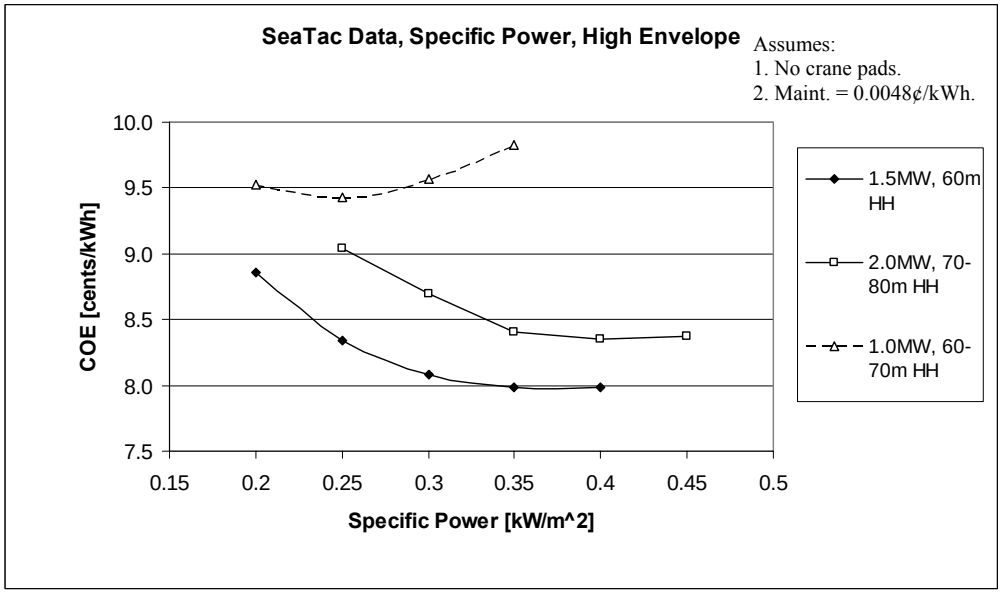

Figure 38. COE Investigation for SeaTac Data, High Envelope

The 1.5MW rated turbines are again found to be the best fit for the Maury Island application. With the wind resource derived from the SeaTac data, the COE from ten 1.5MW turbines is estimated to be between 8¢/kWh and 10¼¢/kWh. This is obviously much cheaper than the COE estimates using the Beall Data.

The specific power trend discussed from the Beall data results are continued in the SeaTac data results. As before, the optimum specific power is lower for lower turbine ratings. Similarly, the optimum specific power is seen to increase for higher wind speeds (from low envelope to high envelope). The optimum specific powers are larger for the SeaTac data results than those for the Beall data results since the wind speeds are higher for the SeaTac data. The optimum turbine parameters are summarized in Table15.

Table 15. Optimum Specific Power for SeaTac Data

Turbine Parameter	Low Envelope	High Envelope
Rotor Diameter [m]	83.5	80
Generator Rating [MW]	1.5	1.5
Tower Height [m]	70	70
Specific Power [kW/m^2]	0.325	0.35
COE [¢/kWh]	8	10.25

2.3.3 Comparison of Optimum Specific Powers to Those from Previous Studies

The results of the optimum specific power investigation are compared with previous studies in Figure 39. The triangles labeled "Maury Island" are the optimum specific powers found in this study for the average velocities at 70m using the SeaTac high and low envelopes (5.1m/s and 5.8m/s respectively), and for the average velocities at 70m using the Beall data high and low envelopes (3.7m/s and 4.3m/s respectively). The WindPACT [24] and Burton et al. [26] specific power study results are extrapolated to the lower wind speeds of interest. The optimum specific power of the WindPACT and Burton studies predict a much lower optimum specific power than this study found.

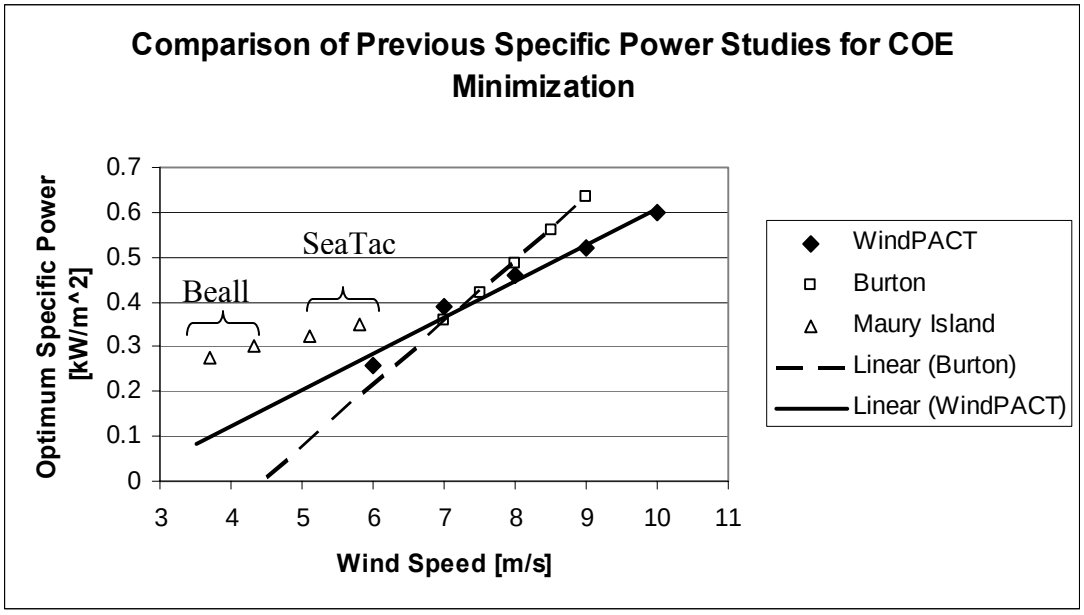

Figure 39. Comparison of Specific Power Study

The difference in optimum specific ratings between the studies can be explained by differences in the distribution of wind speeds. The previous studies assume a wind regime which has a perfect Rayleigh wind speed distribution (i.e. Weibull shape parameter, k = 2). However, this is not the case for the Maury Island site. The wind resource assessment in Chapter 1 showed that the best Weibull distribution fit for the projected wind speeds at the turbine sites had much smaller Weibull shape parameters, k = 1.6 to 1.7. According to the WindPACT study [24], the optimum specific power significantly increases with a smaller Weibull shape parameter. This phenomenon is explained by the overlap of the wind speed distribution and the turbine power curve.

Recognizing that the optimum specific power is dependent on both average wind speed and Weibull shape parameter is an important point for a wind farm developer looking to utilize the findings. That is, optimizing wind turbines for a given wind regime require an investigation into the total statistical description of the site. It is not adequate to simply assess the average wind speeds.

A comparison of the COE found in this study and the COE found in the WindPACT study [24] is shown in Figure 40. The data points marked "Maury Island" are the results of this study for the SeaTac data high and low envelope results and the Beall data high and low envelope results. These results are slightly higher than the extrapolation of the WindPACT study [24] might predict. The long distance spacing of the turbines on the Maury Island coastline resulted in relatively large balance-of-station costs for the wind farm compared to that of the WindPACT study [24]. Also, this study adopts a philosophy to make conservative choices when assumptions are necessary, and the results reflect this philosophy.

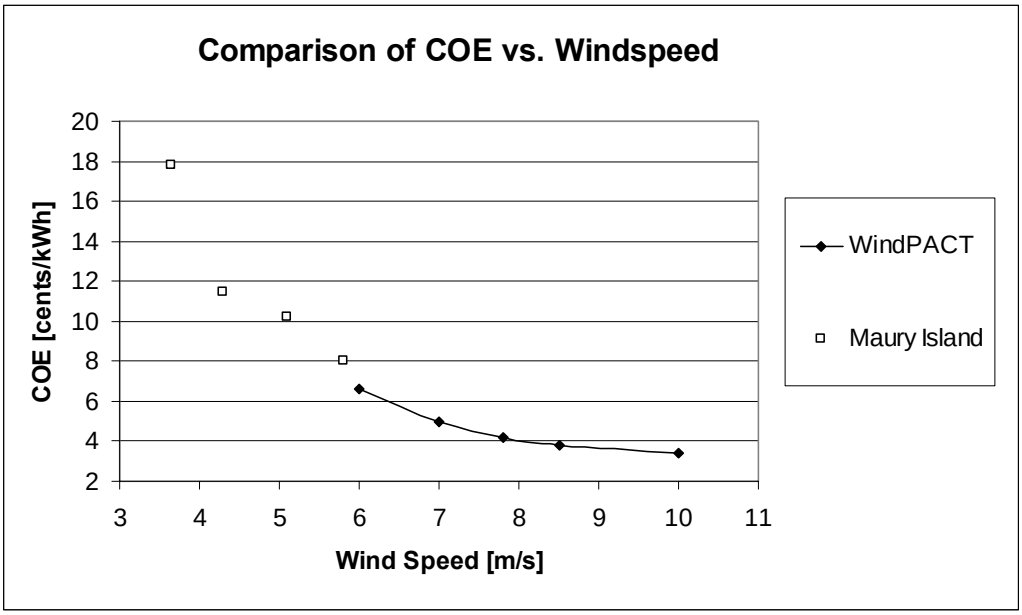

Figure 40. Comparison of COE vs. Wind Speed

2.3.4 Energy Production

Energy production from the 10 turbine wind farm is not considered in the previous section, but is investigated here. Energy consumption by the community on Vashon/Maury Island is expected to be about 26GWh per year after energy conservation measures are put into place [60]. The energy production for the two envelopes and two data sets are shown in Figure 41 through Figure 44. The black circles identify the

optimum specific power for the respective turbine rating and therefore, the minimum COE.

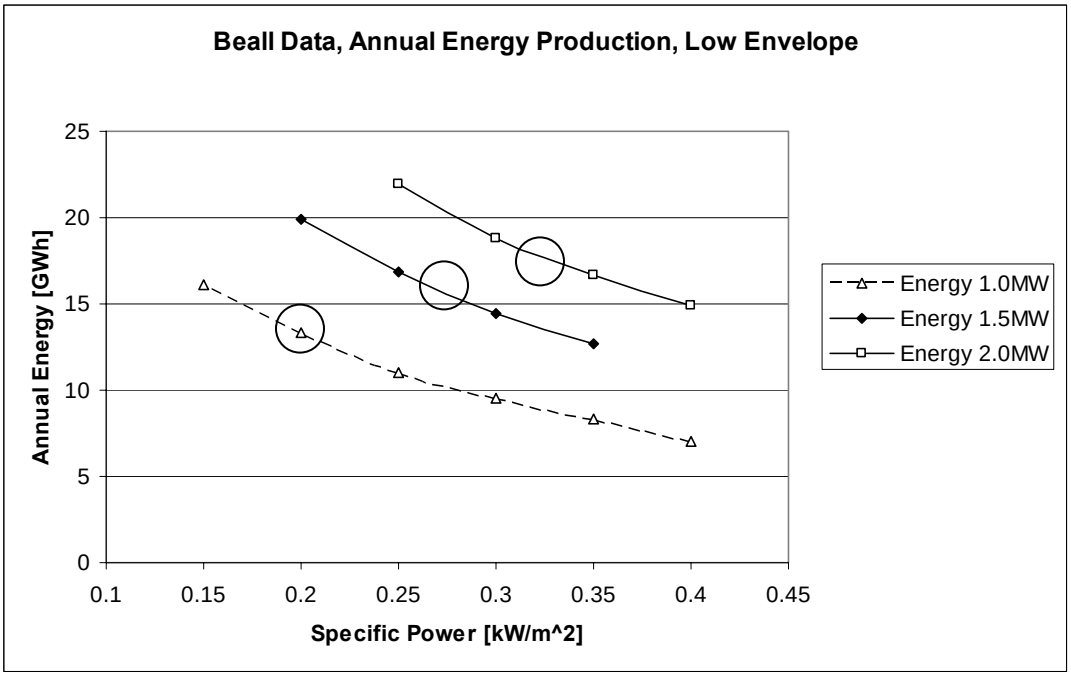

Figure 41. Annual Energy Capture for Beall Data, Low Envelope

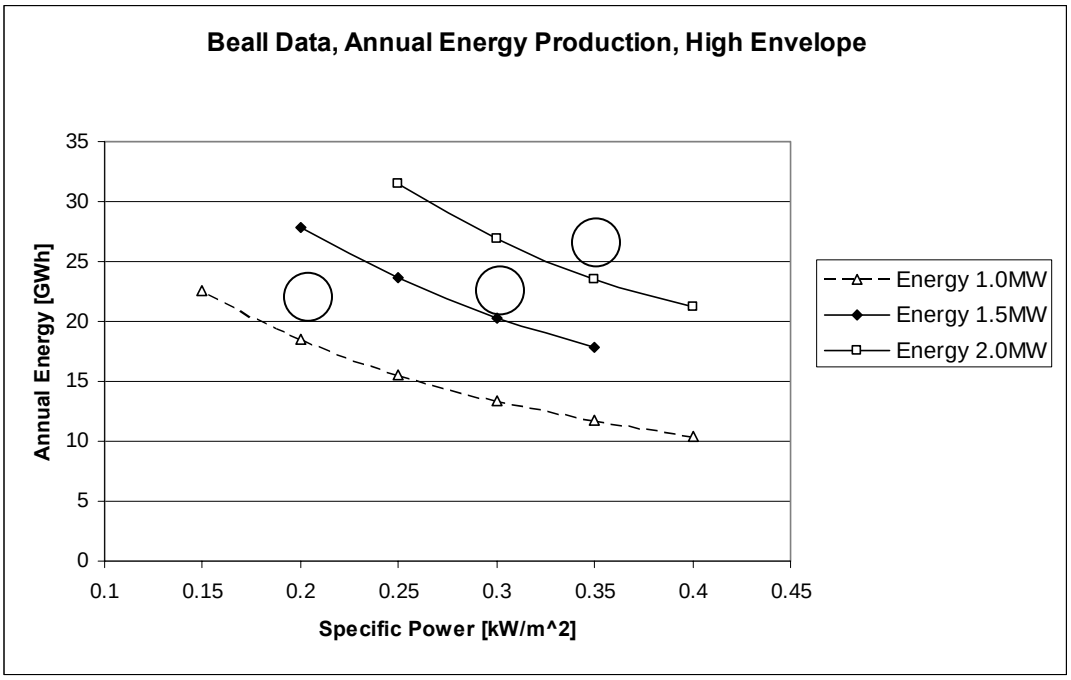

Figure 42. Annual Energy Capture for Beall Data, High Envelope

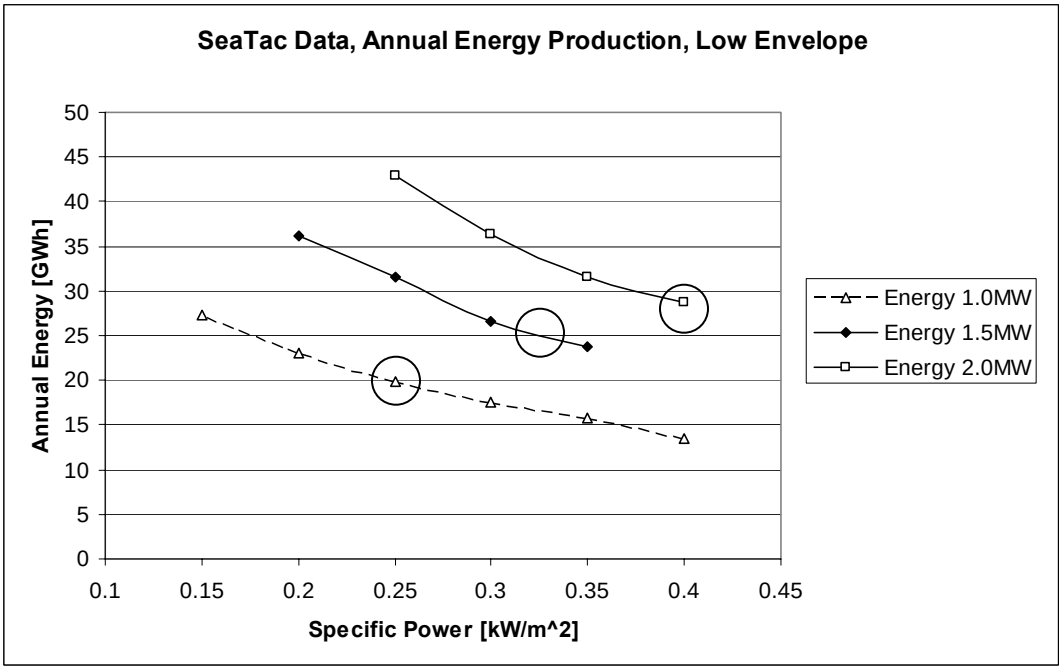

Figure 43. Annual Energy Capture for SeaTac Data, Low Envelope

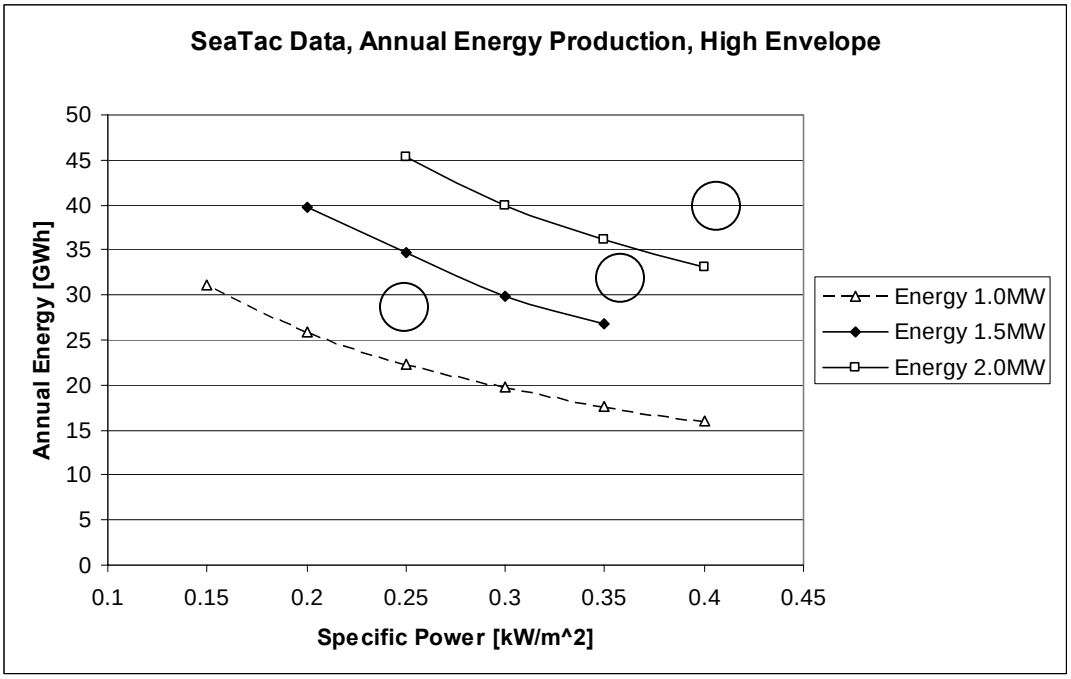

Figure 44. Annual Energy Capture for SeaTac Data, High Envelope

The results from the Beall data analysis show that 26GWh of energy can only be produced at the minimum COE if more wind turbines are installed. An additional three to six turbines would need to be installed to produce the 26GWh for the Beall data high and low envelopes respectively. This is assuming that the additional turbine sites have the same average annual energy production potential as the original ten sites.

A turbine design with a lower specific power and/or a higher hub height could also be used to produce 26GWh if it is necessary to maintain only ten turbine sites. For example, the Beall data high envelope results would require ten 1.5MW turbines to have specific powers of 0.25kW/m^2 and 80 meter towers to produce 26GWh annually. However, this would increase the cost of energy for the high envelope from 11.5¢/kWh to 11.7¢/kWh.

The analysis using the SeaTac data shows that roughly 26GWh of energy could be produced at the minimum COE with no additional turbines. For the low envelope, about

25GWh could be produced from ten 1.5MW turbines. For the high envelope, about 27GWh could be produced from the ten 1.5MW turbines.

2.4 Future Component Cost Reduction

There are a number of wind turbine systems and components that are still areas of active design improvements, including the blade airfoil shape, the speed control system, the gearbox, and the electrical generation system. For example, with more carbon fiber being used in rotor blades, concepts of an airfoil shape that changes with increasing wind speed to maximize efficiency using the inherent properties of composites, called flap-twist coupling, may be coming closer to reality [32]. These design optimizations can be considered applicable to all wind regimes.

The Low Wind Speed Turbine program of the US Department of Energy calls for a 40-50% reduction of COE for low wind speed sites by 2010 [2]. The WindPACT studies [30,32,39,40] indicate that cost reductions will come in every major system of wind turbines. The description of how technology is expected to change and predicted cost reductions are quantified in the following system description.

2.4.1 Drivetrain

Many conceptual drivetrain designs are reviewed in the WindPACT Drivetrain Design study [30], but the medium speed, single permanent magnet generator design was found to provide the largest decrease in COE from the baseline design. The recent price decrease in permanent magnets helps facilitate this reduction in cost.

The baseline drivetrain design is similar to those incorporated in variable speed machines from GE and several turbine manufacturers in Europe. It consists of a modular bedplate design using a three stage gearbox with the rear bearing integrated into the gearbox. The

gearbox drives a doubly fed generator with a stator that is connected directly to the grid through the turbine pad mounted transformer.

The single permanent magnet (PM) generator drivetrain design integrates the generator, gearbox, mainshaft, and mainshaft bearing into one housing. The housing is supported by a tubular bedplate structure and the drivetrain is enclosed by a fiberglass nacelle cover. The gearbox has only one stage which drives a liquid-cooled permanent magnet generator. A silicon controlled rectifier (SCR) power electronic system is used to passively convert the generator output. Additional filtering and a VAR control component are added at the substation. The overall cost of energy decrease was approximated at 13% from the baseline design. Details are in Appendix F.

2.4.2 Power Electronics

The power electronics system the WindPACT study [30] adopts is a SCR AC-to-AC conversion system as apposed to the current industry trend of insulated gate bipolar transistor (IGBT) AC-to-AC conversion system. The IGBT systems have been developed from apparently similar industries for motor-controllers and grid-tied converters. Since these systems were not designed for wind turbines, they have undesirable characteristic for wind turbine applications. The IGBT system requires large amounts of filtration and an isolated DC bus. This design suffers inefficiencies and increased costs for additional transformers. The development of new advanced algorithmic methods for controlling the SCR's produces better output wave forms, extremely low dV/dt (changes in voltage relative to changes in time) which reduces the need for filtering, and a high efficiency. At the same time the SCR system eliminates the need for DC isolation [38].

2.4.3 Self-Erecting Tower and Nacelle

Similar to the WindPACT drivetrain design study [30], the self-erecting tower and nacelle study [39,40] investigated numerous designs and strategies for erecting wind turbine towers and nacelles. The self-erecting towers and nacelle installation strategies seek to minimize the cost of cranes, crane transport, and crane pads required for installation. Of the many strategies investigated, the Barnhart designed climbing frame with a counterbalance weight [39] was found to reduce the cost of tower and nacelle erection significantly. This strategy is shown in Figure 45.

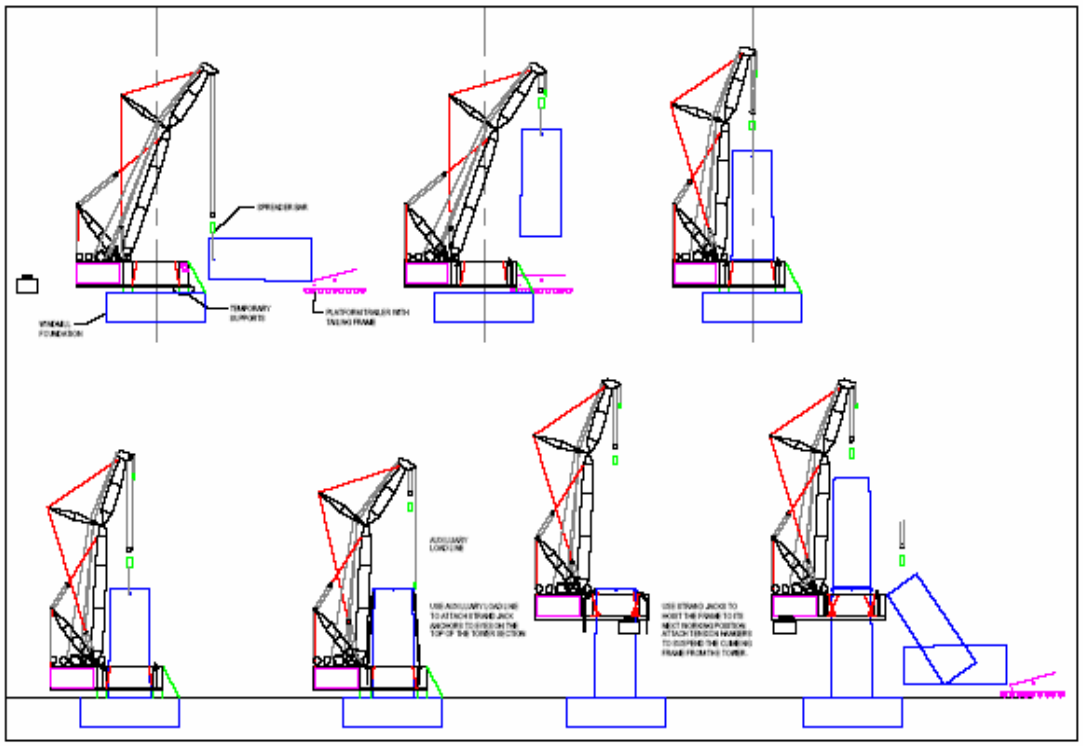

Figure 45. Self-Erecting Tower Concept [39]

The Barnhart climbing frame is comprised of a pair of longitudinal truss members attached to either side of the turbine tower. Another pair of truss members is secured to these trusses forming a box around the tower. A boom, mast and jib are crane structures that are attached to the trusses with sufficient capacity to lift the turbine components. An

engine and hoist are also mounted to the frame to provide the power to lift of the turbine parts. Counterbalance weights move along a track on the underside of the frame to counterbalance the loads that are being lifted. A pair of strand jacks is installed on each section during installation in order for the climbing frame to lift itself via cables to the top of the next section.

The adjustments to the component cost model include an elimination of the crane pad cost, a reduction in the crane cost, and a reduction in the installation cost. A support crane would be necessary to assist in assembling the wind turbine, but this could be accomplished with a much smaller and less expensive crane than those required for traditional installation. Without the need for a large crane, there is no need for a large and expensive crane pad to be constructed for each turbine. In addition, the cost of assembling and disassembling the large crane for each site using the traditional installation methods would be avoided, driving down the overall installation costs.

The WindPACT study [39] had Barnhart estimate the costs to design and build the climbing frame, transport the frame to the wind farm site, and install the wind turbine using the climbing frame. These costs, turbine hub heights, and quantity of turbines in the wind farm are developed into a linearly interpreted lookup table. The table is included in Appendix F.

2.4.4 Rotor Design

The WindPACT Rotor Design study [32] investigates the effects of rotor blade design changes. The study found that three features had beneficial effects for entire turbine configurations investigated:

- Tower feedback in the control system
- Incorporation of flap-twist coupling in the blade
- Reduced blade solidity in conjunction with higher tip speeds

Tower feedback controls and flap-twist coupling decrease loads on the turbine which result in smaller section modulii, weights and costs of many components. However, flap-twist coupling calls for the inclusion of expensive carbon fibers into the blades and coning of the blades (an angling of the blades away from the tower) to achieve sufficient stiffness to avoid tower contact. Reduced blade solidity with higher tip speeds reduces the weight of the rotor and the loads on the turbine as well.

The effects of these features were quantified in the WindPACT study [32] by incorporating the features into a turbine load model which identifies new component sizes and weights. A comparison of the reduced component sizes and weights with those of the baseline case is performed here and conclusions are drawn for the effects on the cost model for the Maury Island study. The following effects are applied:

- Rotor solidity is changed from 0.05 to 0.038
- The rotor blade mass is reduced by 50%
- The hub mass is reduced by 50%
- The bedplate mass is reduced an additional 5% after the effects of the rotor and hub masses are accounted for
- The tower diameters and thickness are reduced an additional 10% after the effects of the rotor solidity are accounted for

2.4.5 COE with Technical Improvements

The technical changes and cost improvements are applied to the Maury Island wind farm model. The analysis assumes that ten 1.5MW turbines are installed in the same manner as in the original analysis. COE results for both the Beall data and the SeaTac data are discussed below.

The COE reductions using the Beall data are significant. The minimum COE for the low and high envelopes are reduced from 11.5¢/kWh and 17.8¢/kWh to 8.5¢/kWh and 13¼ ¢/kWh, respectively. This is a reduction of about 25%. Also apparent is the increase in energy capture of 2-4GWh at the optimum specific power. This is partially due a decrease in the optimum specific power. The optimum specific power decreases mainly because of the cost reduction in the rotor warranting an increase in the optimum rotor diameter and energy capture. The results of the optimum turbine parameters, COE and the annual energy capture for the ten turbines are shown in Table 16.

Table 16. Optimum Turbine Parameters for Beall Data

Turbine Parameter	Low Envelope	High Envelope
Rotor Diameter [m]	88	88
Generator Rating [MW]	1.5	1.5
Tower Height [m]	70	70
Specific Power [kW/m^2]	0.25	0.25
COE [¢/kWh]	13.25	8.5
Annual Energy [GWh]	18	25

The COE for the SeaTac data analysis also decreases while the annual energy capture increases. The COE reduces from 8¢/kWh and 10¼¢/kWh for the high and low envelopes to 6¼¢/kWh and 8¢/kWh, respectively. Similar to the Beall data results, this is a reduction of about 25% in COE. The optimum specific power also goes down due the cheaper rotors facilitating larger optimum rotor diameters. The results are shown in Table 17.

Table 17. Optimum Turbine Parameters for Beall Data

Turbine Parameter	Low Envelope	High Envelope
Rotor Diameter [m]	80	80
Generator Rating [MW]	1.5	1.5
Tower Height [m]	70	70
Specific Power [kW/m^2]	0.30	0.30
COE [¢/kWh]	8	6.25
Annual Energy [GWh]	28	31

2.5 Summary and Conclusions

This chapter identifies the minimum COE for a ten turbine wind farm on Maury Island by determining the optimum wind turbine design for the Maury Island wind regime. A turbine design and cost model is developed that functions as a tool to assess the COE while varying the rotor diameter, generator capacity, and tower height. These turbine parameters are used for tailoring the wind turbines to the Maury Island wind regime.

The minimum COE is found to range between 8 and 17.8¢/kWh depending on the wind regime assumed. The SeaTac data low envelope result is probably the most realistic wind resource estimate in this study and has a minimum COE of 10.25¢/kWh. The optimum specific power is 0.325kW/m^2 with turbine design characteristics of 1.5MW generator rating, an 83.5m rotor diameter, and a 70m tower height. Slight differences with previous studies are easily explained, and the COE of this study may well be slightly high because of the conservative approach to the study. The ten turbines would be sufficient to produce 26GWh of energy annually for the SeaTac data high and low envelope results, but three to six more turbines would be necessary for the Beall data high and low envelope results.

Over the next ten years, design improvements and cost reductions in the turbine subsystems may reduce the COE by 25%, bringing it down to 6.25 to 13.5¢/kWh. The SeaTac data low envelope result would fall to 8¢/kWh. Improvements are expected in the rotor, drivetrain, tower and power electronics.

3.0 Grid Integration and Energy Storage

Wind energy is by nature an unpredictable and variable energy source. These characteristics make the energy produced from a wind farm less valuable for two reasons. The first is the ancillary cost imposed back onto the wind farm due to the necessity of the grid operator to keep reserve generators online to maintain grid balance between load and generation. The second is that the wind may come at times of low energy demand and therefore low market price. Incorporating energy storage into wind energy systems can have economical benefits for a wind farm by mitigating these two phenomena.

Chapter 3 investigates the impact of the Maury Island Wind Farm on the Puget Sound Energy (PSE) grid. The goal is to determine the financial costs that PSE is likely to require for integrating the wind farm. Additionally, the economic benefits of adding an energy storage system to the wind farm are assessed.

The Chapter 3 outline is as follows:

3.1 Grid Operation Background and Wind Energy Impacts: This section discusses the operation of electrical grids and how wind energy impacts this operation. It is important for a wind farm developer/operator to understand the system with which the wind farm is integrating.

3.2 Wind Speed Forecasting: The wind speed forecasting methodologies that are used to predict wind farm energy output are introduced in this section.

3.3 Integration Timescales Definitions: The three time scales for grid operation are defined. These time scales are important for understanding how wind energy will impact grid operation.

3.4 Ancillary Services and Previous Studies of the Financial Impacts of Wind Energy Integration: In this section, ancillary services and their necessity for wind integration are discussed. Previous studies into the cost of ancillary services for wind integration are also presented.

3.5 Maury Island Wind Farm Forecasting Errors and Impact on Puget Sound Energy System Forecasting Errors: This section estimates the energy production forecasting errors from the Maury Island wind farm, the PSE system, and the PSE system with the Maury Island wind farm interconnected. These errors will facilitate the estimation of the financial impact of interconnecting the Maury Island wind farm into the PSE system.

3.6 Financial Impacts of Interconnecting the Maury Island Wind Farm: The costs for interconnecting the Maury Island wind farm to the PSE grid are estimated in this section.

3.7 Energy Storage: A system study into the financial benefit of an energy storage system is discussed in this section including an optimal system design description.

3.8 Summary and Conclusions

3.1 Grid Operation Background and Wind Energy Impacts

In any energy supply grid, the energy generation must be balanced with the loads on the grid by a grid operator in real time. This is done not only by matching the instantaneous generation with the load by ramping up or ramping down generators, but also by planning which generators a grid operator should have on line the following day based on capacity and economic considerations. The balancing of the generation and the load therefore occurs over a significant range of timescales. Short term fluctuations in load are matched using automatic generation control (AGC) software that sends electronic signals to

generators to ramp up or down. However, some generators may take hours to warm up or cool down between operational periods and so must be coordinated well in advance [41].

The stochastic nature of wind energy makes the balancing of generation and loads a more difficult task for the grid operator. Since an operator is unable to count on the predicted production of energy from a wind farm, the operator must have traditional generating sources online that are able to be ramped up or ramped down according to the difference in predicted and actual production from a wind farm. Often, the reserve generators are not loaded to the capacity for which they are purchased because the wind farm energy output differs little from the predicted output [41]. In other words, operator may keep more reserve generation on line than is necessary to account for the actual wind energy forecast error.

The grid load demand itself is unpredictable in nature and analysis of the increase in variability of the grid from integrating wind energy should reflect this. Fluctuations of wind power need not be met by counter fluctuations in generation from other sources; it is the fluctuation in the aggregate load that must be met by corresponding changes in the aggregate generation. Therefore, balancing of the grid must be done through the correlated components from the generation and load aggregates [41]. For example, a utility predicts the load demand on its system for an hour to be 1000MW. It schedules 990MW of fossil fuel generation and 10MW of wind farm generation. However, the load demand on the system turns out to only be 900MW and the wind farm produces only 5MW. In this case the wind farm forecast error assisted the utility because the utility had to ramp down only 95MW of generation instead of 100MW of generation. This example shows that it is the aggregate load and aggregate demand that must be matched by the grid operator: the grid operator did not need to ramp up a generator to meet the 5MW that the wind farm fell short.

3.2 Wind Power Forecasting

Wind energy is not a preferred source of energy because it cannot be produced on demand. However, wind energy can be "firmed up" if good prediction methodologies are employed. If the amount of wind energy that a wind farm will produce is known, it can become a more valuable source and would require less ancillary services from the grid operator. This is what makes wind speed prediction and forecasting highly valuable.

Forecasting and prediction methods are becoming increasingly better at determining the wind conditions for wind farms [41]. Since accurate forecasts can be quite valuable to a wind farm, accurate methodologies are desired. There are two basic types of forecasting techniques: statistical and meteorological.

3.2.1 Statistical Forecasting

Statistical forecasting involves using power or wind data from a previous time to predict the power output from a wind farm in the future. The most basic method uses a persistence model where the predicted value in power from a wind turbine in the next unit of time (e.g. the next 10 minutes or hour) is equal to the current power output:

$$\hat{P}_k = P_{k-1}$$

Where: P_{k-1} = the current power output

$\hat{P}_k$ = the predicted power at a later time, $t + \Delta t$

More complex models use more data points than just the single previous data point. These models are called autoregressive (AR) models [26]. Autoregressive models may use previous errors between predicted and actual data points, as well as exogenous data such as measured wind speed to further refine predictions. These models are termed autoregressive moving average (ARMA) and autoregressive moving average exogenous

(ARMAX) models [26]. Other models that have been developed to improve predictions include techniques utilizing recursive least squares, neural networks, fuzzy logic, wavelet-based methods, diurnal variations, and meteorological forecasts [26, 53].

3.2.2 Meteorological Forecasting

Meteorological forecasting involves the use of global weather models, meso-scale models and boundary layer models for predicting weather and wind speeds. These models are discussed in Sections 1.1.2 and 1.1.4. The integration of these models with statistical forecasting methodologies provides for the best available prediction of wind farm power outputs. These predictions are given to the grid operator for use in integrating the wind farm into the grid.

3.3 Integration Timescales

The cost of integrating wind energy into a grid is a function of the ancillary generating capacity necessary to backup the expected capacity of the wind farm. Forecasts of expected wind generation must be supplemented by maintaining excess generating capacity to make up for expected power that may not be produced. The three time scales for the planning and operating an electrical utility are day-ahead, load-following, and regulation.

3.3.1 Unit-commitment (day-ahead)

The unit-commitment time frame has a horizon of one day to one week with one-hour time increments [44]. Typically, utilities and regional transmission operators (RTOs) schedule generators to provide power 12 hours in advance of the subject day. The generators are largely scheduled according to their operating cost (or bid) [42]. A power output forecast is provided by a wind-farm operator this time.

3.3.2 Load following (intra-hour balancing)

The horizon for load following is one hour with five to 10-minute increments (intra-hour) to several hours (inter-hour) [44]. Load following is the matching of electrical generation with electrical load in these timescales. In typical operation, a system operator will match generation to load by running an economic-dispatch model every five to 10 minutes to determine the least cost combination of increasing or decreasing on line generator outputs with the use of unscheduled generators. These unscheduled generators are providing load following ancillary services [42].

3.3.3 Regulation

Regulation has a horizon of one minute to one hour with one to five-second increments [44]. Automatic-generation-control (AGC) systems automatically respond to correct minute-to-minute load imbalances in the system by dispatching those generators providing regulation ancillary services [42]. These generators provide what is often referred to as *spinning reserves* because they must be online and spinning to react within a minute of request.

3.4 Ancillary Services and Imbalances

Generation and load on the electrical grid must be balanced to North American Electric Reliability Council (NERC) control standards. These are limits imposed on statistical quantities of over and under generation as percentage levels of occurrence in a year and magnitude of occurrence. The wind farm operator is ultimately responsible for imbalance charges created by the wind farm. These imbalance charges incurred in each of the integration time scales have differing costs defined by the type of back up generating capacity necessary to cover the imbalances [47]. These charges represent the difference in cost of the utility integrating a firm energy source of the same capacity versus the wind farm during a period of time. It is not easy to define these costs

universally because they are dictated by what generators are available in the particular grid area at a given time. Definitions and a discussion of previous studies of ancillary services for wind energy integration follow.

3.4.1 Regulation Definition

Regulation power sources are characterized as being online, and connected to automatic generation control that can respond rapidly to system-operator requests for up and down movements. AGC is used to track the minute-to-minute fluctuations in system load and to correct for unintended fluctuations in generator output to comply with NERC's Control Performance Standard (CSP) 1 and 2 [41]. The typical duty cycle of regulation power sources is characterized by responses within about one minute to continuously correct grid imbalance fluctuations, and ranges from two to 10 cycles per hour [45].

3.4.2 Spinning Reserve Definition

Spinning reserve power sources are online and synchronized to the grid. They can increase output immediately in response to a major generator or transmission outage and can reach full output within 10 minutes to comply with NERC's Disturbance Control Standards (DCS). The typical duty cycle is an immediate response reaching full power within about 10 minutes and providing full power for up to two hours, called upon five to 20 times per year [45].

3.4.3 Supplemental Reserve Definition

Supplemental reserves are the same as spinning reserve, but need not respond immediately. These units can be offline, but still must be capable of reaching full output within the required 10 minutes. Typical duty cycles for supplemental reserves are full power within about 10 minutes which providing full power for up to two hours, called upon five to 20 times per year [45].

3.4.4 Replacement Reserve Definition

Replacement reserves are the same as supplemental reserves, but with a 30-minute response time rather than 10 minutes. They are used to restore spinning and supplemental reserves to their pre-contingency status. The typical duty cycle of replacement reserves is full power within about 30 minutes which providing full power for up to two hours, called upon five to 20 times per year [45].

3.4.5 NREL Nation-wide Review Study

The NREL nation-wide review study [44] summarizes the analytic frameworks and estimated costs of wind integration from several studies. The study found the following key points:

- Ancillary costs of low levels of wind power are low, but rise with increasing wind penetration.

- The cost is driven by the uncertainty in the unit-commitment time frame, or day-ahead market. Improving the accuracy of the wind forecast will result in lower cost of ancillary services.

- At high penetration levels (proportional levels of wind power in a power system), the cost of required reserves is significantly less when the combined variations in load and wind plant output are considered, as opposed to considering the variations in wind plant output alone.

- Even at moderate wind penetrations, the need for additional generation to compensate for wind variations is substantially less than one-for-one (i.e. 1MW of additional generation for 1MW of scheduled wind power) and is generally small relative to the size of the wind plant.

A summary of the studies performed to estimate the ancillary costs of wind energy integrations are in Table 18. These studies investigate integration costs for wind energy at multiple penetration levels and integrating with grids comprised of different resource mixes.

Table 18. Summary of Wind Integration Cost Estimate Studies [44]

		$/MWh			
Study	Relative Wind Penetration (%)	Regulation	Load Following	Unit Commitment	Total
UWIG/Xcel	3.5	0	0.41	1.44	1.85
PacifiCorp	20	0	2.50	3.00	5.50
BPA	7	0.19	0.28	1.00-1.80	1.47-2.27
Hirst	0.06-0.12	0.05-0.30	0.70-2.80	Na	Na
We Energies I	4	1.12	0.09	0.69	1.90
We Energies II	29	1.02	0.15	1.75	2.92
Great River I	4.3				3.19
Great River II	16.6				4.53
CA RPS Phase I	4	0.17	na	na	na

3.4.6 A Study of Impacts of Wind Generation on the Puget Sound Energy System

Puget Sound Energy (PSE) hired an outside consultant, Golden, to perform an impact assessment of integrating varying amounts of wind energy into the PSE system [46]. The study assessed the impacts to PSE regulation, operating reserves, hour-ahead and day-ahead balancing. Golden used two sources of wind data for the analysis: wind speed data from six anemometer towers located near Ellensburg, and wind energy output data from the 25MW Columbia River Basin (CRB) wind farm which sells energy to PSE. The data are available for ten minute increments. The day-ahead and hour-ahead wind energy forecast from the CRB windfarm are utilized in the day-ahead and load-following impact costs.

The wind energy impacts on the PSE system are unique from other systems because the PSE system is subject to additional operating constraints of the Mid-Columbia (Mid-C) dams (including the Wells, Rocky Reach, Rock Island, Wanapum and Priest Rapids dams [59]). Typically, the Mid-C is operated such that the largest allowable amount of water is run through the dam during on-peak times, and the least allowable amount during off-peak times. Minimum and maximum allowable water flow constraints leveraged by environmental and recreational concerns result in constraints on minimum and maximum generation availability. Wind generation affects the optimum operation of the Mid-C by necessitating a larger degree of flexibility of generation capacity, or in other words, larger off-peak sales and smaller on-peak sales. In addition, a "dual-constraint" exists when only a small range of water flows is allowed for dam operation. During these conditions, the Mid-C dam may not have the flexibility to account for errors between forecasted and actual wind generation, and PSE may be required to purchase or sell energy on the open market. The results are shown in Table 19.

Table 19. Wind Energy Impacts to PSE Power System [46]

Wind Generation Net Capacity [MW]	Regulation [$/MWh]	Operating Reserves [$/MWh]	Hour-Ahead Costs [$/MWh]	Day-Ahead Costs [$/MWh]	Total Costs [$/MWh]
25	0.16	0	2.72	0.84	3.73
50	0.16	0	2.73	0.84	3.73
100	0.16	0	2.75	0.84	3.75
150	0.16	0	2.78	0.84	3.77
200	0.16	0	2.81	0.83	3.80
250	0.16	0	2.85	0.84	3.85
300	0.16	0	2.89	0.83	3.88
350	0.16	0	2.93	0.83	3.92
300	0.16	0	2.97	0.82	3.96
450	0.16	0	3.01	0.89	4.06

The cost of regulation that Golden estimated for wind energy does not change with the installed generation capacity and is small. This is consistent with most other studies [42, 47]. The lack of a fluid intra-hour trading market in the Pacific Northwest, coupled with

the limited flexibility of the Mid-C result in hour-ahead impact costs that are much greater than those assessed in other studies. In the analysis of estimated forecasted and actual wind generation imbalance impacts, Golden may not be considering the impact of wind energy forecast errors combined with the forecast errors of the PSE system (the aggregate imbalance). Failure to consider the aggregate system imbalance would likely skew assessed cost impacts towards much higher values. This is because PSE would be accounting for the wind farm forecast error separately instead of the entire PSE system imbalance of which the wind farm would be only a part.

Extrapolating the results of the PSE system study for a 15MW wind farm (the size of the proposed Maury Island wind farm), the total impact costs of the Maury Island wind farm would be $3.70/MWh or about $96,000 per year for 26GWh of energy per year. The extrapolated results are shown in Table 20. These extrapolated results will be compared with the results of the analysis in the next section.

Table 20. Wind Energy Impacts to the PSE System Extrapolated to 15MW

Wind Generation Net Capacity [MW]	Regulation [$/MWh]	Hour-Ahead Costs [$/MWh]	Day-Ahead Costs [$/MWh]	Total Costs [$/MWh]
15	0.16	2.70	0.84	3.70

3.5 Maury Wind Farm Integration into PSE System Analysis

The ancillary service costs incurred by PSE for interconnecting the Maury Island wind farm will realistically be passed onto the wind farm operator. The wind farm operator is therefore quite interested in these costs. A statistical analysis is necessary to determine the ancillary service costs, and will be carried out in the following steps:

- Determine the power forecasting errors of the Maury Island wind farm for the
  1. day-ahead,
  2. load-following,

3. and regulation timescales.

- Determine the load forecasting errors of the PSE system before and after the Maury Island wind farm is integrated for the
  1. day-ahead,
  2. load-following,
  3. and regulation timescales.

- Determine the cost of ancillary services incurred to PSE due to the wind farm integration.

The ideal situation to perform this analysis would be to have coincident real time data on a minute-by-minute basis for both the PSE grid generation and load, and the wind farm's power output. However, no real time data are available from PSE and only 10 minute wind velocity data are available from the Beall anemometer for four months. The analysis that follows therefore must make assumptions to quantify ancillary service costs.

3.5.1 Maury Island Wind Farm Day-Ahead Forecast Error

The impact assessment of the day-ahead forecast error from a wind farm on Maury Island can be done with the available wind data using a bounding technique. Simple forecast error boundaries can be used to bound the day-ahead forecast error by assuming that the wind farm power forecast is either the daily average or monthly average power output [42]. The daily average power output should be closer to the actual output for the day of interest than the monthly average energy output.

For the day-ahead forecast error, the SeaTac data for the year 1997 is used. Each velocity is correlated to a power output of the ten proposed turbines. A matrix referred to here as the "Power Lookup Table" is created by averaging the power output for each wind speed and each directional sector from the four envelopes developed in Chapter 1 (Beall high

and low envelopes, and SeaTac high and low envelopes). Turbines with 1.5MW ratings, 0.32kW/m^2 specific powers, and 70 meter towers are assumed. The Power Lookup Table transforms the velocity measured by the SeaTac anemometer to an average predicted power output from the ten turbines on Maury Island. The total yearly energy output (for 1997) from the wind farm using the Power Lookup Table is 23.5GWh. This is well within expected yearly variation from 26GWh. It is satisfactory for an analysis of wind energy integration impacts.

The lower boundary for the day-ahead forecast error was found by summing the difference in wind farm output based on the hourly average wind speed and the wind farm power output based on the daily average energy output [42].

$$E_{daily,1} = \frac{\sum_{n=1}^{24} \left| P_{ave,d} - P_{hour,n} \right|}{24 P_{ave,d}}$$

Where: $P_{ave,d}$ = average daily power

$P_{hour,n}$ = power for hour n

The daily average hourly error was summed for the year and averaged. The lower error bound was found to be 1515kWh. This is about 65% of the average hourly energy generation, 2350kWh.

The upper boundary for the day-ahead forecast error was found by summing the difference in wind farm power output based on the hourly wind speed and the wind farm power output based on the monthly average wind speed [42].

$$E_{daily,2} = \frac{\sum_{n=1}^{24} \left| P_{ave,m} - P_{hour,n} \right|}{24 P_{ave,m}}$$

Where: $P_{ave,m}$ = monthly average power

$P_{hour,n}$ = power for hour n

The daily average hourly error was again summed for 1997 and averaged. The upper error bound used for this analysis was found to be 2350kWh. This is 100% of the average hourly energy generation.

To make a simple and clear analysis, a single value for the average day-ahead forecast error is preferred. The day-ahead forecast error used for further analysis assumes the average value of the upper and lower bounds previously developed. The results are shown in Table 21.

3.5.2 Maury Island Wind Farm Load-Following Forecast Error

Load-following forecast errors have previously been calculated using prediction models such as persistence or ARMA models. In reality, the load-following forecast error will be the error between the actual wind farm power output and the forecast energy power on an intra-hour basis (such as ten minutes). Use of a persistence model and 10-minute wind velocity data will give a conservative assessment of load-following error that can be expected for a real wind farm [42].

For the load-following error, Beall data is used for about 4 months from December, 2005 through March, 2004. Similar to the day-ahead forecast error analysis, the Power Lookup Table is used to transform wind velocity data into wind farm power output values. One additional step is used: the Beall-SeaTac correlation coefficients are applied to the wind speed data. This transforms wind speed data from the Beall anemometer site to the predicted power output for the ten proposed turbines at Maury Island.

A simple persistence model is developed for the analysis. The load following error is calculated for each ten-minute increment using the hourly average energy forecasted by

the persistence model and the calculated 10-minute energy production from the wind farm. The load following absolute average hourly forecast error and standard deviation are shown in Table 21.

3.5.3 Maury Island Wind Farm Regulation

To asses the regulation forecast errors, data is needed in at least one minute increments [48]. Since the SeaTac and Beall data were taken in hourly increments and ten-minute increments respectively, a separate assessment here of regulation impacts is not possible. However, the work done for both PSE [46] and the Bonneville Power Administration (BPA) [42] show that regulation costs would be minimal. The cost derived by Golden for PSE is used here at a rate cost of 0.16$/MWh [46]. At a production rate of 26GWh of energy per year, the total cost that would be imposed onto the wind farm would be $4,160.

The estimated forecast errors (or cost impact) for the Maury Island wind farm for the day-ahead, load-following and regulation timescales are shown in Table 21.

Table 21. Maury Island Wind Farm Estimated Hourly Forecast Errors

Forecast Error Time Frame	Absolute Average Error [kWh]	Absolute Standard Deviation [kWh]
Day-ahead	1930	2020
Load Following	1000	1460
Regulation	0.16$/MWh	

3.5.5 PSE Forecast Errors

While the PSE forecast errors are unknown, some conservative assumptions can be made to represent them. The average electrical load for the PSE system in 2004 was 2268 MW or about 19.97 TWh of energy per annum [49]. Hirst found that the BPA day-ahead

forecast was quite accurate [42]. The day-ahead and load following error averages and standard deviation for BPA were found to be between 3% and 5%.

The assumption of an accurate forecast error for PSE will provide conservative estimates for wind integration impacts, since the wind energy forecast errors will have a larger relative effect on the combined forecast errors. Based on the average connected load of PSE, the day-ahead and load following errors of PSE were calculated based on similar errors to those of BPA as a percent of load.

Table 22. Estimated PSE Forecast Errors

	Absolute Average Error		Absolute Standard Deviation	
Forecast Error Time frame	Value* [MW]	Percent of Load	Value* [MW]	Percent of Load
Day-ahead	79	3.5	64	2.8
Load Following	57	2.5	45	2

* Based on an average connected load of 2268MW

3.5.6 Combination of Maury Island and PSE Forecast Errors

Considering the cost impact of the wind farm forecast errors alone does not correctly represent the integration of wind energy into an electric grid. The forecast errors of the wind farm will help to offset the forecast errors of the integrating utility about 50% of the time [42]. Therefore it is necessary to consider both the PSE load forecast errors and the forecast errors of the Maury Island wind farm in concert.

A real time data analysis for the Maury Island wind farm integrated into the PSE grid was not possible due to lack of real time data from PSE; therefore, statistical assumptions of the two forecast errors must be made. It is assumed here that both the PSE forecast errors for the day-ahead and load-following timescales, and the forecast errors for the Maury Island wind farm are normal distributions with a mean about zero and standard deviations found in the previous sections. This means that PSE is assumed to not err more on the

positive side than the negative side for load forecast errors. This is also assumed true for the Maury Island wind farm forecast errors.

3.5.6.1 Combining Averages

The summation of the estimated PSE energy forecast error and the estimated wind farm energy forecast error is the summation of two random variables. The linear combination of random variables requires the sum of the average of the two random variables [50]:

$$FEA_{PSE+wind} = FEA_{PSE} + FEA_{wind}$$

Where: $FEA_{PSE+wind}$ = the average forecast error for PSE and wind farm combined
FEA_{PSE} = the average forecast error for PSE
FEA_{wind} = the average forecast error for the wind farm

Since the average forecast error of the Maury Island wind farm and the assumed average forecast errors for the PSE errors are both zero for the day-ahead and the load-following timescales, the sum of the average forecast errors is zero.

3.5.6.2 Combining Standard Deviations

The question of how the standard deviations of the two errors combine is a question of how correlated the forecast errors are in both the day-ahead time frame and the load-following time frame. The three cases to be considered here are a perfect negative correlation, no correlation, or a perfect positive correlation. Hirst found that the day-ahead forecast errors are uncorrelated [42]. The forecasting errors in both the day-ahead and the load-following time frame are assumed to be perfectly uncorrelated in this analysis. The total standard deviation for a perfectly uncorrelated system is [50]:

$$\sigma_{total} = \sqrt{\sigma_{PSE}^2 + \sigma_{wind}^2}$$

Combining the standard deviation for the PSE forecast errors and for the Maury Island wind farm forecast errors according to this equation for the day-ahead and load-following time frames yields the results in Table 23.

Table 23. Combined Standard Deviation of Hourly Forecast Errors.

	Load Following [MW]	Day-ahead [MW]
PSE System	45	64
Maury Wind Farm	1.46	2.99
PSE System w/ Wind Farm	45.02	64.03

It is worthwhile to note that if real time data were known for both the PSE load forecast errors, and the Maury Island wind farm forecast errors were available, a statistical analysis could be done in both the load-following and day-ahead time frames to find the correlation of the two errors.

3.5.7 Ancillary Services Cost Analysis

The average price quoted for 2003 for ancillary services are listed in Table 24. The California costs for spinning reserves per hour are used for the analysis which follows.

Table 24. California and New York Average Ancillary Service Prices for 2002 [45]

Service	NY East	NY West	CA
--	$/MW-hr	$/MW-hr	$/MW-hr
Regulation	18.63	18.63	13.69
Spinning Reserve	3.04	2.82	3.89
Supplemental Reserve	1.51	1.37	1.57
Replacement Reserve	1.23	1.23	0.86

Assuming a normal distribution of forecasting errors, cumulative distribution functions are used to model the hourly average absolute errors of the PSE system with and without the Maury Island wind farm. These cumulative distribution functions are comprised of discretized buckets representing a small range of errors (similar to the velocity buckets of the cumulative distribution function in Chapter 1). The probability of each bucket is based on the standard deviations developed for the PSE system forecast errors with and without the wind farm. Average hourly costs are calculated for both the day-ahead and load-following impacts. The cost of additional reserves for integrating the wind farm is about 0.26 $/MWh or about $6,630 per year for 26GWh of annual energy production. This amount is very small because of the very small penetration of wind into the system (about 1%). The results are shown in Table 25.

Table 25. Estimated Financial Impacts of Maury Island Wind Farm on PSE System

Regulation	Load Following	Day-ahead	Total
0.16 $/MWh	0.052 $/MWh	0.043 $/MWh	0.26 $/MWh
4160 $/yr	1350 $/yr	1120 $/yr	6,630 $/yr

3.5.8 Comparison of Financial Impacts with Those of PSE Study

The analysis done here reaches much different conclusions than those done for the PSE system. This analysis finds that integrating a 15MW wind farm into the 2268MW PSE grid results in very small change in the system forecasting errors. The total ancillary service cost per year including regulation, load following and day-ahead time frames for the system would be about $6,630. The projected ancillary cost for the wind farm from the PSE study would result in a total yearly cost of $96,200. The results are compared in Table 26.

Table 26. Comparison of Financial Impacts of Maury Island Wind Farm on PSE System

Results	Regulation [$/MWh]	Load-Following Costs [$/MWh]	Day-Ahead Costs [$/MWh]	Total [$/MWh]	Total Cost for 26GWh/yr [$]
PSE [46]	0.16	2.70	0.84	3.70	96,200
Maury Island Study	0.16	0.052	0.043	0.26	6,630

It is quite possible that the PSE study analyzed only the impacts of forecasting errors from a wind farm and not the impacts on the system forecasting error. There is no Federal Energy Regulation Commission (FERC) requirement mandating that a utility assess ancillary costs by the increase in the total system forecasting errors rather than the wind farm forecasting errors only. Additionally, the Maury Island wind farm study is not able to capture additional imbalance costs that would be incurred onto the PSE system. These costs are system dependent and require a thorough understanding of the system [47]. Therefore, it is likely that PSE would require the Maury Island wind farm to pay the larger cost of $96,200 per year (or 3.70$/MWh). This assumption is used in the Energy Storage section which follows.

3.6 Energy Storage

Energy storage comes in many forms; from fossil fuels and dammed waterways to batteries and flywheels. The storage of energy in the form of fossil fuels and dammed waterways represents long term energy storage that has rather large flexibility of when the energy is used. The use of energy storage for shorter timescales has been limited by the economics of storage systems, including timescales such as fractions of a second to one minute [45]. In the US, about 2.5% of the total electric power consumed is cycled through an energy storage facility; mainly pumped hydro, but some utility scale compressed air and battery storage facilities exist [45].

An energy storage system may be economically beneficial to the Maury Island wind farm. The storage system would store energy when the wind farm is producing power above the forecasted amount, and could provide energy when the wind farm is producing power below the forecasted amount. The costs of the ancillary services that would have been imposed for the forecast error would be avoided. Energy storage is ideal for providing regulation or spinning reserves if it is not limited by life cycles, since regulation requires frequent cycles and zero total energy storage [45]. Cycles for an energy storage system are defined as a transition from an inactive state or a state of storing energy to a state of discharging energy, or vice versa. Energy storage can provide regulation services when idle or in concert with another primary function [45].

An additional economic benefit that an energy storage system could provide to the Maury Island wind farm is load shifting. The economic benefit is created by storing energy produced from periods of low energy value (night time) and then discharging the energy to the grid during the periods of high energy value (day time). This action is called load shifting.

3.6.1 Energy Storage Requirements

Energy storage systems may be designed for many different specific applications or combination of applications. An ideal energy storage system for the Maury Island wind farm would perform the following functions:

- Regulation Control: smooth the wind farm power output to that forecasted on a minute to minute basis
- Load Following: maintain the energy output of the system to that forecasted for the hour
- Day-Ahead: maintain the energy output of the system to that forecasted for the hour

- Load Shift: shift the energy output of the wind farm from off peak hours to on peak hours

Energy storage capacity needs generally increase from top to bottom of this list. However, the number of cycles required by the system generally increases from bottom to top of this list since the balancing time frames become smaller and smaller. For an energy system to meet all of these functions, it must be able to accommodate frequent shallow cycles as well as less frequent deep cycles. The storage media must also have a fast response time to meet short-term energy demands (i.e. regulation and load following time frames).

The requirements for regulation and day-ahead support may be neglected because of the small economic impact of these two time frames and the difficult requirements they pose on the storage system. Regulation ancillary services are seen to have the lowest overall cost impact in most studies [42, 44]. The day-ahead ancillary service in this study are almost nil, and represent only about one quarter the cost of the load-following ancillary service impacts in the PSE study [46]. Therefore, the storage system for the Maury Island wind farm only needs to provide load following support and load shifting capabilities.

3.6.2 Energy Storage Options

An investigation into the available energy systems for the Maury Island application revealed that flow batteries are considered the best choices for long duration discharge and long term storage [45]. Some flow batteries also show good response times and are able to endure a large number of cycles without detriment. Flow batteries are recognized as being a good technology for large systems due to their inherent scalability, which offers flexibility in the system design. The design chosen for the Maury Island application is a Vanadium Redox-Flow Battery (VRB) system.

VRBs operate on a reaction between vanadium ions. The reaction is shown below:

Positive Electrode: $V^{4+} \Leftrightarrow V^{5+} + e^-$

Negative Electrode: $V^{2+} \Leftrightarrow V^{3+} + e^-$

Two electrolyte tanks pump electrolytes to the two halves of the cell. At the positive electrode, V^{5+} is converted to V^{4+} by accepting an electron during the charging phase. During the discharging phase, the reaction is reversed. Similarly, at the negative electrode, V^{3+} is converted to V^{2+} by accepting an electron during the discharging phase and vice versa. The two halves of the cell are divided by a proton exchange membrane which allows protons or H^+ ions to pass and complete the electrical circuit. A schematic of a VRB system is shown in Figure 46.

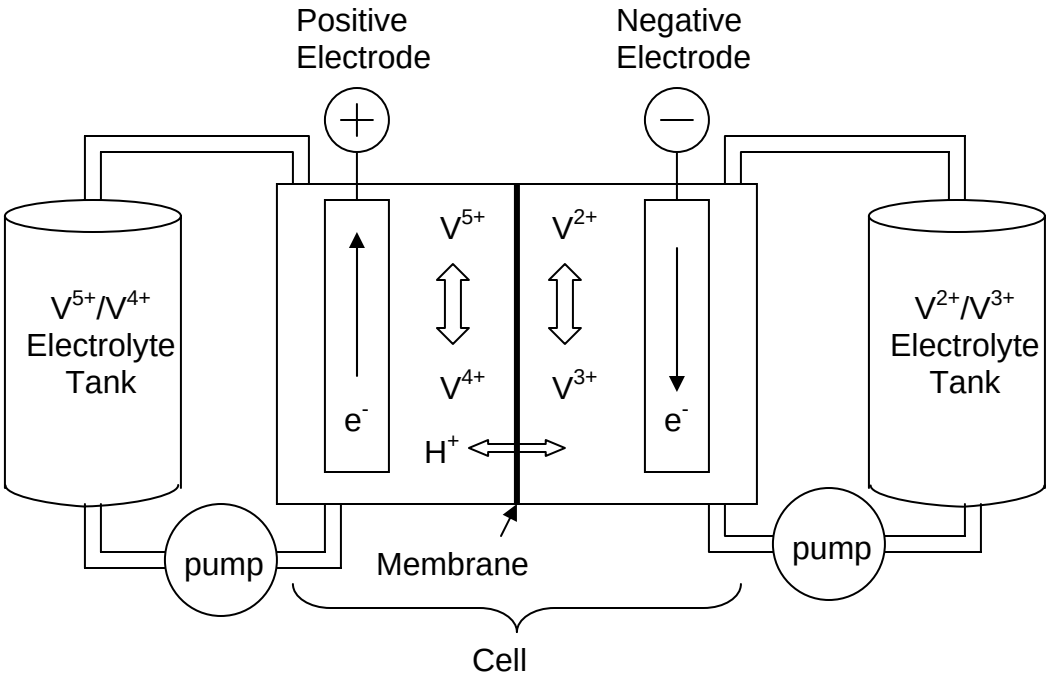

Figure 46. Schematic of Vanadium Redox Battery System

The electrolyte is comprised of a vanadium and sulfuric acid mixture. Electrolyte concentrations and volume determine the amount of energy that can be stored. The battery has an almost instantaneous response time of 350 microseconds [52].

Environmental impact is quite low as the stacks, plumbing and tanks are made of recycled plastics. Additionally, the electrolytes can be refurbished and reused, so no toxic chemicals disposal is required.

VRB systems are already being used in wind systems. They have a long lifetime for deep charge/discharge cycles [52, 45], making them appropriate for stabilization of wind turbine outputs as well as for load-leveling. The round trip efficiency is about 75-80% over the lifetime of the battery.

VRB systems are commercially available and have been used in numerous projects. One application of a VRB system is the stabilization of power output from a wind turbine. The system is able to store or provide 170kW for up to 6 hours. Uninterruptible Power Source (UPS) and peak shaving VRB applications also exist including a system design that is able to store or provide 1.5MW for one hour [45].

3.6.3 Benefits of Energy Storage

The benefit of the energy storage system is quantifiable for the load-following timescale and for load shifting. The load-shifting benefit can be calculated simply by multiplying the energy shifted from off-peak times to on-peak times by the difference in the value of energy (minus the energy losses from the shift). PSE identified the average difference between on-peak and off-peak energy values as $6.74/MWh [51]. This value is quite low compared to other sources [45], but is used since it is accurate to the PSE system.

The PSE study [46] identifies the load following cost of integrating a 15MW wind farm at 2.70$/MWh as shown in Table 26. For the purposes of the energy storage analysis, a

reduction in the load-following forecast error from the wind farm is assumed to correlate to an equal reduction in the cost identified by the PSE study. For example, if the storage system is able to reduce the load following forecast error by 50%, then the assumed benefit is a 50% reduction in load following costs from 2.70$/MWh to 1.35$/MWh.

3.6.3.1 Load Shifting

Load shifting requires the storage system to charge during off peak hours and discharge during on peak hours. The Mid Columbia index (Mid-C) market defines on-peak as 6am to 10pm Monday through Saturday. All other hours including all day Sunday are considered off-peak [51]. The benefits from load shifting are available to be captured 313 days of the year.

The hourly wind velocities and projected hourly energy production is important information when considering load shifting. If the majority of the energy produced at the Maury Island site is during on-peak hours, than the energy storage capacity required to shift all the energy is smaller. Likewise, the more energy that is produced in the off-peak hours, the larger the storage system must be to shift it. The wind velocities at SeaTac for 1997 and the projected energy production of the Maury Island wind farm are shown in Figure 47.

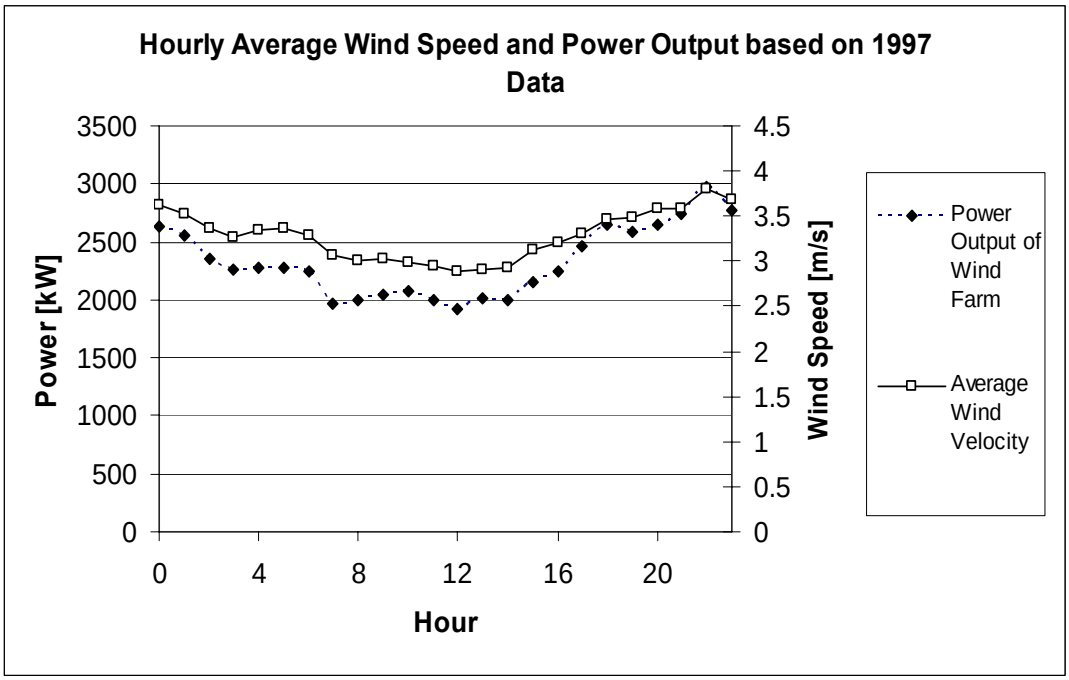

Figure 47. Hourly Wind Speed at SeaTac and Energy Output from the Maury Island Wind Farm

The amount of energy that can be shifted was investigated using a simple system algorithm which charges from 10pm to 6am until fully charged. The storage system would then discharge during the on-peak hours. Three inefficiencies in the system are considered:

1. The power electronic conversion efficiency from the turbine AC output to a DC input to the storage unit, 95%.
2. The storage unit conversion efficiency, 80%.
3. The power electronic conversion efficiency from the DC output from the storage unit to AC input to the grid, 95%.

The total yearly energy that could be stored and the total yearly energy loss are calculated for 1997. The results are shown in Figure 48.

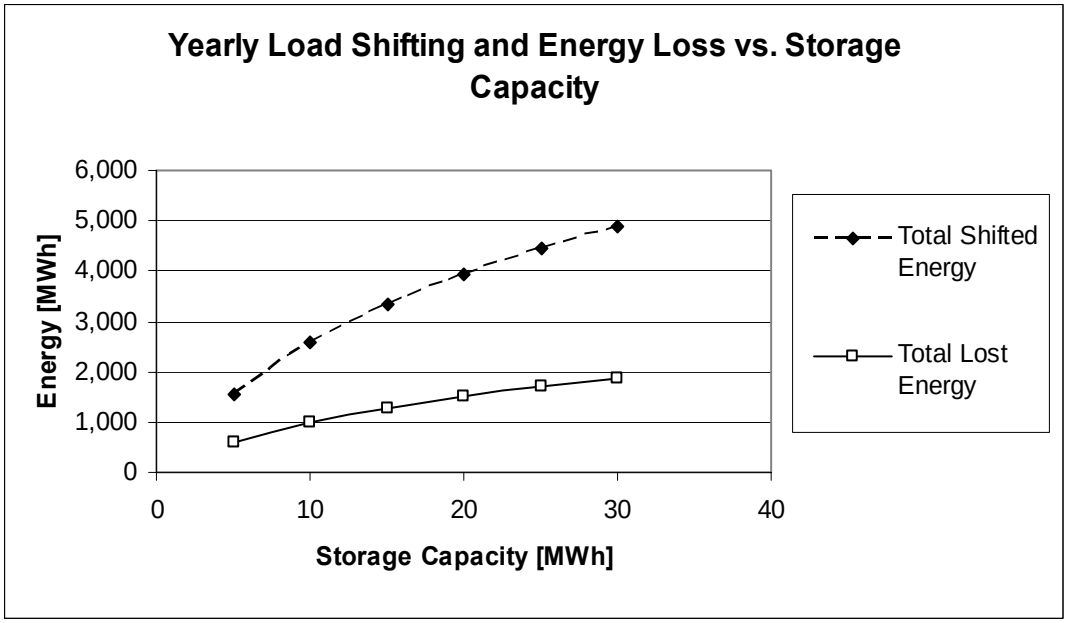

Figure 48. Yearly Load Shifted and Energy Loss.

The amount of energy that can be shifted and the energy loss increase with increasing storage capacity at logarithmic rates.

3.6.3.2 Load-Following Timescale Benefits

The reduction in load-following forecast errors realized through the use of energy storage is quantified by a separate analysis. An algorithm is created that allows the storage system to be charged when the load-following forecast error is positive (actual power greater than predicted power), and for the storage system to discharge when the load following forecast error is negative. The storage system is able to charge until the capacity of the system is reached or discharge until the storage system is fully depleted. Three inefficiencies in the system are considered:

1. The power electronic conversion efficiency from the turbine AC output to a DC input to the storage unit, 95%.
2. The storage unit conversion efficiency, 80%.

3. The power electronic conversion efficiency from the DC output from the storage unit to AC input to the grid, 95%.

The reduction in the average absolute load following error value and the absolute load following deviation are shown in Figure 49. The load following error average and standard deviation are normalized to the wind farm values without any energy storage.

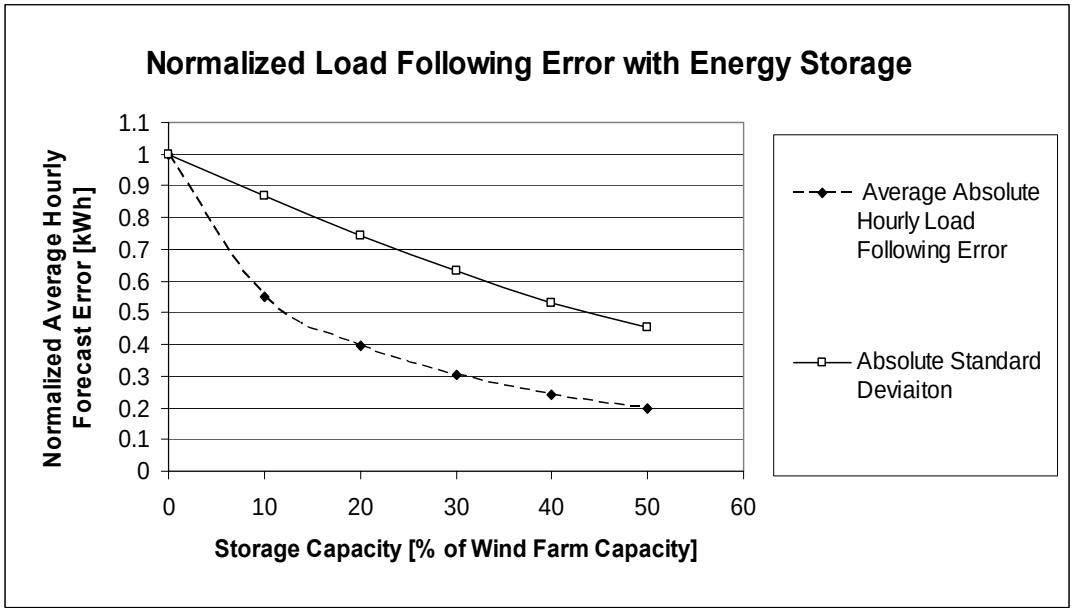

Figure 49. Normalized Load Following Error Reductions with Energy Storage

The reduction in the normalized average absolute load following error is asymptotic. The largest incremental error reduction occurs with a system capacity of 10% of the wind farm capacity with increasing capacity bringing decreasing benefit. The important value to consider in Figure 49 is the average absolute error value, since this is the quantity that PSE is likely to consider according to the study done for them [46].

Energy cycling through the storage system causes energy losses from inefficiencies in the storage and conversion system. The energy losses are shown in Figure 50.

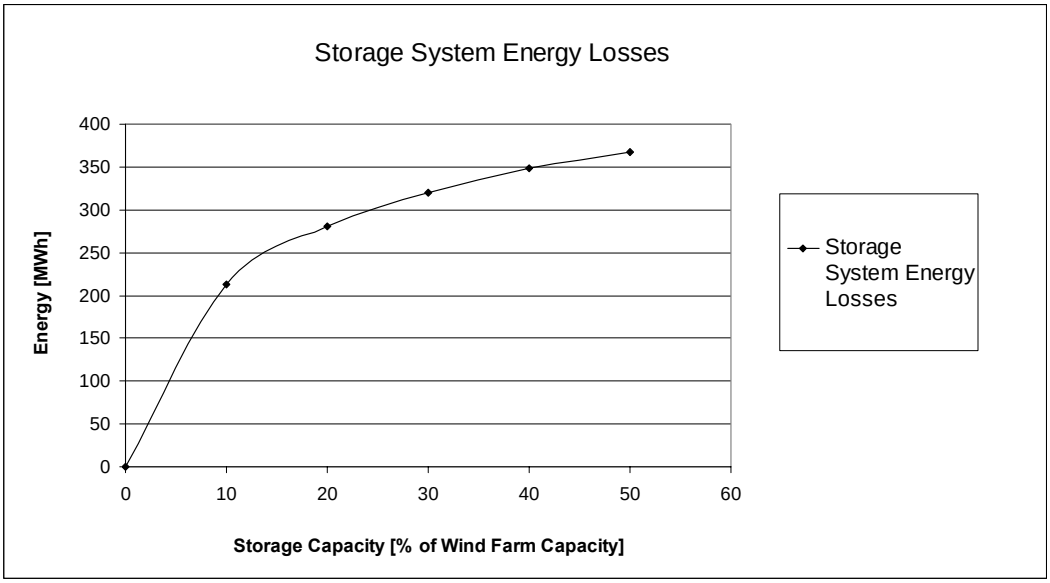

Figure 50. Losses of Energy Storage System for Load Following

The energy losses increase with storage system capacity at a logarithmic rate. They are much lower in the load shifting case (Figure 48) because less energy is being stored and discharged by the storage system.

3.6.3.3 Cost of the Energy Storage System

The baseline energy storage system is assumed to be a full VRB battery system with a twenty year lifetime. Battery cost data from a VRB battery manufacturer is readily available and is used in the analysis [52]. The remaining costs are derived from the DOE study [45].

Table 27. VRB Energy Storage System Costs [45, 52]

System Component	**Cost**
Power Conversion System Initial Cost, $/kW	400
Balance of Plant Initial Cost, $/kW	100
Battery Initial Cost, $/kWh	728*
O$M Cost – Fixed, $/kW-year	54.8
O$M Cost – Variable, $/kW-year	2.4

* From manufacturer quote [52]

3.6.3.4 Value of the Energy Storage System

The value of the energy storage system needs to be compared to the cost of the energy storage system in the present time. The net present value of the energy storage system can be defined by the following equation:

$$PV = \sum_{t}^{n} \frac{NB - O\,\&\,M}{(1+r)^t}$$

Where: PV = the present value of the energy storage, $

NB = the yearly net benefits, $/yr

$O\&M$ = the O&M costs, $/yr

r = the real discount rate, 7.5%

t = time period, years

n = the number of time periods, 20

The yearly benefits for this analysis include the avoided costs of load following ancillary services and load shifting benefits. The avoided cost of the load following services is calculated by multiplying the percent reduction in load following error by the total load following costs (Annual Energy Production in MWh * $2.70/MWh). The benefit from load shifting is calculated by multiplying the total amount of energy shifted by the increased value in energy ($6.74/MWh). The energy losses associated with these benefits must also be included. A value of 3.5¢/kWh or 35$/MWh is assumed for the value of the energy lost. The total net benefits, NB, are thus calculated by:

$$NB = \%LF_{red} * AEP * \$2.70 + AES * \$6.74 - AEL * \$35$$

Where: $\%LF_{red}$ = the percent reduction in load following ancillary services

AEP = Annual energy production from the wind farm in MWh

AES = Annual energy shifted from off-peak to on-peak in MWh

AEL = Annual energy lost due to load shifting and LF mitigation in MWh

3.6.3.5 Economic Analysis

The initial capital cost (ICC) and the present value of the storage system were calculated for storage systems ranging in size from 7.5MWh to 32.5MWh. Comparing the ICC of the system with the present value of the system determines the economic benefit of the energy storage system for the Maury Island wind farm. The results of the analysis show that no economic benefit is gained with the energy storage system. In fact, ignoring the capital cost of the system, the present value becomes negative at about 18MWh capacity as can be seen in Figure 51. This is due to the O&M costs and energy loss costs outweighing the benefit of load shifting and avoided load following ancillary costs.

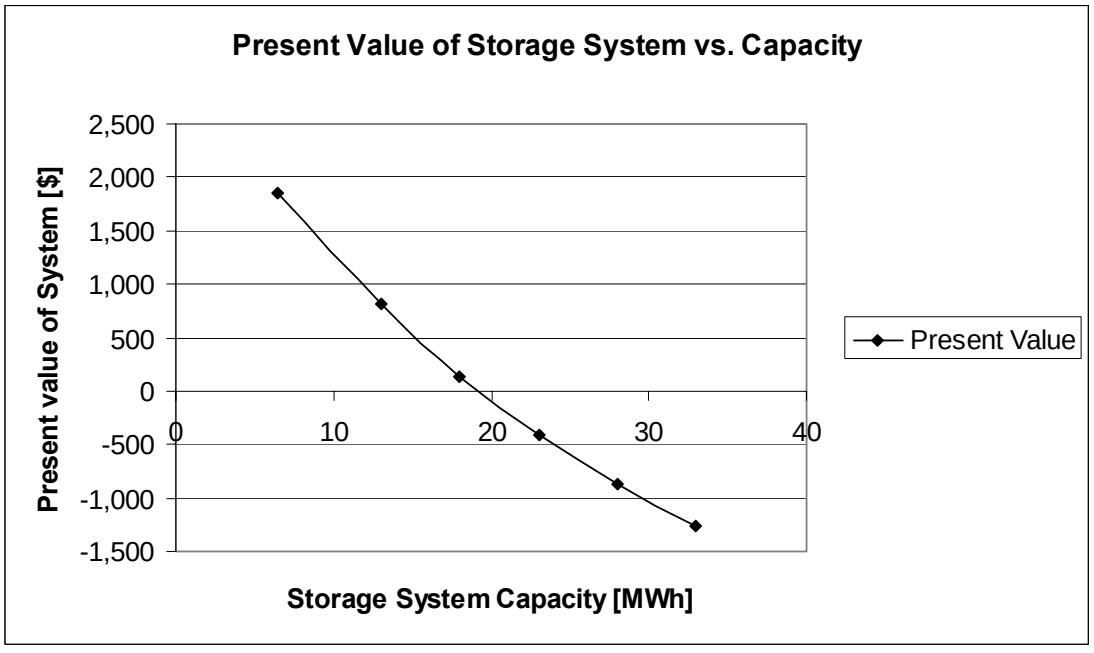

Figure 51. Present Value of the Energy Storage System

A comparison of the present value of the system and the ICC of the system is shown in Figure 52. As can be seen, the ICC is always much greater than the present value of the

system. For the energy storage system to be economically beneficial, the present value would have to be greater than the ICC. This is clearly not the case.

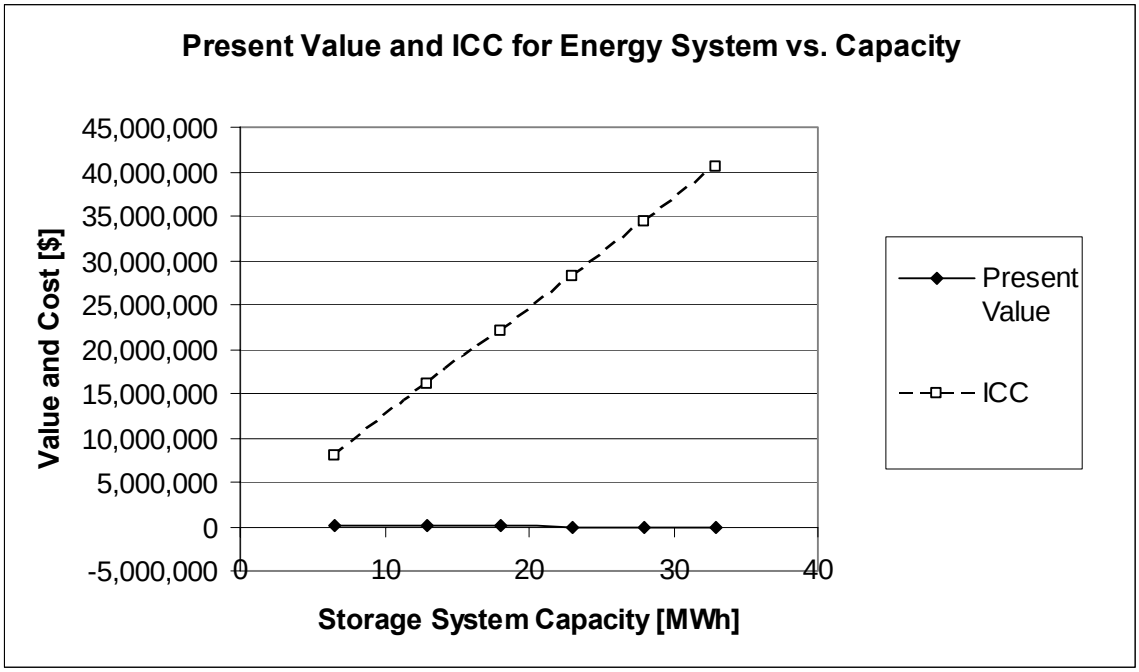

Figure 52. Energy Storage System Present Value and ICC

3.7 Summary and Conclusions

The cost of interconnecting the Maury Island wind farm into the PSE grid is estimated in this chapter and compared with previous studies. The Maury Island wind farm power output forecasting errors are calculated for the three timescales of importance: the day-ahead, the load-following, and the regulation timescales. These forecast errors are statistically combined with those estimated for the PSE system. A cost analysis is developed based on ancillary service costs incurred by the PSE system with and without the Maury Island wind farm integration. The ancillary service costs are much smaller than those found in a similar study done by Golden [46] for PSE. This is likely due to either the lack of information regarding the PSE operational restrictions for the Maury Island wind farm study, or to Golden basing ancillary service costs on the wind farm

power output forecast errors alone and not in combination with the PSE system. The ancillary service cost results are shown in Table 28.

Table 28. Comparison of Financial Impacts of Maury Island Wind Farm on PSE System

Results	Regulation [$/MWh]	Hour-Ahead Costs [$/MWh]	Day-Ahead Costs [$/MWh]	Total [$/MWh]	Total Cost for 26GWh/yr [$]
PSE [46]	0.16	2.70	0.84	3.70	96,200
Maury Island Study	0.16	0.052	0.043	0.26	6,630

An energy storage system design for the Maury Island wind farm is developed, but is not economically beneficial. Vanadium Redox Flow batteries meet the load-following and load-shifting requirements for the wind farm. The benefits of avoided ancillary costs and greater profits on energy shifted from off-peak to on-peak times are inconsequential when compared to the ICC of the energy storage system. Energy losses that occur when cycling energy through the storage system also serve to negate the benefit of the storage system. Since the Maury Island wind farm is a grid-tied system and is not the only energy system for the Vashon/Maury Island community, there is no need for an energy storage system.

Conclusion

A system study is performed here to identify the wind farm that could produce a minimum of 26GWh of energy on Vashon/Maury Island at the least cost of energy (COE). This study characterizes the wind regime at ten proposed wind turbine locations and identifies the optimum turbine designs for the wind regime. Investigations into the effect of technology improvements on the COE and annual energy capture were also investigated. Finally, the costs of integrating the wind farm into the grid are analyzed as well as the potential for energy storage to mitigate these costs.

To determine the wind resource potential of the island, a wind regime analysis is performed. The wind resource assessment is developed from data from the SeaTac airport anemometer and from the Institute for Environmental Research and Education anemometer at the Beall site. Guidelines for assessing surface terrain effects are utilized to determine the wind regime at the ten proposed turbine sites on Maury Island. Weibull distributions and frequencies are developed for thirty degree directional sectors, revealing that the two southwestern sectors represent the largest energy resource by far (50-70%). The average wind speed at 50 meters for the ten turbine sites is estimated to be 4.85 m/s

A rigorous investigation into the optimum wind turbine design reveals the lowest cost of energy and the annual energy production from ten turbines. This is a particularly interesting study because wind turbines are not typically designed for low wind speed regimes such as those in the Puget Sound. The optimum wind turbine is found to have a 1.5MW rating with an 83.5m rotor diameter, and a tower height of 70 meters. The COE best estimate from these turbines is about 10.25¢/kWh. Improvements to turbine system technology are expected to bring the COE down by 25% over the next ten years.

The integration costs of the wind farm are calculated based on statistical estimates of the energy forecast errors in the three integration timescales: day-ahead, load-following and

regulation. The forecasting errors for a wind farm with this small of a capacity compared to those of the integrating utility, PSE, are quite small. The impacts of these forecasting errors are estimated to cost $6,630 a year in ancillary services. However, a study done for the PSE system estimates these costs to be much higher. An investigation of an energy storage system to help mitigate ancillary service costs and to shift loads from off-peak to on-peak hours is performed, but the results show the system to not be an economically beneficial option.

References

1. Northwest Sustainable Energy for Economic Development. Wind Power Maps.org. Retrieved May, 2005 from http://www.windpowermaps.org..
2. Calvert, S., Thresher, R., Hock, S., Laxson, A., and Smith, B. "Low Wind Speed Technology Development in the U.S. Department of Energy Wind Energy Research Program (Preprint)." National Renewable Energy Laboratory. Golden, CO. NREL/CP-500-32512. May, 2002.
3. International Electrotechnical Commission. Safety of Wind Turbine Conversion Systems. 61400-1. 1998.
4. EWEA, European Commission, Directorate-General for Energy. Wind Energy – The Facts. Volume 1: Technology. 2004.
5. Troen, I. and Petersen, E.L. European Wind Atlas. Risø National Laboratory, Roskilde. (1989).
6. US Geological Survey. Burien, Washington, United States 6/13/2002. Retrieved May, 2005 from http://terraserver-usa.com.
7. National Climatic Data Center. Global Hourly Surface Data for SeaTac Airport. Retrieved May, 2005 from http://www.ncdc.noaa.gov.
8. USGS. 7.5' Map of Olalla, Vashon, Gig Harbor, Tacoma North. 2000.
9. Bowen, A.J., Mortensen, N.G. "WAsP Prediction Errors Due to Site Orography." Riso National Laboratory. Roskilde, Denmark. Rido-R-995(EN) December, 2004.
10. Jackson, P.S., and Hunt, J.C.R. "Turbulent wind flow over a low hill." Quart. J. Royal Meteorological Society. 101 (1975).
11. Mason, P.J., and Sykes, R.I. "Flow Over an Isolated Hill of Moderate Slope." Quart. J. Royal Meteorological Society. 105 (1979).
12. Walmsley, J.L., Salmon, J.R., and Taylor, P.A. "On the Application of a Model of Boundary-Layer Flow Over Low Hills to Real Terrain." Boundary Layer Meteorology. 23 (1982).
13. Frank, H.P., Rathmann, O., Mortensen, N.G., Landberg, L. "The Numerical Wind Atlas – the KAMM/WAsP Method." Riso National Laboratory. Roskilde, Denmark. Rido-R-1252(EN) June, 2001.
14. Taylor, P.A. and Lee, R.J. "Simple Guidelines for Estimating Wind Speed Variations Due to Small Scale Topographic Features." Climatological Bulletin. 18(2) (1984).
15. Hunt, J.C.R. "Wind Over Hills." In Workshop on the Planetary Boundary Layer. American Meteorological Society, ed. J.C. Wyngaard. Boston, MA, 1980.

16. Elliot, W.P. "The Growth of the Atmospheric Internal Boundary Layer." Transactions of the American Geophysical Union. 39 (1958).

17. Walmsley, J.L., Taylor, P.A., and Salmon, J.R. "Simple Guidelines for Estimating Wind Speed Variations due to Small-scale Topographic Features – An Update." Climatological Bulletin. 23 (1989).

18. Woods, N. "The Onset of Separation in Neutral, Turbulent Flow Over Hills." Boundary Layer Meteorology. (1995)

19. Hau, E. Wind Turbines Fundamentals, Technologies, Applications and Economics. Springer. Germany. 2000.

20. Seguro, J.V. and Lambert, T.W. "Modern estimation of the parameters of the Weibull wind speed distribution for wind energy analysis." Journal of Wind Engineering and Industrial Aerodynamics. 85 (2000).

21. Lun, I.Y.F., and Lam, J.C. "A study of the Weibull parameters using long-term wind observations." Renewable Energy. 20 (2000).

22. EWEA, European Commission, Directorate-General for Energy. Wind Energy – The Facts. Appendices. 2004.

23. Jackson, K., van Dam, C.P., and Yen-Nakafuji, D. "Wind Turbine Generator Trends for Site-specific Tailoring." Wind Energy. In Press. 2005.

24. Malcolm, D.J., and Hansen, A.C. "WindPACT Turbine Rotor Design, Specific Rating Study." National Renewable Energy Laboratory. Golden, CO. NREL/SR-500-34794. November, 2003.

25. Janganshetti, S.H., and Rau. V. G. "Normalized Power Curves as a Tool for Identification of Optimum Wind Turbine Generator Parameters." IEEE Transactions on Energy Conversion. 16(3) (2001).

26. Burton, T., Sharpe, D., Jenkins, N. and Bossanyi, E. Wind Energy Handbook. Wiley. England. 2001.

27. Griffin, D.A. "WindPACT Turbine Design Scaling Studies Technical Area 1 – Composite Blades for 80- to 120-Meter Rotor." National Renewable Energy Laboratory. Golden, CO. NREL/SR-500-29492. March 2001.

28. Global Energy Concepts, LLC. "WindPACT Turbine Design Scaling Studies. Technical Area 2 – Turbine, Rotor and Blade Logistics. Final Report." National Renewable Energy Laboratory Subcontract YAM-0-320203-01. December, 2000.

29. Harrison, R., Hau, E., and Snel, H. Large Wind Turbines, Design and Economics. John Wiley & Sons, Ltd. 2000.

30. Poore, R. and Lettenmaier, T. "Alternative Design Study Report: WindPACT Advanced Wind Turbine Drive Train Designs Study." National Renewable Energy Laboratory. Golden, CO. NREL/SR-500-33196. August 2003.

31. Shafer, D.A., Srawmyer, K.R., Comley, R.M., Guidinger, J.H., Wilkie, D.C. and Zellman, T.F. "WindPACT Turbine Design Scaling Studies: Technical Area 4 – Balance-of-Station Cost." National Renewable Energy Laboratory. Golden, CO. NREL/SR-500-29950. July, 2001.

32. Malcolm, D.J., and Hansen, A.C. "WindPACT Turbine Rotor Design Study." National Renewable Energy Laboratory. Golden, CO. NREL/SR-500-32495. August, 2002.

33. de Vries, Eize. "Global Wind Technology." RE Wind Power. January 7, 2004.

34. EWEA, European Commission, Directorate-General for Energy. Wind Energy – The Facts. Volume 1: Technology. 2003.

35. Hansen, L.H., Helle, L., Blaabjerg, F., Ritchie, E., Munk-Nielsen, S., Bindner, H., Sorensen, P., and Bak-Jensen, B. "Conceptual Survey of Generators and Power Electronics for Wind Turbines." Riso National Laboratory. Roskilde, Denmark. December, 2001.

36. EWEA, European Commission, Directorate-General for Energy. Wind Energy – The Facts. Volume 2: Costs &Prices. 2004.

37. IEEE Standard 835-1994. Standard Power Cable Ampacity Tables. 1994.

38. "Wind Power Electronics: Achieving Lower Cost, Higher Efficiency, and Superior Reliability." Refocus. May/June, 2004.

39. Global Energy Concepts. "WindPACT Turbine Design Scaling Studies Technical Area 3 – Self-Erecting Tower and Nacelle Feasibility." National Renewable Energy Laboratory. Golden, CO. NREL/SR-500-29493. May, 2001.

40. Global Energy Concepts. "Addendum to WindPACT Turbine Design Scaling Studies Technical Area 3 – Self-Erecting Tower and Nacelle Feasibility." National Renewable Energy Laboratory. Golden, CO. NREL/SR-500-29493A. October, 2002.

41. Parsons, B., Milligan, M., Zavadil, B, Brooks, D., Kirby, B., Dragoon, K., and Caldwell, J. "Grid Impacts of Wind Power: A Summary of Recent Studies in the United States." Draft to be presented at: European Wind Energy Conference. Madrid, Spain. June, 2003.

42. Hirst, Eric. "Integrating Wind Energy with the BPA Power System: Preliminary Study." (Consulting in Electric-Industry Restructuring, Oak ridge, TN. September, 2002.)

43. Bonneville Power Administration. Wind Integration Services. March 2004.

44. Smith, J.C., DeMeo, E.A., Parsons, B., and Milligan, M. "Wind Power Impacts on Electric Power System Operating Costs: Summary and Perspective Work to Date. (Preprint)." National Renewable Energy Laboratory. Golden, CO. NREL/CP-500-35946. March, 2004.

45. EPRI-DOE. Handbook of Energy Storage for Transmission and Distribution Applications. Final Report. December, 2003.

46. Golden Energy Services, Inc. "Short-term Operational Impacts of Wind Generation on the Puget Sound Energy Power System, Phase 2 Studies." (Puget Sound Energy, March, 2005).

47. Dragoon, K., and Milligan, M. "Assessing Wind Integration Costs with Dispatch Models: A Case Study of PacifiCorp." National Renewable Energy Laboratory. Golden, CO. NREL/CP-500-34022.

48. Kirby, B., and Hirst, E. "Customer-Specific Metrics for the Regulation and Load-Following Ancillary Services." Oak Ridge National Laboratory. ORNL/CON-474. January, 2000.

49. Puget Sound Energy. "2005 Least Cost Plan, Chapter VI – Demand Forecast." (Puget Sound Energy, 2005)

50. Montgomery, D.C., and Runger, G.C. Applied Statistics and Probability for Engineers. Wiley. US. 1994.

51. Richardson, Michael, Puget Sound Energy. Phone conversation, April, 2005.

52. VRB Power Systems Inc.. "Executive Summary." (VRB Power Systems, Inc., 2004).

53. Korpas, Magnus. "Distributed Energy Systems with Wind Power and Energy Storage." (PhD Thesis. Norweigian University of Science and Technology. Trondheim. 2004).

54. Milligan, M., Schwartz, M.N., and Wan, Y. "Statistical Wind Power Forecasting for U.S. Wind Farms, Preprint." National Renewable Energy Laboratory. Golden, CO. NREL/CP-500-35087. November 2003.

55. Kottenstette, R., and Cotrell, J. "Hydrogen Storage in Wind Turbine Towers." National Renewable Energy Laboratory. NREL/TP-500-34656. September, 2003.

56. Muller, S., Deicke, M., De Docncker, R.W. "Doubly Fed Induction Generator Systems for Wind Turbines." IEEE Industry Applications. May/June, 2002.

57. Princeton Energy Resources International, LLC, "Preliminary Engineering and Economic Assessment of Energy Consumption and Renewable Energy Production Potential for Vashon-Maury Island." (Institute for Environmental Research and Education, 2004).

58. Chang, J.E. Electrical Cost Data. RS Means. 2004.

59. Puget Sound Energy. "2005 Least Cost Plan, Chapter IX – Electric Resources." (Puget Sound Energy, 2005)

60. Schenck, Rita, Institute for Environmental Research and Education. Meeting 4/24/05.

Appendix A. Wind Resource Figures

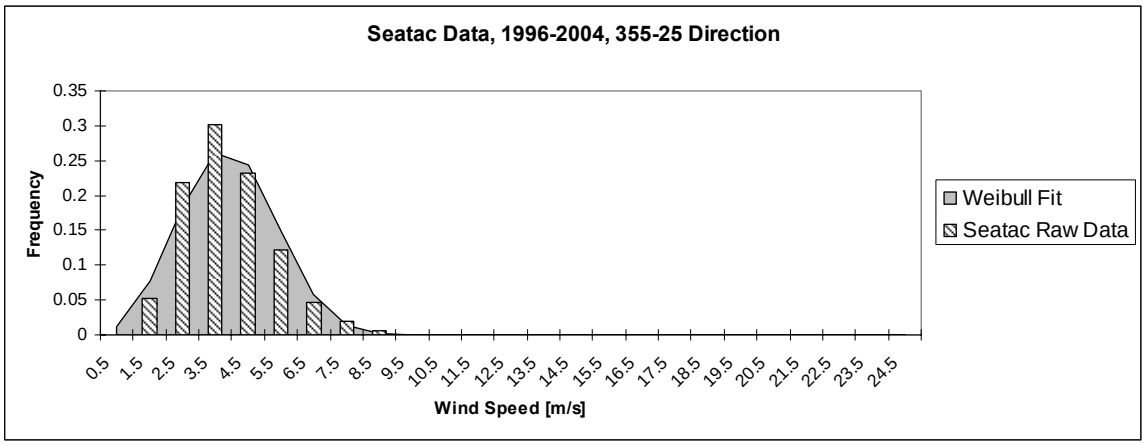

Figure A.1

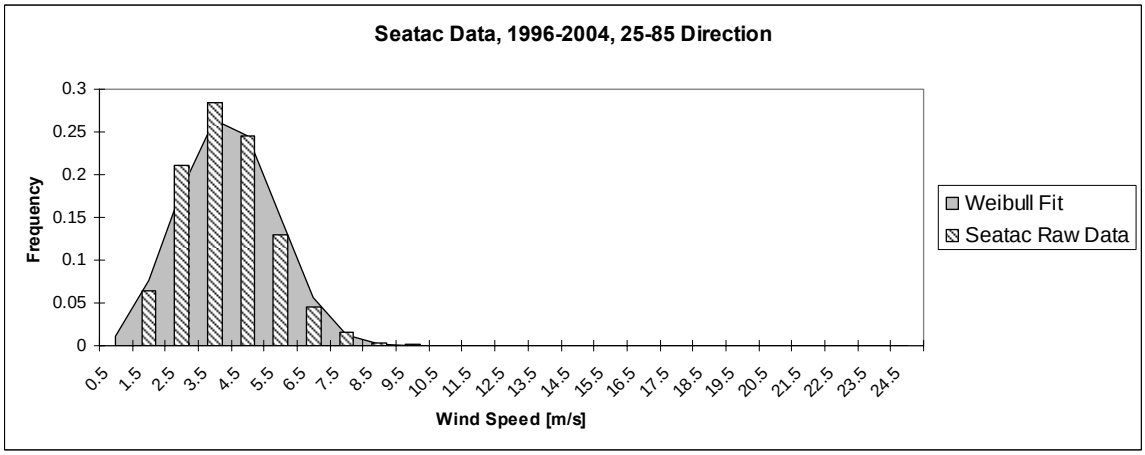

Figure A.2

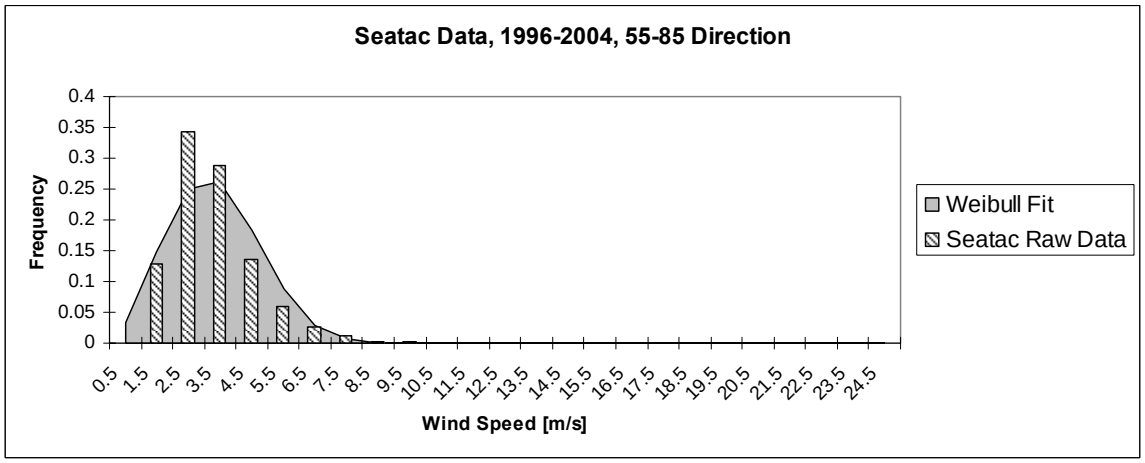

Figure A.3

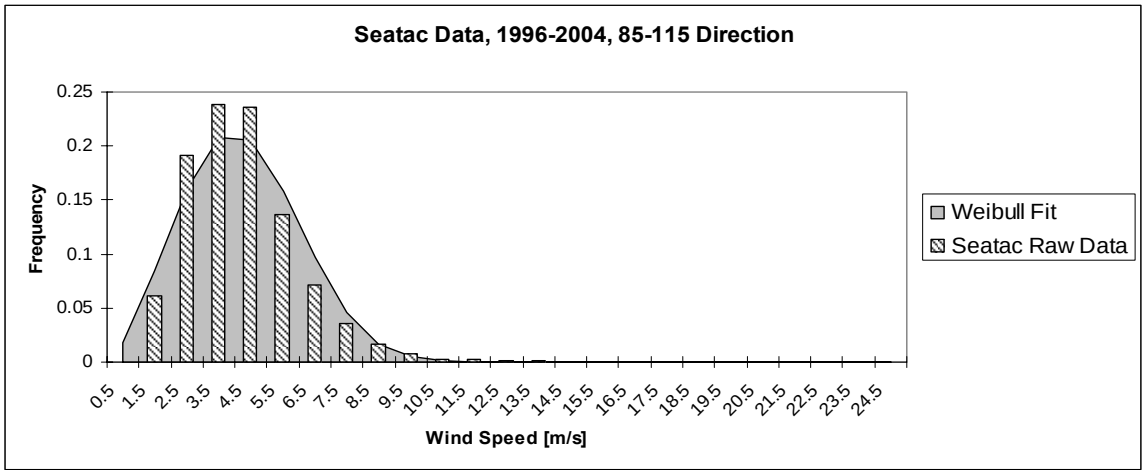

Figure A.4

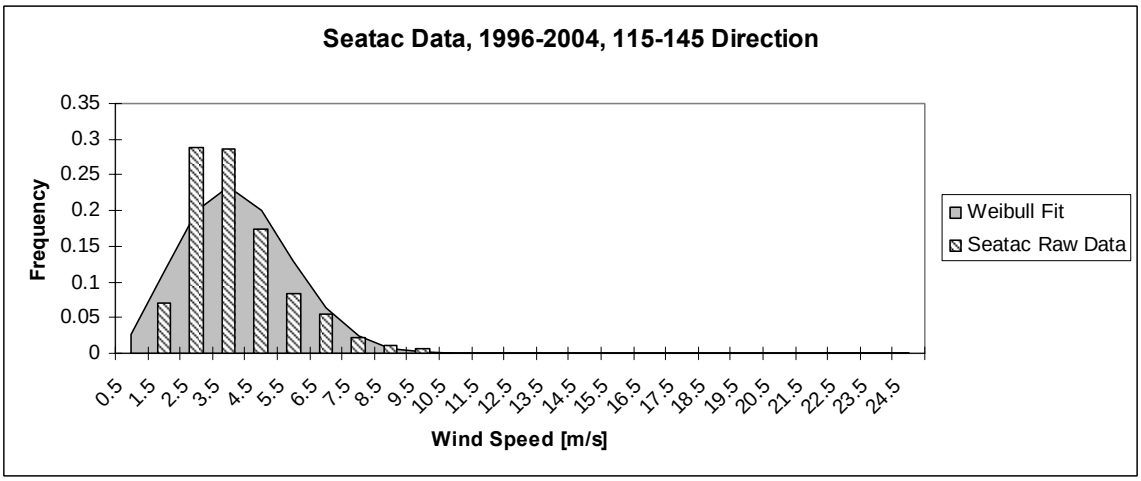

Figure A.5

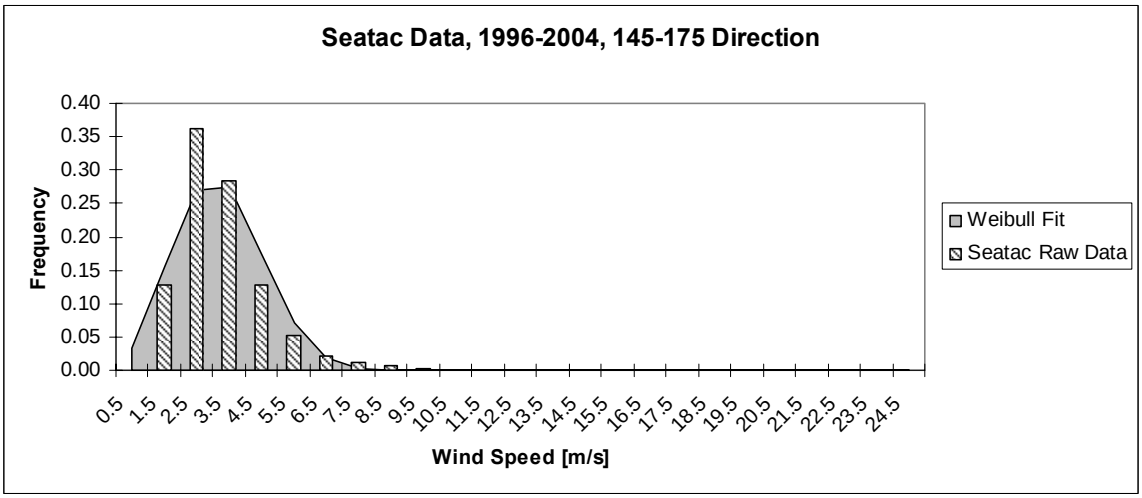

Figure A.6

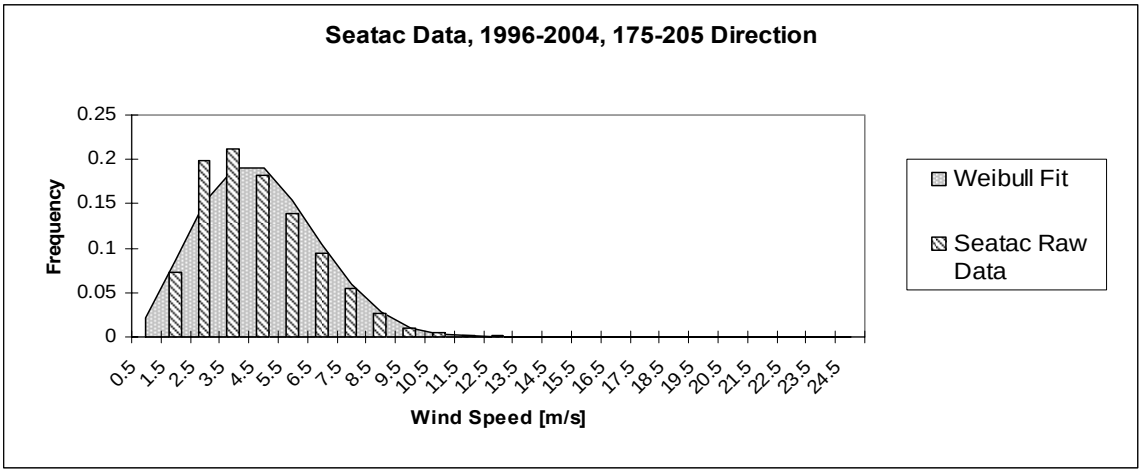

Figure A.7

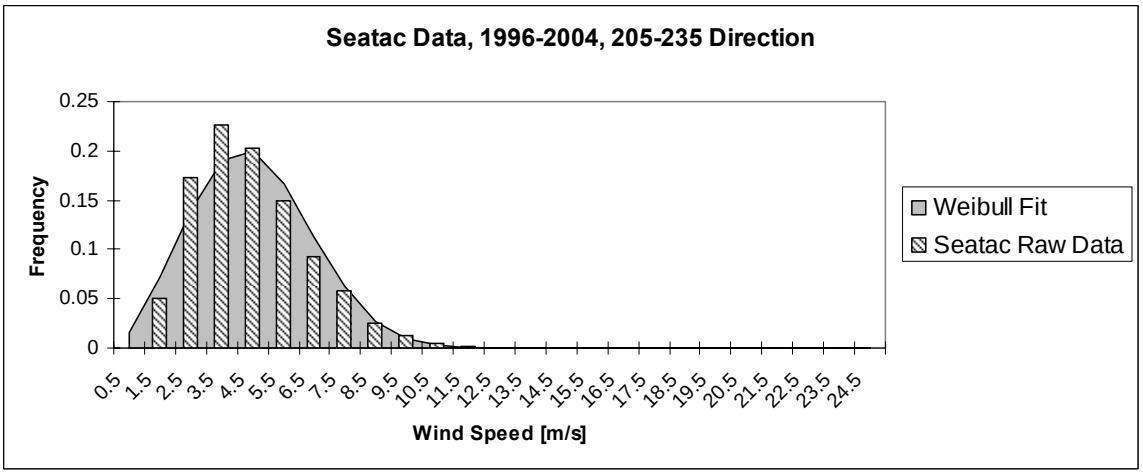

Figure A.8

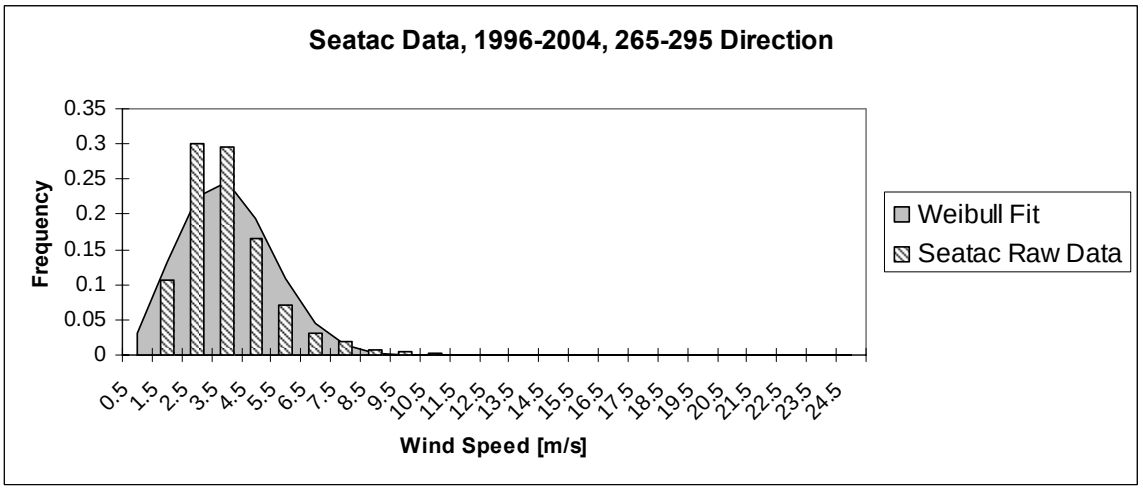

Figure A.9

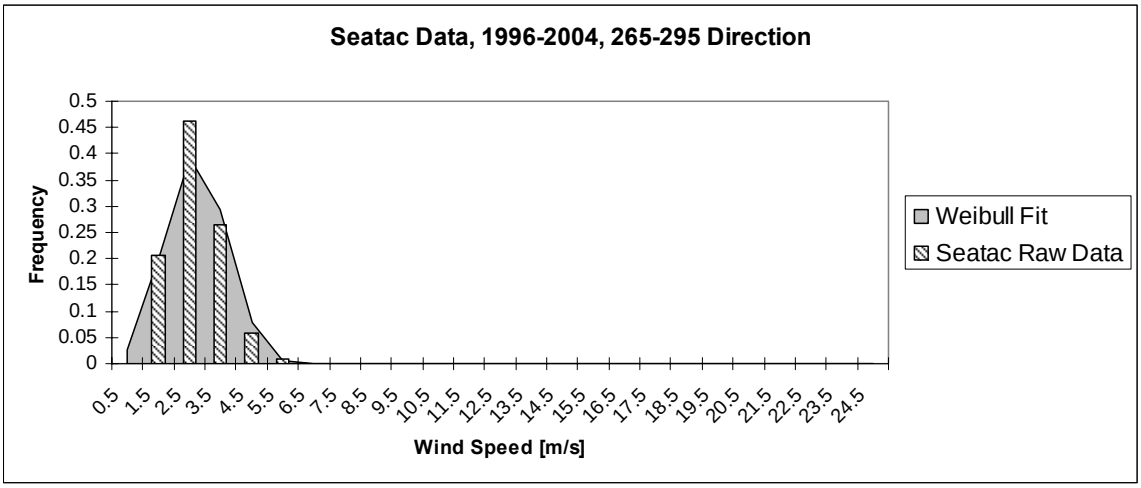

Figure A.10

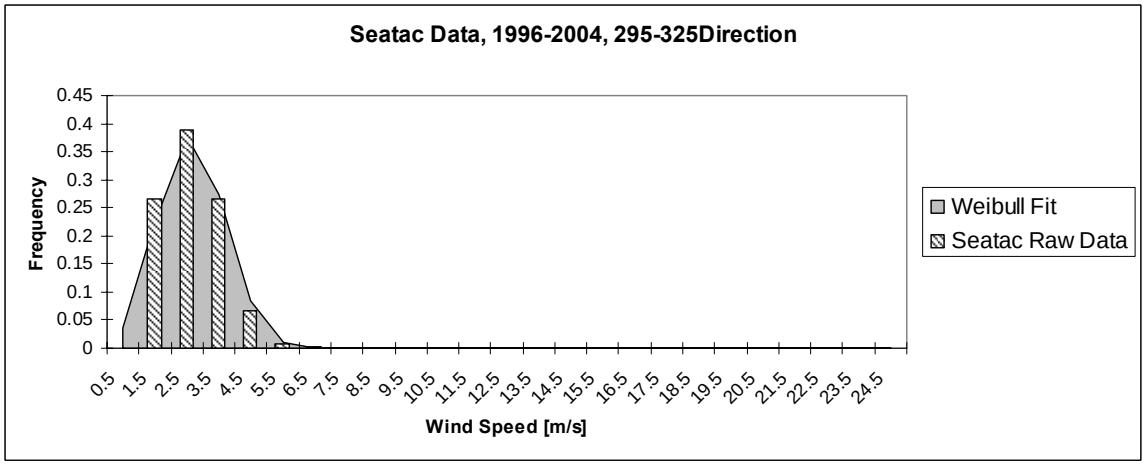

Figure A.11

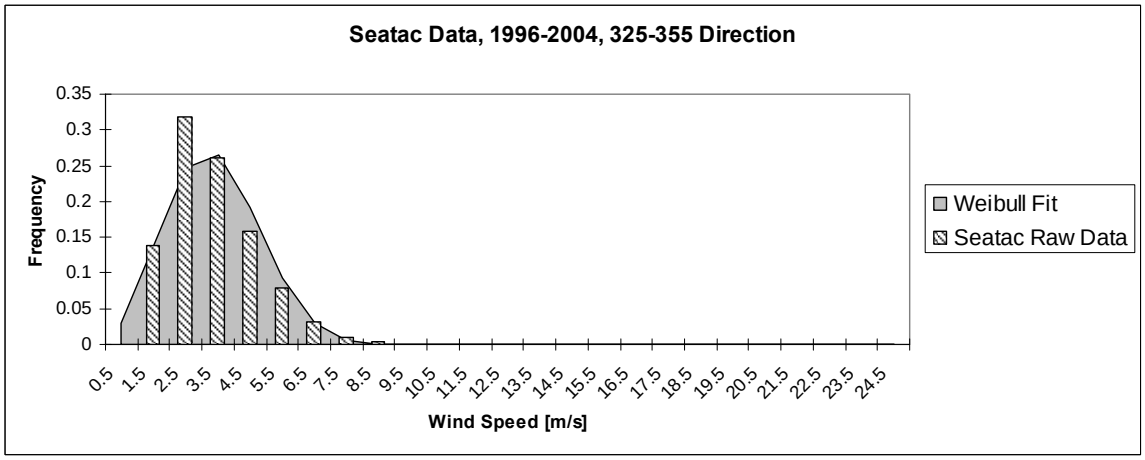

Figure A.12

Appendix B. Turbine Site Description

The turbine site descriptions are given below for the twelve sites and ten directional sectors. The key is as follows:

r = distance to the coastline [m]

h = height of the ridgeline [m]

L = distance to half the total height of the ridge [m]

z_{ou} = roughness length [m]

m = grad of the slope

	Turbine 1					Turbine 2				
Direction	r [m]	h [m]	L [m]	z_{ou} [m]	m	r [m]	h [m]	L [m]	z_{ou} [m]	m
355-25	-	-	-	0.6	-	-	-	-	0.6	-
25-55	-	-	-	0.6	-	-	-	-	0.6	-
55-85	-	-	-	0.6	-	-	-	-	0.6	-
85-115	-	-	-	0.6	-	-	-	-	0.6	-
115-145	-	-	-	0.6	-	-	-	-	0.6	-
145-175	-	-	-	0.6	-	-	-	-	0.6	-
175-205	600	115	400	1.E-03	0.29	500	120	300	1.E-03	0.40
205-235	600	115	300	1.E-03	0.38	600	120	300	1.E-03	0.40
235-265	600	115	400	1.E-03	0.29	-	-	-	0.6	-
265-295	700	115	450	0.01	0.26	-	-	-	0.6	-
295-325	-	-	-	0.6	-	-	-	-	0.6	-
325-355	-	-	-	0.6	-	-	-	-	0.6	-

	Turbine 3					Turbine 4				
Direction	r [m]	h [m]	L [m]	z_{ou} [m]	m	r [m]	h [m]	L [m]	z_{ou} [m]	m
355-25	-	-		0.6	-	-	-	-	0.6	-
25-55	-	-		0.6	-	-	-	-	0.6	-
55-85	900	-		1.E-03	-	500	-	-	1.E-03	-
85-115	600	105	450	1.E-03	0.23	300	105	150	1.E-03	0.70
115-145	500	105	450	1.E-03	0.23	300	105	200	1.E-03	0.53
145-175	350	105	200	1.E-03	0.53	400	105	300	1.E-03	0.35
175-205	300	105	150	1.E-03	0.70	400	105	250	1.E-03	0.42
205-235	400	105	150	1.E-03	0.70	-	-	-	0.6	-
235-265	-	-	-	0.6	-	-	-	-	0.6	-
265-295	-	-	-	0.6	-	-	-	-	0.6	-
295-325	-	-	-	0.6	-	-	-	-	0.6	-
325-355	-	-	-	0.6	-	-	-	-	0.6	-

	Turbine 5					Turbine 6				
Direction	r [m]	h [m]	L [m]	z_{ou} [m]	m	r [m]	h [m]	L [m]	z_{ou} [m]	m
355-25	-	-	-	0.6	-	-	-	-	0.6	-
25-55	-	-	-	0.6	-	-	105	300	0.6	0.35
55-85	500	-	-	1.E-03	-	300	105	350	1.E-03	0.3
85-115	300	115	150	1.E-03	0.77	250	105	200	1.E-03	0.525
115-145	400	115	150	1.E-03	0.77	300	105	150	1.E-03	0.7
145-175	500	-	-	1.E-03	-	400	105	150	1.E-03	0.7
175-205	700	-	-	1.E-03	-	-	-	-	0.6	-
205-235	-	-	-	0.6	-	-	-	-	0.6	-
235-265	-	-	-	0.6	-	-	-	-	0.6	-
265-295	-	-	-	0.6	-	-	-	-	0.6	-
295-325	-	-	-	0.6	-	-	-	-	0.6	-
325-355	-	-	-	0.6	-	-	-	-	0.6	-

	Turbine 7					Turbine 8				
Direction	r [m]	h [m]	L [m]	z_{ou} [m]	m	r [m]	h [m]	L [m]	z_{ou} [m]	m
355-25	-	-	-	0.6	-	-	-	-	0.6	-
25-55	-	-	-	0.6	-	-	-	-	0.6	-
55-85	-	-	-	0.6	-	-	-	-	0.6	-
85-115	200	110	150	1.E-03	0.73	400	130	150	1.E-03	0.87
115-145	250	110	150	1.E-03	0.73	400	130	200	1.E-03	0.65
145-175	300	110	150	1.E-03	0.73	500	130	200	1.E-03	0.65
175-205	300	110	150	1.E-03	0.73	900	130	200	1.E-03	0.65
205-235	-	-		0.6	-	-	-	-	0.6	-
235-265	-	-		0.6	-	-	-	-	0.6	-
265-295	-	-		0.6	-	-	-	-	0.6	-
295-325	-	-		0.6	-	-	-	-	0.6	-
325-355	-	110	1200	0.6	0.09	-	-	-	0.6	-

	Turbine 9					Turbine 10				
Direction	r [m]	h [m]	L [m]	z_{ou} [m]	m	r [m]	h [m]	L [m]	z_{ou} [m]	m
355-25	-	-	-	0.6	-	-	-	-	0.6	-
25-55	-	-	-	0.6	-	-	-	-	0.6	-
55-85	-	-	-	0.6	-	-	-	-	0.6	-
85-115	400	135	250	1.E-03	0.54	-	-	-	0.6	-
115-145	400	135	250	1.E-03	0.54	500	120	150	1.E-03	0.8
145-175	400	135	300	1.E-03	0.45	300	120	150	1.E-03	0.8
175-205	500	135	350	1.E-03	0.39	-	-	-	0.6	-
205-235	-	-	-	0.6	-	-	-	-	0.6	-
235-265	-	-	-	0.6	-	-	-	-	0.6	-
265-295	-	-	-	0.6	-	-	-	-	0.6	-
295-325	-	-	-	0.6	-	-	-	-	0.6	-
325-355	-	-	-	0.6	-	-	-	-	0.6	-

Appendix C. Wind Resource Model Sensitivities

To make a sensitivity comparison, a baseline must be created. The baseline has the following assumptions that will be discussed in the subsequent sections:

Upstream (water) Roughness Length: $z_{ou} = 0.001$
Maury Island Roughness Length: $z_{op} = 0.8$
Beall Roughness Length: $z_{or} = 0.5$
Puget Sound Roughness Length: $z_{ps} = 0.5$
Critical Slope: $\theta_c = 0.6$
Applicable Velocities: $U_{start} > 3$m/s at $\Delta z_r = 49$m

The results of the analysis are in Figure C.1. The assumed parameters and results are discussed subsequently.

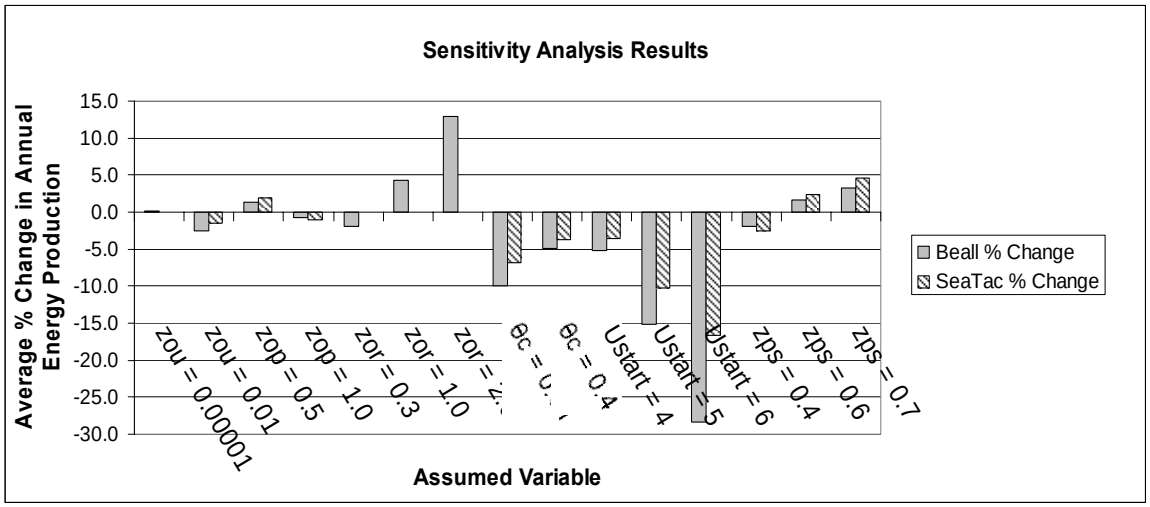

Upstream (water) Roughness Length, z_{ou}

The roughness length of the water upstream of the turbine sites is given in most texts as 10^{-5} to 10^{-3} [4,5,14]. Changing the upstream roughness length produced a small change in the total annual energy from the ten turbines.

Maury Island Roughness Length

The vegetation coverage on Maury Island consists of fairly dense forest. However, unlike much of the forests in the Puget Sound, the forests on Maury Island have large amounts of deciduous trees. The surface roughness lengths for forests vary over a wide range from reference to reference, from $z_o = 0.5$ to $z_o = 6.0$. The effects on the annual energy production due to roughness lengths of $z_o = 0.5$ and $z_o = 1.0$ were investigated. A change in the roughness length for Maury Island did not change the annual energy production values significantly.

Beall Roughness Length

The Beall roughness length analysis produced results of $z_{or} = 0.6$ to 7.4, which are predominantly off the EWA scale [5] and fall largely within the range of suburban areas, forests or city centers according to Taylor and Lee [14], and EWEA [4]. None of these descriptions fit the Beall site very well. It is quite likely that the significant change in roughness lengths surrounding the turbine create high turbulence. Changing the roughness length from the EWA [4] 'shelter belts' case of $z_{or} = 0.3$ to the maximum value of suburban areas according to Taylor and Lee [14] of $z_{or} = 2.0$ had the following effects.

The total annual energy production model is quite sensitive to the roughness length at the Beall anemometer site. A maximum variation of -3 to 21% was found when varying the roughness length from $z_{or} = 0.3$ to 2.0 respectively. Again, it is unlikely that the roughness length is as high as $z_{or} = 2.0$ according to the references used in this study.

Critical Slope

The critical slope of a fill or valley is the slope required to produce a zero surface stress somewhere over the hill [18]. This means that wind flow passing over the hill or valley will begin to separate from the surface. Speed-up factors predicted from the Guidelines

would likely begin to diverge from actual flows. Walmsley, Taylor and Salmon [17] set this limit as $\theta_c = 0.6$. For slopes greater than this, they suggest the slope to be set to 0.6. They argue that this gives reasonable estimates for steep terrain because ΔS_{max} is kept realistic and the speed-up factor has a slower exponential decay with height. Applying the same strategy for the critical angle found by Woods [18] of $\theta_c = 0.31$ and that found by investigation into the EWA [5] software estimates of $\theta_c = 0.4$, produces significant impact on the total annual energy production.

Applicable Velocities

Since wind speeds less than 3m/s are probably dominated by non-aerodynamic effects, the references used in this study suggest applying the guideline estimates to speeds greater than these [14,17]. The references argue that the guidelines are most appropriate for wind speeds greater than 6m/s [14,17]. The model was adjusted to investigate the effect of applicable velocities.

The velocities below the applicable velocity limit are simply adjusted for the surface roughness at the site using the surface layer similarity laws. The effect of this variation on the total annual energy production is quite significant and shows this parameter to be the most sensitive in the model. By taking the applicable velocity limit to be greater than 3m/s, the model will be more conservative than it would be if it used the suggestions from the references.

Puget Sound Region Roughness Length

The roughness of the land surrounding the Puget Sound in the Maury Island vicinity include cities, suburbs and woodlands. An average roughness length is assumed, and here it is varied from $z_{or} = 0.4$ to $z_{or} = 0.7$. The impact of the land surrounding the Puget Sound has only a slight impact on the annual energy production.

Appendix D. Turbine Component and System Design Description and Formulas

This appendix describes the turbine components and systems and their associated weight and cost formulas.

D.1 Rotor Blades

The rotor blades are an important and complex component of wind turbine design. The blades are important to the aerodynamic efficiency which directly influences the energy capture. The loads which the blades experience are due to aerodynamic, dynamic, and static effects. Proper material selection and design techniques must be employed to minimize rotor blade costs. The WindPACT study [32] shows that an approximation to the rotor mass is given by the formula:

$$M_{blade} = 0.21 * (D/2)^{2.89} \qquad \text{[kg]}$$

The WindPACT study [32] found the cost of the blades on a per mass basis to be $10.95/kg for traditional glass fiber and epoxy rotor blades.

D.2 Hub

The hub of a wind turbine is one of its most highly stressed components. These stresses are cyclical in nature (they are the result of rotor forces and moments) and thus the fatigue of the design must be considered to avoid stress concentrations. The three designs used today are welded steel, cast steel and forged components. Forged components offer the best solution for strength and fatigue characteristics, but cast hubs are beginning to become common since they are cheaper and better inspection techniques are available [19]. The WindPACT Rotor Blade and Logistics [28] study gives the hub mass as a function of the rotor diameter as:

$$M_{hub} = 0.24 * D^{2.5765} \qquad \text{[kg]}$$

The cost of the hub is estimated as $4.25/kg [32].

D.3 Pitch Mechanism and Bearings

The pitch mechanism for a turbine rotor allows each blade to pitch separately. The system consists of a bearing, a speed reducer, an electric drive motor (or a hydraulic drive), a controller, and a power supply. Each blade is mounted to the hub on rotating bearings and is turned using a pinion drive. The mass and cost model adopted by the WindPACT study [32] is:

$$M_{pitch} = 0.0220\left(\frac{Moment_{\max}}{D}\right)^{1.489} \qquad \text{[kg]}$$

Where: $Moment_{max} = 0.0136 * D^{3.0104}$ [kNm]

$$Cost_{pitch} = M_{pitch} * 6.689 + 953 \qquad \text{[\$]}$$

The maximum applied moment was estimated from the mass data in the WindPACT Rotor Design study [32] using an exponential fit of Residual = 1.

D.4 Low-Speed Shaft

The low speed shaft connects the hub to the gearbox and is assumed to be a hollow cylinder with a flanged end. The length of the shaft is assumed to be 0.03 multiplied by the rotor diameter, and the inner-to-outer diameter is fixed at 0.5. The shaft is assumed to be made from high-strength steel with a characteristic yield of 828 MPa and an endurance limit of 186 MPa. The cost of the shaft based on its mass (with a density of 7.85 g/cm^3) is assumed to be $7.00/kg [32]. The outer diameter of the shaft is calculated from [29] (modified to reflect a hollow shaft instead of a solid shaft) with the following equation:

$$D_o = \sqrt[3]{\frac{19.6}{0.9375} * \left[\left[\frac{Q_{LSS}}{\sigma_y} \right]^2 + \left[\frac{M_{LSS}}{\sigma_e} \right]^2 \right]^{1/2}} \quad \text{[mm]}$$

Where: $Q_{LSS} = 3 * Q_R$

$M_{LSS} = 0.25 * Length * g * M_{rotor}$ [kg]

D.5 Main Bearings

The main bearings which hold the shaft in place are considered to be of a standard type. The WindPACT study [32] suggests the following formula to calculate the bearing and housing masses:

$M_{bearing} = 2.613E\text{-}5 * (D_o)^{2.77}$ [kg]

$M_{housing} = 6.744E\text{-}5 * (D_o)^{2.64}$ [kg]

Where: OD_{shaft} = the outer diameter of the low speed shaft [mm]

The cost of both the bearings and housings is estimated as $17.60/kg.

D.6 Gearbox

The gearbox takes the low speed shaft input and produces a high speed output suitable for generator operation. The baseline design used here is a multiple-stage gearbox model developed by the University of Sunderland [29]. The model is quite complicated and is not described here, and the information is readily available from the reference. The cost of the gearbox is a function of the generator rating [32]:

$Cost_{gearbox} = (0.000647 * Rating + 13.26) * M_{gearbox}$

Where: *Rating* = the electrical rating of the turbine [kW]

$M_{gearbox}$ = the mass of the gearbox [kg]

D.7 Generator

The generator transforms the mechanical shaft energy into electrical energy. The generator chosen for this model is a doubly fed induction generator which allows variable speed operation with power electronics rated only at about 33% of the electrical capacity. The mass of this generator is described by [29]:

$$M_{generator} = 3.3 * Rating + 471$$

The cost of the generator is $52.00/kW [30].

D.8 Variable-speed electronics

The variable speed power electronic system is the means by which the variable frequency AC current is transformed into grid compatible constant frequency 60 Hz AC current. The traditional topology for power electronic (PE) systems of this magnitude is an IGBT-IGBT (Insulated Gate Bipolar Transistor) topology. The variable-speed power electronics are assumed to be rated to 33% the capacity of the doubly-fed induction generator. The cost of the power electronic system is $54.00/kW [30].

D.9 Bedplate

The bedplate is the structural component which transfers all of the rotor forces to the tower and supports the drivetrain components. The bedplate is necessarily a heavy component to meet strength and stiffness requirements. The bedplate is commonly made of longitudinal and cross sectional welded steel beams, but cast bedplates can provide a considerable reduction in cost. The bedplate weight is simulated according to the relation developed by the University of Sunderland [29]:

$$W_{BPQ} = 8.8E-3 * Q_R \quad \text{[kg]}$$

$$W_{BPTHR} = 1.58E-3 * T_R * Dia_{top} \quad \text{[kg]}$$

$$W_{BPRWT} = 1.5E-2 * (M_{blade} + M_{hub}) * Dia_{top} \quad \text{[kg]}$$

$$L_{BP} = 8.3E-2 * D \quad \text{[m]}$$

$$A_{BP} = 0.5 * L_{BP}^2 \quad [\text{m}^2]$$

$$W_{BPQ} = 100 * A_{BP} \quad \text{[kg]}$$

$$M_{bedplate} = W_{BPQ} + W_{BPTHR} + W_{BPWT} + W_{BPAREA} \quad \text{[kg]}$$

$$Cost_{bedplate} = 4.25 * M_{bedplate} \quad \text{[\$]}$$

Where: W_{BPQ} = Weight due to rotor torque

W_{BPTHR} = Weight due to rotor thrust

W_{BPRWT} = Weight due to rotor weight

L_{BP} = Length of bedplate

A_{BP} = Area pf bedplate

W_{BPQ} = Weight due to bedplate area

Dia_{top} = the top diameter of the tower

The cost of the bedplate including casting and machining costs is $4.25/kg [32].

D.10 Nacelle Cover

Nacelle covers encase the drive train assembly and bedplate, and are typically made of fiberglass reinforced composites. They also provide insulation for noise from the drivetrain and for protection of the electrical components from temperature and humidity. The fiberglass cladding has a mass per unit area equal to 84.1 kg/m^2 and a cost if $10.00/kg [32]. The estimated surface area is calculated from the University of Sunderland [29] report:

$$A_{CLAD} = 2 * L_{BP}^2 \qquad [m^2]$$

$$M_{nacelle} = 84.1 * A_{CLAD} \quad [kg]$$

Where: A_{CLAD} = the cladding area

D.11 Mechanical Brake, High-Speed Shaft, Coupler

The high speed shaft connects the output of the gearbox to the generator. The mass of the high-speed shaft and coupler is calculated using the following equation [29]:

$$M_{brake,HSS,} = 0.0375 * Torque_{HSS,rated} \qquad [kg]$$

Where: $Torque_{HSS,rated}$ = the rated torque of the high-speed shaft found in the gearbox calculations [N-m]

The cost estimate for these items is $10.00/kg [32].

D.12 Yaw Drive and Bearing

The yaw drive has the task of orienting the rotor and nacelle into the wind. The drive is powered by either an electric or hydraulic motor with the recent trend moving towards electric motors due to their increased ease of control. The mass of the system is calculated using the University of Sunderland report [29]:

$$W_{YAW} = M_{blade} + M_{hub} + M_{pitch} + M_{bearing} + M_{LSS} + M_{gearbox} + M_{generator} + M_{bedpkate} + M_{nacelle} + M_{brake,HSS} \qquad [kg]$$

$$M_{yaw} = W_{YAW} * 4E - 4 * D + 0.975 * T_R * Dia_{top} \qquad [kg]$$

$$Cost_{yaw} = 2* (Mass_{yaw} * 6.689 + 953) \qquad [\$]$$

D.13 Electrical Connections

The electrical connections of the wind turbine include the switchgear, transformer, cable, cabinets, and other small electrical connectors. These items make the turbine ready to "plug in" to a wind farm collection scheme. The cost estimated for these items together is based on the WindPACT Balance-of-station study [31] and is $40.00/kW. The electrical connections do not include the controls and power electronics.

D.14 Hydraulic and Lubrication System

The hydraulic system is used only for the brakes, cooling, and lubrication, including the equipment used for cooling the gearbox and bearings. The cost estimated in the WindPACT study [32] is as follows:

$$Cost_{hydraulic} = \$4.50/kW$$

D.15 Controls and Safety System

The control and safety system is a composite of sensors, actuators, hardware and software that together are required to maintain efficient and safe operation of the turbine. Inputs include data from the anemometer, wind vane, power output, and rotor speed. The controller is used to control pitch, generator torque, yaw, and tower vibration. The safety system may take corrective action in the case of rotor over speed, excessive vibration, controller malfunction, emergency stop button actuation or other faults [26]. The cost of the controls as a function of the diameter of the turbine is as follows [29]:

$$Cost_{control} = 9500 + 10 * D \qquad [\$]$$

D.16 Tower

The tower is one of the major components in a wind turbine. It usually comprises 10-20% of the turbine costs. A tubular steel tower with a material yield stress of 350MPA is

assumed [32]. The tower is designed for peak loads at both its top and base. The cost of the tower is $1.50/kg. The tower dimensions and mass are iterated twice to meet the applied loads [28]. The drag coefficients used in the analysis were back calculated from the data in the study [28] and applied to the simulation for the Maury Island project. The tower calculations are as follows:

$$M_{initial} = \frac{1.35 * T_R * Height}{(0.85)^2}$$

$$SM_{initial} = \frac{M_{initial}}{YS}$$

$$Dia_{Base,Initial} = 0.784 * \frac{SM_{initial}}{\left(\pi/64 * 0.03587\right)^{1/3}}$$

$$Drag_{initial} = 1.89 * 0.75 * Dia_{base,initial} * Height * \rho * \frac{V_{EX}^2}{2}$$

$$M_{Base,initial} = \frac{0.89 * Drag_{initial} * Height}{2}$$

$$M_{base,characteristic} = 0.74 * \left(M_{base,initial} + M_{initial}\right)$$

$$Section_{\text{mod}} = 1.35 \frac{M_{base,characteristic}}{YS_{tower}}$$

$$Dia_{base} = Feed\_red * 0.784 * \left(\frac{Section_{\text{mod}}}{\frac{\pi}{64} * 0.03587} \right)^{1/3}$$

$$Dia_{top} = \frac{Dia_{base}}{2}$$

$$Thick_{base} = \frac{Dia_{base}}{220}$$

$$Area_{base} = \frac{\pi}{4}\left(Dia_{base}^2 - \frac{218}{220} Dia_{base}^2 \right)$$

$$Thick_{top} = \frac{Dia_{top}}{220}$$

$$Area_{top} = \frac{\pi}{4}\left(Dia_{top}^2 - \frac{218}{220} Dia_{top}^2 \right)$$

$$Tower_{mass} = \rho_{tower} * Height * \frac{Dia_{base} + Dia_{top}}{2}$$

$$Tower_{cost} = 1.50 * Tower_{mass}$$

Where: Dia_{base} = the tower base diameter

Dia_{top} = the tower top diameter

YS_{tower} = yield strength of the tower

$Thick_{base}$ = the thickness at the base of the tower

$Thick_{top}$ = the thickness at the top of the tower

ρ_{tower} = the density of the tower

Appendix E. Balance-of-station Design Description and Cost Analysis

The balance-of-station for the sites along Maury Island is considered here. The layout of the turbine sites are summarized in Figure E-1 through Figure E-3, and a description of the layout follows:

- The numbered circles represent the turbine locations.
- The dashed lines in the figures represent new roads that would have to be built to install and service the proposed turbines on Maury Island.
- The solid lines represent underground electric cables (or possibly overhead lines) that are necessary to connect the turbines to a common recloser and riser assembly. Cable will also be run along the road lengths in red. The total cable length at a site is therefore the distance of the blue and red lines combined.
- The squares represent the recloser (connection devices similar to circuit breakers) and riser assemblies which connect the underground cables to the medium voltage overhead lines.

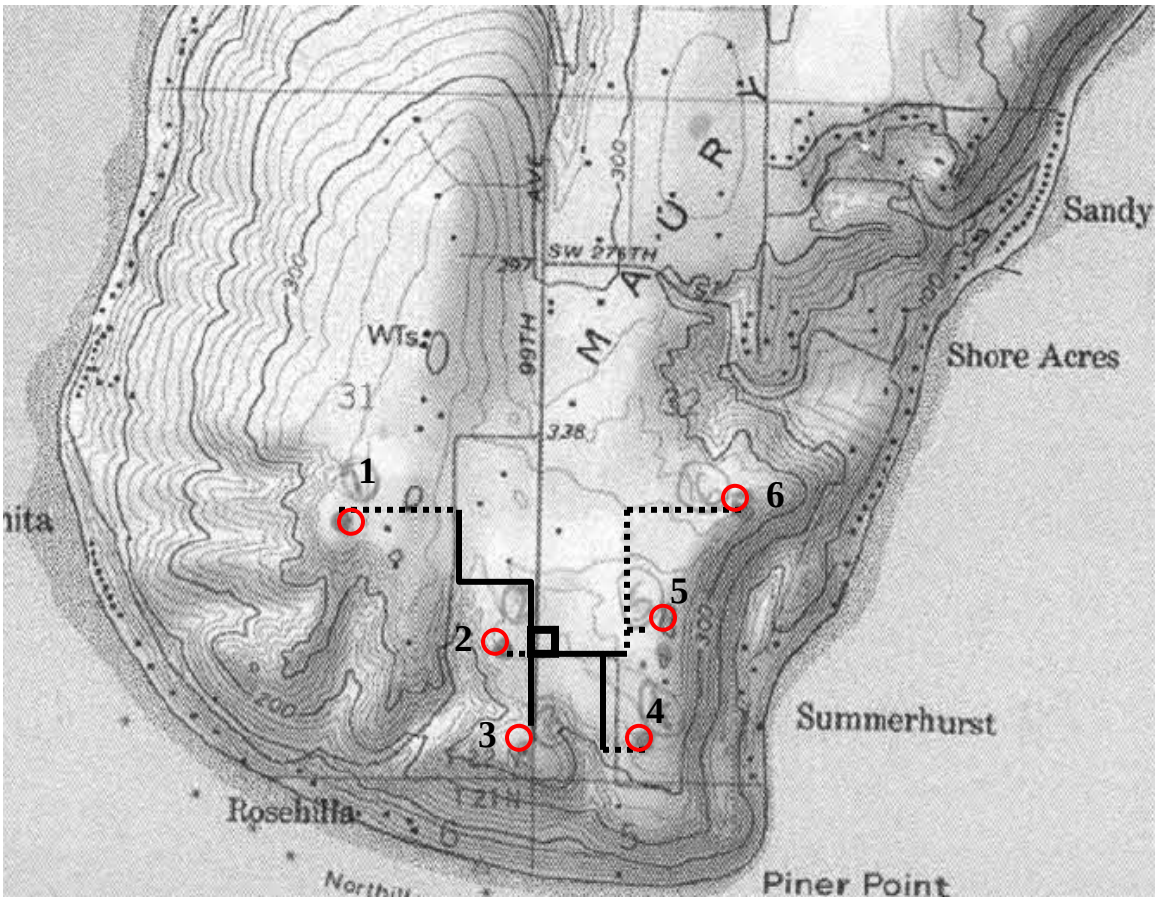

Figure E-1. Location A on the southern tip of Maury Island [8]

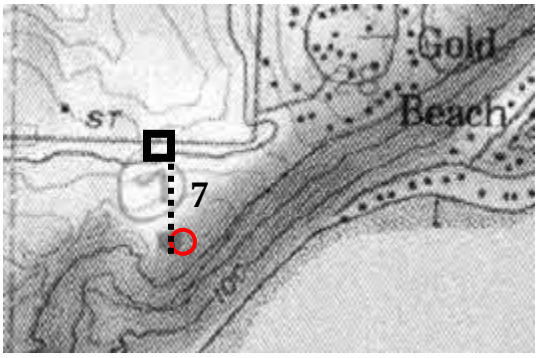

Figure E-2. Location B on the south-eastern shore of Maury Island [8]

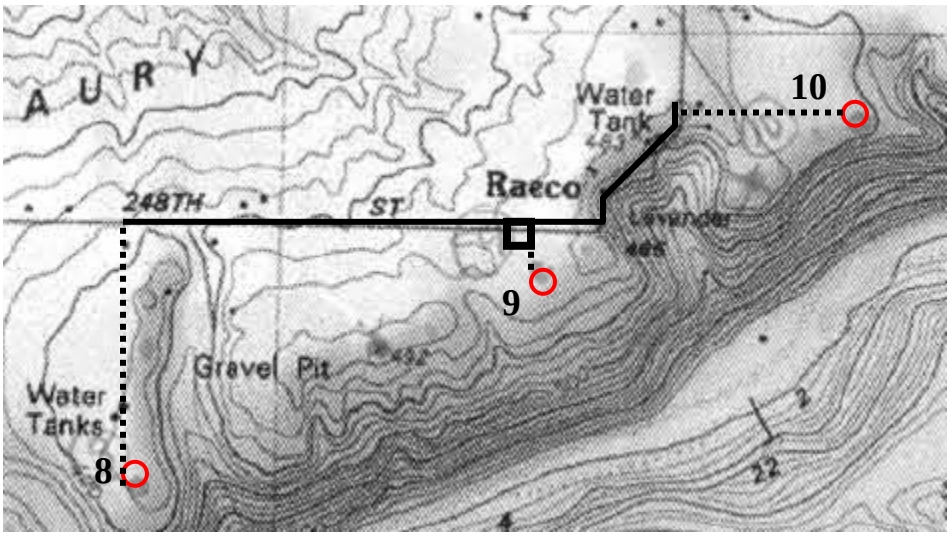

Figure E-3 Location C along the eastern shore of Maury Island

Table E-1. Summary of the Location Descriptions

Site	Turbines	Length of Underground Cable [km]	Service Road [km]	Area [km^2]
A	6	2.3	1.2	0.36
B	1	0.2	0.2	0.04
C	3	2.5	1.1	0.24
Total	10	5	2.5	0.64

E.1 Electrical Interface/Connections

The collection system is the electrical pathway by which the power from the turbines is transmitted to the electrical grid. A system with a capacity this large would have to be interconnected to the grid at a substation rather than directly through the distribution system nearest the turbines [26]. Voltages of the collection system are typically 15kV, 25kV, and 35kV with new wind farms tending towards 35kV [30,31]. The voltage must be stepped up from the wind turbine generator voltage to reduce line losses. A thorough analysis of the collection system would include a trade study into the optimum voltage, but was outside the scope of this study. The voltage chosen for the collection system is 25kV. The step-up transformers (which step the voltage from the turbine generator

output (690V) to the medium voltage cable lines (25kV)), the turbine circuit breakers, and switches are included in the turbine electrical connections cost.

It is assumed that the Maury Island wind farm can interconnect to the grid at the existing utility substation on Maury Island. This 115kV substation is where the cable from the mainland connects to overhead lines. Major equipment required to interconnect the collection system at 115kV include: a 115kV/25kV transformer, a 25kV circuit breaker (three pole), a switch (three pole), and current and potential transformers all rated at 15MVA.

The medium voltage cables link the power output from the wind turbines together at each site. The cables are buried conduit cables which will provide protection against someone digging and hitting the lines. Additionally, if a section of cable fails, it does not have to be dug up to be replaced; the faulted section can simply be pulled through the conduit. The conductor current rating is found by the following formula:

$$I_{1\phi} = \frac{N_{turbine} * Rating}{\sqrt{3} * V_{med}}$$

Where: $I_{1\varphi}$ = the single phase current in each line

$N_{turbine}$ = the number of turbines at each area

$Rating$ = the wind turbine generator rating

V_{med} = 25kV, the medium voltage line voltage

The rated currents and appropriate aluminum cables found by using IEEE standards [37] (and linear extrapolation) are listed in Table E-2. The abbreviation AWG stands for American Wire Gauge.

Table E-2. Underground Single-Phase Currents and Conductor Types

Turbine Rating	One Turbine [Amps]	Copper Conductor Type*	Two Turbines [Amps]	Copper Conductor Type*	Three Turbines [Amps]	Copper Conductor Type*
1.0MW	23.1	6 AWG	46.2	4 AWG	69.3	2 AWG
1.5MW	34.6	4 AWG	69.3	2 AWG	103.8	1 AWG
2.0MW	46.2	4 AWG	92.4	1 AWG	138.6	1 AWG
Length	4.5 km		0.25 km		0.25 km	

*25 kV single conductor, shielded, extruded, direct buried conduit, aluminum, 75% load factor, 90ºC conductor, 90Ω earth resistivity [37]

The underground cable would be run to the edge of the site where it would be connected to a main collector line. The main collector line is assumed to be a conventional three-phase overhead distribution line that would be built for the purpose of the wind farm and would run along a roadway from site to site and then to the substation. The overhead lines are assumed to be Aluminum Conductor Steel Reinforced (ASCR) 25kV lines. The total length of the collector line running from the turbine area recloser and riser assemblies to the Maury Island substation is 11.5 km. The rated currents for the line segments and appropriate aluminum cables are listed in Table E-2.

Table E-2. Single Phase Line Currents and Conductor Types for Overhead Lines

Turbine Rating	Site A to Site B Current [Amps]	Copper Conductor Type*	Site B to Site C Current [Amps]	Copper Conductor Type*	Site C to Substation Current [Amps]	Copper Conductor Type*
1.0MW	139	1AWG	163	1/0	233	4/0
1.5MW	208	3/0	243	4/0	347	350kmils
2.0MW	278	250kmils	321	350kmils	460	750kmils
Length	5 km		3.25 km		3.25 km	

*25kV single conductor, shielded, extruded, free air, full Sun, V_{wind} = 2ft/s, 90ºC Conductor, 40 ºC Ambient [37]

Between the underground cable and the overhead distribution line would be a fault-interrupting device called a recloser. A recloser is like a utility scale circuit breaker which will isolate the two sections in the event of an electrical fault. With three sites, the project would require three reclosers. A riser assembly is also required to connect the

underground cables to the overhead lines. The cost for the reclosers and risers is $25,880 each [31].

Table E-3. Overhead Line Calculations [31,58]

Overhead Lines					From Site A to Site B, 5km		
Item	Quant.	Cost	Cost per Mile	Cost per km	1AWG Cond	1/0 Cond	4/0 Cond
Poles	12	335	4020	2498	12492	12492	12492
Holes	12	252	3024	1879	9397	9397	9397
Erect, etc.	12	2125	25500	15848	79242	79242	79242
Disposal	1	105	105	65	326	326	326
Crossarms	24	1120	26880	16706	83530	83530	83530
Disposal	1	54.5	54.5	34	169	169	169
Conductor	3	-	-	-	53431	58999	74040
Material handling	1	650	650	404	2020	2020	2020
Joints	1	1650	1650	1025	5127	5127	5127
Sagging	1	860	860	534	2672	2672	2672
Clipping (1/2 factor)	12	167.5	2010	1249	6246	6246	6246
Jumpers (1/2 factor)	12	587.5	7050	4382	21908	21908	21908
Ground Wire	1	7400	7400	4599	22996	22996	22996
Insulators (0.9 factor)	180	68.5	12323	7659	38295	38295	38295
Disposal	1	52.5	52.5	33	163	163	163
SubTotal			91579	56917	338016	343584	358625

Table E-3 (Continued)

Overhead Lines	From Site B to Site C, 3.25km			From Site C to Substation, 3.25km		
Item	3/0 Cond	4/0 Cond	350kmils Cond	250kmils Cond	350kmils Cond	750 kmils Cond
Poles	26390	26390	26390	26390	26390	26390
Holes	19851	19851	19851	19851	19851	19851
Erect, etc.	167398	167398	167398	167398	167398	167398
Disposal	689	689	689	689	689	689
Crossarms	176457	176457	176457	176457	176457	176457
Disposal	358	358	358	358	358	358
Conductor	0	0	0	0	0	0
Material handling	4267	4267	4267	4267	4267	4267
Joints	10832	10832	10832	10832	10832	10832
Sagging	5646	5646	5646	5646	5646	5646
Clipping (1/2 factor)	13195	13195	13195	13195	13195	13195
Jumpers (1/2 factor)	46281	46281	46281	46281	46281	46281
Ground Wire	48578	48578	48578	48578	48578	48578
Insulators (0.9 factor)	80898	80898	80898	80898	80898	80898
Disposal	345	345	345	345	345	345
SubTotal	601185	601185	601185	601185	601185	601185

Table E-2. Underground Cable Calculations [31,58]

Underground Cables		1000 kW Turbine		
Item	Quantity	6 AWG Cond, 4.5km	4 AWG Cond, 0.25km	2 AWG Cond, 0.25km
Direct burial PVC, 4"	1	148408	8245	8245
Conductors	3	42964	2497	2672
Terminals (3P)	13	40430	0	0
Fuses (3P)	10	18000		
Connectors, etc 20%	20%	52109		
Total		323569		

Underground Cables		1500 kW Turbine			2000 kW Turbine	
Item	Quantity	4 AWG Cond, 4.5km	2 AWG Cond, 0.25km	1 AWG Cond, 0.25km	4 AWG Cond, 4.5km	1 AWG Cond, 0.5km
Direct burial PVC, 4"	1	148408	8245	8245	148408	16490
Conductors	3	44944	2672	2795	44944	5589
Terminals (3P)	13	40430	0	0	40430	0
Fuses (3P)	10	18000			18000	
Connectors, etc 20%	20%	52540			54772	
Total		326277			328632	

E.2 Roads and Civil Works

It is realistic to assume that existing roads on the island could be utilized to move equipment between each turbine site without the need for new roadway construction. However, roadways to allow for construction and maintenance of the wind turbines are necessary where existing roadways are not available. The roadway will be a paved road wide enough for the heavy maintenance equipment and moving cranes to pass, but may not be large enough for the equipment (cranes) during the initial construction of the towers and rotors. This means the cranes may need to be disassembled when moving from one turbine location to the next. The cost of the paved roadway is $90.00/ft [31].

E.3 Crane Pads

The remaining civil works that are included in this section of the analysis are the crane pads. A crane pad is necessary for a large crane to safely erect the tower and rotor of a large wind turbine if the ground is not level enough. An expression is developed from the WindPACT balance-of-station study [31] for crane pad cost as a function of hub height:

$$Cost_{cranepad} = 1.3348 * (HH)^{2.3081}$$

Where: HH = the hub height of the turbine [m]

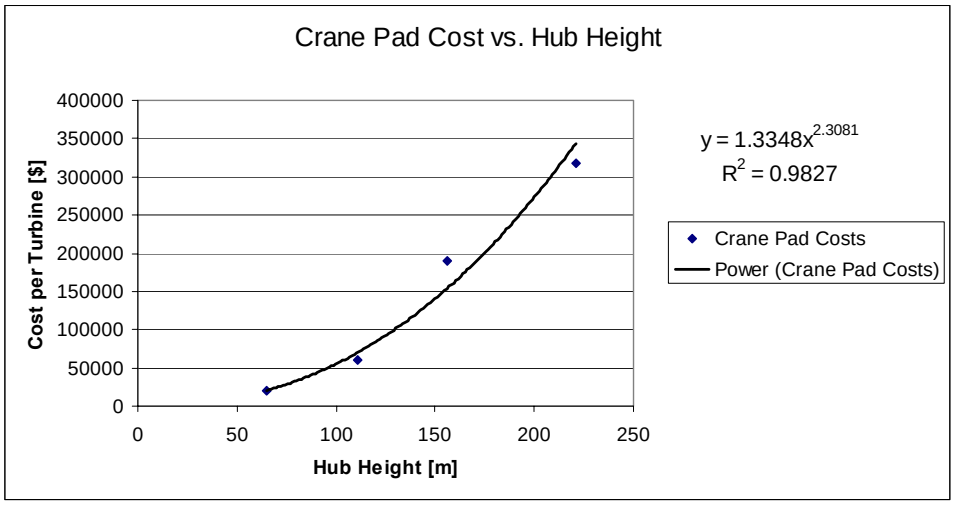

Figure E-4. Crane Pad Costs

E.4 Foundations

The foundation size is determined by the size of the wind turbine, loading on the tower, and the local geological condition. Foundations are exclusively constructed of steel reinforced concrete. The geological condition of the site determines whether flat standard foundations are required or if foundations with piles are required (for weak soils). Maury Island is assumed to have solid soil and thus a flat foundation is assumed. The cost of a flat foundation is based on the maximum overturn moment due to an extreme wind gust [31]:

$$Cost_{foundation} = 510*(Moment_{max,\ base})^{0.465}$$

Where: $Moment_{max,\ base}$ = the maximum moment at the base of the tower [kNm]

E.5 Blade Transport

The average distance to national suppliers of rotor blades is 1380 miles. Transportation of the rotor blades can be accomplished most economically by tractor-trailer. However, blades with length beyond 45 m and up to 49 m, requires the use of rear-steering

equipment in addition to the tractor-trailer. For rotor blades longer than 49 m, the use of water transportation is necessary. In this case, only blade manufacturers on the west coast are considered with an average cost of $125 per metric ton or cubic meter, whichever is greater [28]. The costs per blade follow.

From US less than 49 m (by truck):

$$Cost_{blade,transport} = 0.1722 * D^{2.4181} \quad [\$]$$

From US greater than 49 m (by ocean vessel):

$$Cost_{blade,transport} = 125 * 0.0018 * D^{3} \quad [\$]$$

E.6 Hub Transport

Hubs are considered to be supplied from Tehachapi, California [28] at 1100 miles. Both truck and rail options are viable transport options with trucking being about half the cost.

$$Cost_{hub,\ transport} = 0.782 * D^{2.0083} \quad [\$]$$

E.7 Nacelle Transport

The origin of the nacelles is considered the same as those for the hubs. Viable transport options include trucks and rail for the lighter nacelles and ocean going ship for the larger nacelles. For chartered ocean vessels, the average transportation cost is $125 per metric ton or cubic meter, whichever is greater [28].

$$Cost_{nacelle,transport} = 0.3251 * D^{2.4212} \quad [\$]$$

E.8 Tower Transport

Three tower manufacturers located in Rancho Cucamonga, CA, Irvine, CA, and Tarzana, CA at an average of 1160 miles are considered. For towers with base diameters larger than 4.83m, the towers are considered to be quartered to avoid either shipment by ocean vessel or the added cost of removing overhead lines. The assembly of the tower sections is accounted for in the assembly and installation costs. The cost function is [28]:

$$\text{Cost}_{\text{tower, transport}} = \left(\frac{1160}{1111}\right) * 0.0121 * (HH)^{3.3649} \qquad [\$]$$

E.9 Transportation to Vashon Island

Once the turbine components arrive in Seattle or Tacoma, they will need to get to Vashon Island by some means. Most major turbine components would not be able to be transferred by ferry due to size and weight limitations. Therefore, all components are considered to be transported by barge.

A rough estimate for the cost of the barge was provided by a barge service at the Port of Seattle. A rough per diem cost would be $1000 per day for a large barge and about $2100 for transportation to Vashon ferry terminal. There will be a standby charge of $300 per hour while on-loading/off-loading in addition to other mobilization costs.

The barge loading assumptions were that two tractor-trailers would fit per barge and 1.5 trips per day could be made. The average on-loading and off-loading time would be four hours per trip. The number of tractor-trailors required for a turbine was taken directly from the road transportation numbers developed previously. The costs are broken down into two categories: (1) the costs for the tower and (2) the costs for the rotor, nacelle, and hub. Expression for the barge costs are then developed for each group as a function of the hub height and the rotor diameter respectively. The functions developed are:

Tower head costs (blades, hub, nacelle):

3-bladed: $Cost_{barge,head} = 1830.9 * D^{0.3716}$ [$]

Tower costs:

$Cost_{barge,tower} = 0.0406 * D^{2.8291}$ [$]

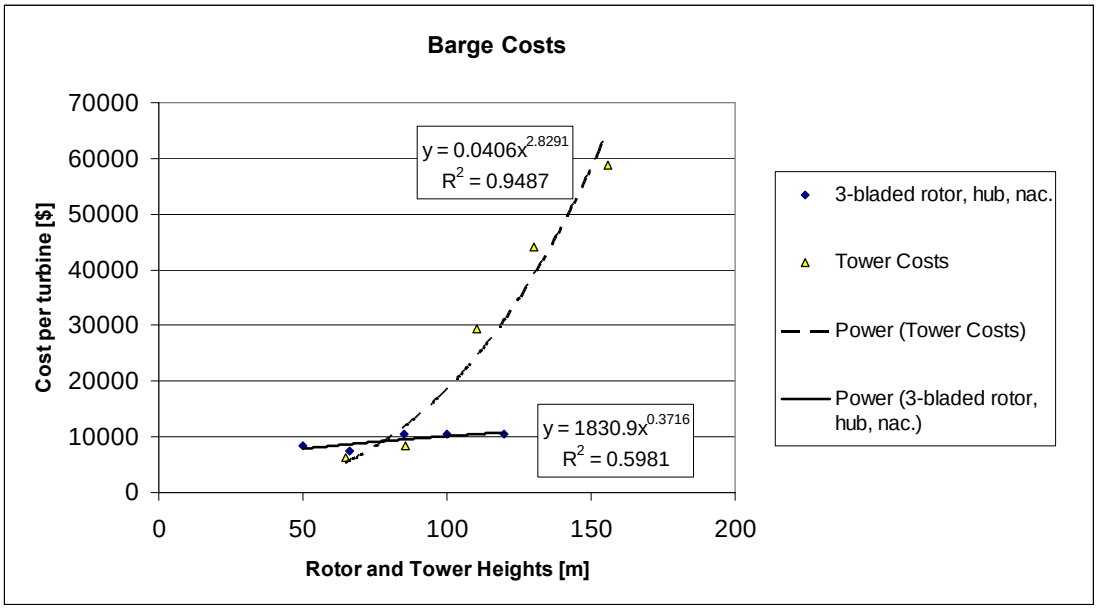

Figure E-5. Barge Costs

E.10 Crane Costs

The crane costs were investigated in the WindPACT logistics study and were found to be dependent on the height of the nacelle installation rather than weight of the nacelle, tower sections or rotor [31]. This is because cranes being designed to handle much larger weights for a given height than those required for wind turbine assembly. The data developed in the WindPACT study [31] is curve fit as a function of the hub height:

$Cost_{crane} = 0.017 * (HH)^{3.3058}$ [$]

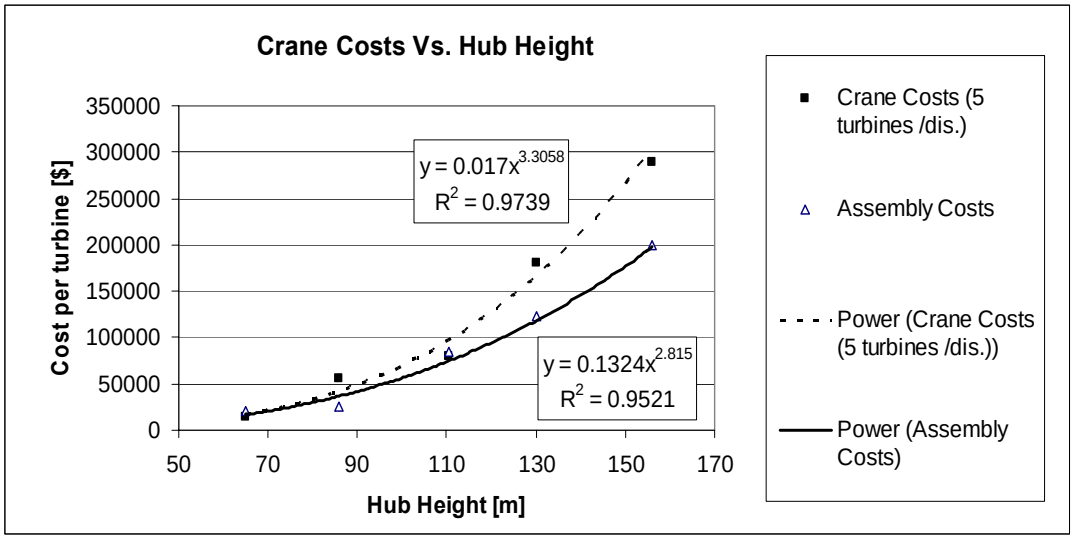

Figure E-6. Crane Costs

E.11 Assembly and Installation

The per turbine assembly costs found in the WindPACT study are used here with the knowledge that this is a non-conservative assumption. The assumption is not expected to effect the overall capital cost of the project significantly (i.e. <1%). A trend line is developed to represent as a function of the hub height as follows [31]:

$$Cost_{installation} = 0.1324 * (HH)^{2.815} \quad [\$]$$

E.12 Permitting Costs

The permits and engineering as a function of the rating of the turbine [31]:

$$Cost_{permits} = 9.94E\text{-}4*Rating + 20.31 \quad [\$/kW]$$

E.13 Engineering Costs

The engineering costs are those costs for the development of the wind farm and supporting civil infrastructure. This cost is estimated at 7% of the subtotal of the balance-of-station costs [31].

$$Cost_{engineering} = 0.07 * \text{Balance Subtotal} \qquad [\$]$$

E.14 Surveying Costs

The surveying costs are calculated on a per square kilometer basis [31]:

$$Cost_{surveying} = 6562 * \text{Site Area} \qquad [\$]$$

E.15 Inspection Costs

The inspection costs are considered a flat fee. This covers the inspection cost for the civil infrastructure construction and turbine assembly and installation. This cost is estimated as $10,000 per inspection with 6 inspections over the construction and installation process [31].

$$Cost_{inspection} = 6 * 10{,}000 \qquad [\$]$$

Appendix F. WindPACT Technology Impacts on Cost

The WindPACT studies [30,32,39,40] investigated the COE reductions that may occur with turbine system design improvements over the next ten years. The turbine and balance-of-station models for the Maury Island wind farm use the percent decreases in COE for each system as those found in the WindPACT studies [30,32,39,40]. The decreases in COE are detailed here.

Table F-1. Cost Reduction of Single Stage Gearbox with Permanent Magnet Generator Design [30]

Component	Baseline Drivetrain	Single PM Generator	% of Baseline
Transmission System	155,000	90,000	0.58
Support Structure	34,000	20,000	0.59
External Cooling System	2,400	4,400	1.83
Brake	1,400	3,200	2.29
Coupling	2,400	0	0.00
Nacelle Cover	17,000	8,200	0.48
Generator	60,000	54,000	0.90
Power Electronics	62,000	53,000	0.85
Substation VAR Control	0	12,000	-
Transformer	23,000	26,000	1.13
Cable	18,000	16,000	0.89
Switchgear	12,000	10,000	0.83
Drivetrain Assembly and Test	8,000	5,500	0.69
Annual Energy Production	4,841,000	5,001,000	1.03

Table F-2. Cost Reduction Table for Self-Erecting Tower [39]

Data Table					
Rating	750	1500	2500	3500	5000
Hub Height	65	86	111	130	156
Lump Costs					
Dev. & Cap. Cost (based on ICC payback in 5 years)	219750	281300	348650	474650	586000
Transportation cost/mile	15	20	25	30	33
Miles transported (Memphis to Seattle round trip)	4800	4800	4800	4800	4800
Transportation Cost	72000	96000	120000	144000	158400
Load/Setup/Teardown Cost	8600	9900	11300	12600	13600
Per Turbine Costs					
Operator Cost	4800	6000	7200	9600	10800
Adjustments	7417	8293	9440	10627	12377
Assembly Labor and Materials	25079	33762	53709	66226	107627
Support Crane	1480	2600	2600	2992	3920
Lookup Table					
Number of Turbines					
10	68811	89375	120944	152570	210524
20	53794	70015	96947	121008	172624
30	48788	63562	88947	110487	159991
40	46285	60335	84948	105226	153674
50	44783	58399	82548	102070	149884